THESIS FOR THE DEGREE OF DOCTOR OF PHILOSOPHY IN THERMO AND FLUID DYNAMICS

Modelling of Catalytic Monolith Reactors for Exhaust Aftertreatment

Combining Accurate Experiments with Robust Parameter Tuning

MAGNUS WALANDER

Department of Mechanics and Maritime Sciences
CHALMERS UNIVERSITY OF TECHNOLOGY

Gothenburg, Sweden 2022

Modelling of Catalytic Monolith Reactors for Exhaust Aftertreatment
Combining Accurate Experiments with Robust Parameter Tuning
MAGNUS WALANDER
ISBN 978-91-7905-672-8

Doktorsavhandlingar vid Chalmers tekniska högskola
Ny serie nr. 5138
ISSN 0346-718X

Division of Combustion and Propulsion Systems
Department of Mechanics and Maritime Sciences
Chalmers University of Technology
SE-412 96 Gothenburg Sweden
Telephone: +46 (0)76-833 53 20

Cover Picture: Illustration of length scales involved in a diesel oxidation catalyst.

Chalmers Digitaltryck
Gothenburg, Sweden 2022

Abstract

The incomplete combustion of liquid or gaseous fuels in the internal combustion engine inherently produces several toxic emissions that need to be removed. This is done through a series of catalytic converters, referred to as the exhaust aftertreatment system (EATS), each catalyst with its own purpose. To cope with increasingly stringent emission legislation for the automotive industry, the performance of these catalysts needs to improve. For their development, modelling is an indispensable tool.

This thesis presents a mathematical model, a so-called single-channel 1+1D reactor model, that describes the reactions that occur inside a diesel oxidation catalyst (DOC) - along with the heat and mass transport. The purpose was to improve an already existing model using relevant experiments such as kinetic experiments using a synthetic catalyst activity test (SCAT) bench, gravimetric analysis (GA), temperature programmed desorption (TPD) as well as scanning electron microscopy (SEM).

The inlet conditions for the used catalyst sample in an injection-based SCAT bench along with important model assumptions was validated rigorously. A smart experiment, using a small active DOC core positioned in various radial positions within an inert, larger monolith revealed that there was a radial concentration maldistribution within the SCAT bench. After developing a modified SMX mixer and running the experiments again, it was concluded that the SCAT bench fulfilled the assumptions for single channel models, while still maintaining its transient benefits compared to the alternative premixed design.

After the SCAT bench inlet conditions were verified, an efficient experimental method was developed for identifying mass transfer limitations for a monolith reactor. This experimental method constituted the basis for the experimental observations in paper III and IV. It was shown, using ratios of various timescales that NO oxidation on Pt/Al_2O_3 can be internally mass transfer limited already at 175°C. This agreed fairly well with the modelling findings of paper IV using the same timescales.

Another important modelling assumption that was investigated was the one regarding the assumed uniformly distributed washcoat. This assumption was challenged by developing a parallel, tangentially resolved mass transfer model with local effective diffusivities established using a combination of SEM and IGA. The model shows great promise for monolith reactors with high washcoat loading, however, it showed to be redundant for the catalysts used with uniform washcoat distributions. It might still find uses in reactors that utilize differences in internal mass transfer to promote selectivity for series reactions.

To accompany the experiments performed, without having to perform dedicated experiments for each unknown model parameter, a robust parameter estimation algorithm using response surface methodology (RSM) was integrated into the 1+1D reactor model in Matlab. The tool utilized a design of experiment (DoE) to numerically approximate the objective function for gradient and step size determination. It was shown that different DoEs require different step sizes but a more sophisticated DoE can allow for a faster optimization. One other important aspect for the tuning was the weight function to weigh together the temperature resolved residual - a temperature dependent weight function improved the fit and boosted the importance for external and internal mass transfer parameters. Lastly, the use of an additional, inert washcoat in the experiments showed to be a vital observation for tuning the internal mass transfer.

These findings are relevant for accurate and predictive modelling of catalysts for the automotive industry.

Keywords: Exhaust aftertreatment modelling, EATS, diesel oxidation catalyst, synthetic catalyst activity test, scanning electron microscope, gravimetric analysis, effective diffusivity, washcoat, parameter estimation

Acknowledgements

First of all, I would like to thank my supervisors Associate Professor Jonas Sjöblom and Professor Derek Creaser for giving me the opportunity to work on this project, for guiding me through solving problems and for helping me to create new ones. The two of you have always kept me motivated and interested.

Secondly, I would like to extend my gratitude to several project members. To Björn Agri providing the reactor code, to Stefanie Tamm, Jonas Edvardsson, Niklas Löfgren and Klas Arvidsson for helping me plan experiments and perform industry relevant research. I would also like to thank and apologize to Mats Mannhem, Anna-Lena Lindahl, Iain Hitchcock, Nadezda Sadokhina and Niklas Freiman for helping me performing excellent but sometimes extremely tedious experiments at Johnson Matthey. You are so helpful and I would consider myself lucky if I ever were to work with any of you again. Funding from the Swedish Energy Agency, through FFI project 42814-1 "*Emission control by validated catalytic reactor modelling*", is gratefully acknowledged.

When I started at the Division for Combustion and Propulsion Systems (CaPS) I felt like I did not belong because for the first time in my adult life I was not surrounded by chemical engineers. Well, many thanks to the social people around the lunch and coffee table who proved me wrong; Michael, Sreelekha, Vignesh, Jelmer, Jayesh, Mindaugas, Marco, Andreas, Josefine and Omar. I will miss you deeply. For the lovely PhD students who are here still after me; Nidal, Abhilash, Mohammad and Victor - our (short) coffee breaks has been vital to my well-being for the passed years. To my dear office mate Pratheeba (room mate considering how many evenings we spend together in the office); we may not be the most similar people, but our conversation about anything and everything kept me sane and happy during the most challenging years of my life. I have never met someone who knows so much about so many different fields in chemical engineering. I do not need a search engine, neither a chemical reaction engineering handbook as long as I can turn to you for advice.

Thank you to all my friends in Gothenburg, I promise I will be able to hang out soon, real soon. Thank you dear Anna for teaching me about what is important in life and being the crazy person that you are, cooking fancy roe deer meat on a Tuesday to make me happy.

Last, but most importantly, the biggest and warmest thank you to my family. Thank you to the most persistently loving person in my life. My mother Anki is really the mother of all mothers. Thank you Mats for raising me to be the man that I am today. I miss you every day and thinking of you makes me a little stronger a little longer. Thank you my brother Tomas for always being there for me, whether it is for playing Age of Empires or for just relaxing a weekend in Stockholm.

List of publications

This thesis is based on the work contained in the following publications:

Publication I M. Walander, A. Nygren, J. Sjöblom, E. Johansson, D. Creaser, J. Edvardsson, S. Tamm and B. Lundberg. "Use of 3D-printed mixers in laboratory reactor design for modelling of heterogeneous catalytic converters."
in Chemical Engineering and Processing - Process Intensification (2021) Vol. 164.

Publication II M. Walander, J. Sjöblom, D. Creaser, B. Lundberg, S. Tamm and J. Edvardsson. "Efficient Experimental Approach to Evaluate Mass Transfer Limitations for Monolithic DOCs."
in Topics in Catalysis (2019) Vol. 62, 1–4, p. 391–396.

Publication III M. Walander, J. Sjöblom, D. Creaser, B. Agri, N. Löfgren, S. Tamm and J. Edvardsson. "Modelling of mass-transfer resistances in non-uniformly washcoated monolith reactors."
in Emission Control Science and Technology (2021), Vol. 7, p. 153-162.

Publication IV M. Walander, J. Sjöblom, D. Creaser, J. Edvardsson, N. Löfgren and S. Tamm. "Robust parameter estimation methodology for heterogeneous catalytic reactors."
Submitted to Computers & Chemical Engineering.

List of Figures

List of Tables

Nomenclature

Abbreviations

Symbol	Description
ABS	Acrylonitrile butadiene styrene
ASC	Ammonia Slip Catalyst
CFD	Computational Fluid Dynamics
CPSI	Cells Per Square Inch
CPU	Central Processing Unit
CRT	Continuously Regenerating Trap
CSTR	Continuously Stirred Tank Reactor
DAE	Differential-Algebraic system of Equations
DFT	Density-Functional Theory
DOC	Diesel Oxidation Catalyst
DoE	Design of Experiments
DPF	Diesel Particulate Filter
EATS	Exhaust AfterTreatment Systems
EU	European Union
Euro X	Euro Emission Standard X
GA	Gravimetric Analysis
GHSV	Gas Hourly Space Velocity
HC	HydroCarbon
HDD	Heavy Duty Diesel
ICE	Internal Combustion Engine
IGA	Intelligent Gravimetric Analysis
LNT	Lean NO_x Trap
MFC	Mass Flow Controller
NSR	NO_x Storage and Reduction
ODE	Ordinary Differential Equations
OECD	Organization for Economic Cooperation and Development
PFR	Plug Flow Reactor
PLS	Partial Least Squares
PM	Particulate Matter
POCS	Periodic Open Cellular Substrates

RSM	Response Surface Methodology
SCAT	Synthetic Catalyst Activity Test
SCR	Selective Catalytic Reduction
SDG	Sustainable Development Goal
SEM	Scanning Electron Microscopy
SMX	Name of Mixer
TWC	Three-way Catalyst
US	United States
WHO	World Health Organization

Dimensionless Numbers

Symbol	Description	Unit
Φ	Thiele modulus	[–]
Ψ	Weisz modulus	[–]
Bi_m	mass Biot number	
Da_II	2^nd Damköhler number	[–]
Gz	Graetz number	[–]
$Nu_{\infty,\mathrm{T}}$	Asymptotic Nusselt number	[–]
Re	Reynold number	[–]
Sc	Schmidt number	[–]
Sh	Sherwood number	[–]

Greek Symbols

Symbol	Description	Unit
α_tot	Lumped heat loss coefficient	$[\mathrm{W\,K^{-1}}]$
α_j	Coverage dependency for activation energies	[–]
ΔG_net	Net change in Gibb's free energy	$[\mathrm{J\,mol^{-1}}]$
ΔH^0_net	Net change in enthalpy	$[\mathrm{J\,mol^{-1}}]$
ΔH_j	Reaction enthalpy	$[\mathrm{J\,mol^{-1}}]$
ΔS^0_net	Net change in entropy	$[\mathrm{J\,mol^{-1}\,K^{-1}}]$
Δx_l	Radial distance between layers	[m]
Δz_k	Axial distance between tanks	[m]
η	Effectiveness factor	[–]
$\Gamma_{i,k,l}$	Lumped mass transfer coefficient	$[\mathrm{m^3\,s^{-1}}]$

λ_{g}	Gas phase heat conductivity	$[\mathrm{W\,m^{-1}\,K^{-1}}]$
λ_{s}	Solid phase heat conductivity	$[\mathrm{W\,m^{-1}\,K^{-1}}]$
ν	Kinematic viscosity	$[\mathrm{m^2\,s^{-1}}]$
$\nu_{i,j}$	Stoichiometric coefficient	$[-]$
Ω_{D}	Collision integral	$[-]$
Ω_{g}	Effective diffusion length of gas phase	[m]
Ω_{wsc}	Effective diffusion length of washcoat	[m]
ω_p	RSM: Parameter weight	$[-]$
σ^2_{AB}	Average collision diameter	[m]
τ	Tortuosity	$[-]$
θ_i	Surface coverage of species i	$[-]$
$\varepsilon_{\mathrm{wsc}}$	Porosity of washcoat	$[-]$

Subscripts

Symbol	**Description**	**Range**
g	Gas	$[-]$
s	Solid (washcoat and monolith lumped)	$[-]$
v	Vacant	$[-]$
wsc	Washcoat	$[-]$
i	Species	$[1, I]$
j	Reaction id	$[1, J]$
k	Axial tank	$[1, K]$
l	Radial layer	$[1, L]$
m	Segment	$[1, M]$
o	Experimental observation	$[1, O]$
p	Parameter id	$[1, P]$
bwd	Net backward reaction	$[-]$
fwd	Net forward reaction	$[-]$

Superscripts

Symbol	**Description**	**Unit**
0	Standard state	$[-]$
$< f >$	RSM: Final parameter value	$[-]$
$< i >$	RSM: Initial parameter value	$[-]$

$< s >$	RSM: Scaled parameter value	$[-]$

Species

Symbol	Description
γ-Al_2O_3	"Gamma"-Alumina
$CO(NH_2)_2$	Urea
CO_2	Carbon dioxide
CO	Carbon monoxide
CO	Carbon monoxide
H_2O	Water
N_2	Nitrogen
NH_3	Ammonia
NO_2	Nitrogen dioxide
NO_x	Nitrous Oxides
NO	Nitrogen monoxide
O_2	Oxygen
O_2	Oxygen
O_3	Ozone
SO_2	Sulfur dioxide

Variables

Symbol	Description	Unit
$\check{y_o}(p)$	RSM: Simulated conversion	[%]
$\hat{y}$	Predicted conversion according to RSM	[%]
$\vec{b}$	RSM: Vector of responses	[%]
A_g	Cross-sectional area of gas phase	$[\mathrm{m}^2]$
A_wsc	Cross-sectional area of washcoat	$[\mathrm{m}^2]$
A_j	Frequency factor	$[-]$
A_k	Area between axial tanks	$[\mathrm{m}^2]$
A_l	Area between radial layers	$[\mathrm{m}^2]$
a_s	Washcoat cross-sectional area for segment s	$[\mathrm{m}^2]$
a_{tot}	Total Washcoat cross-sectional area	$[\mathrm{m}^2]$
$c_\mathrm{p,s}$	Solid phase specific heat capacity	$[\mathrm{J\,K^{-1}\,kg^{-1}}]$
$c_{i,\mathrm{surf}}$	Concentration at the gas/washcoat interface	$[\mathrm{mol\,m^{-3}}]$

$c_{i,k,l}$	Concentration	$[\mathrm{m}^3]$
d_o	Hydraulic diameter	$[\mathrm{m}]$
D_AB	Free molecular diffusivity	$[\mathrm{m}^2\,\mathrm{s}^{-1}]$
D_e	Effective diffusivity of washcoat	$[\mathrm{m}^2\,\mathrm{s}^{-1}]$
d_wsc	Washcoat thickness	$[\mathrm{m}]$
d_p	Mean pore diameter	$[\mathrm{m}]$
$D_{\mathrm{AB},i,k,l}$	Free molecular diffusivity	$[\mathrm{m}^2\,\mathrm{s}^{-1}]$
$D_{\mathrm{e},i,k,l}$	Effective diffusivity	$[\mathrm{m}^2\,\mathrm{s}^{-1}]$
D_Kn	Knudsen diffusivity	$[\mathrm{m}^2\,\mathrm{s}^{-1}]$
Ea_j	Activation energy	$[\mathrm{J}\,\mathrm{mol}^{-1}]$
F_tot	Total molar flow rate	$[\mathrm{mol}\,\mathrm{m}^{-3}]$
G	Inhibition term	$[-]$
$g(p)$	RSM: Objective function	$[-]$
$k0_j$	Reference rate coefficient	$[\mathrm{m}^3\,\mathrm{s}^{-1}\,\mathrm{kg}^{-1}]$
k_B	Boltzmann's constant	$[\mathrm{J}\,\mathrm{K}^{-1}]$
K_eq	Equilibrium quotient	$[-]$
K_inh	Inhibition coefficient	$[-]$
k_wsc	Uptake rate coefficient	$[\mathrm{s}^{-1}]$
k_j	Rate coefficient	$[\mathrm{m}^3\,\mathrm{s}^{-1}\,\mathrm{kg}^{-1}]$
$k_{\mathrm{c},i,k,0}$	External mass transfer coefficient	$[\mathrm{m}\,\mathrm{s}^{-1}]$
l	Catalyst length	$[\mathrm{m}]$
$m(t)/m_\infty$	Ratio of mass obsorbed at time t	$[-]$
M_AB	Reduced molecular mass	$[\mathrm{g}\,\mathrm{mol}^{-1}]$
$m_{k,l}$	Mass of catalyst	$[\mathrm{kg}]$
n	Number density	$[\mathrm{mol}\,\mathrm{m}^{-3}]$
n_{multi}	RSM: number of multisteps	$[-]$
$P_\mathrm{g,wsc}$	Perimeter of washcoat/gas interface	$[\mathrm{m}]$
p_p	RSM: Parameter	$[-]$
Q	Reaction quotient	$[-]$
R_wsc	Reaction rate (observed) per volume of washcoat	$[\mathrm{mol}\,\mathrm{m}^{-3}\,\mathrm{s}^{-1}]$
$r_{j,k,n}$	Reaction rate	$[\mathrm{mol}\,\mathrm{s}^{-1}\,\mathrm{kg}^{-1}]$
s_heat	Heat sink due to added mass from catalyst canning and insulation	$[\mathrm{W}\,\mathrm{K}^{-1}]$

t_c	Timescale for Convection	[s]
t_r	Timescale for Reaction (observed)	[s]
t_td	Timescale for Transverse Diffusion	[s]
t_wsc	Timescale for Washcoat diffusion	[s]
T_0	Reference temperature	[K]
T_∞	Effective surrounding temperature	[K]
v	Velocity	$[\mathrm{m\,s^{-1}}]$
$V_{k,l}$	Volume of tank	$[\mathrm{m^3}]$
w_o	RSM: Weight function for observation o	[−]
X	RSM: Design matrix	[−]
y_o	RSM: Experimentally measured conversion	[%]
$y_{i,k,l}$	Gas phase molar fraction	[−]
z^*	Dimensionless axial coordinate	[−]

Contents

1 Introduction

This chapter provides a brief overview of why automotive converters are needed, the basic principle for exhaust aftertreatment along with the objectives of this thesis.

1.1 Environmental and health aspects

The incomplete combustion of liquid or gaseous fuels in the internal combustion engine (ICE) inherently produces small but significant concentration of carbon monoxide (CO), unburnt hydrocarbons (HC) and particulate matter (PM). Furthermore, due to the high temperatures and excess O_2 and N_2, mainly nitrogen monoxide (NO) but also nitrogen dioxide (NO_2) are formed [1]. Lastly, some unique substances may form during combustion depending on fuel impurities - however, their impact can be reduced by having more stringent fuel quality legislation For example, SO_2 emissions from road transportation in the European Union (EU) decreased by 99% between 1990 and 2011 following *Directive 98/70/EC* [2].

These emissions are all harmful to the environment or human health. First off, CO poisoning is likely responsible for more than half of all fatal poisonings world-wide, where roughly 70% of the cases are due to exposure to vehicle exhaust [3]. PM is the emission that has been most clearly linked to premature deaths, where exposure to PM can lead to lung cancer, chronic respiratory or cardiovascular diseases [4]. For example, the World Health Organization (WHO) estimated that the deaths of 3 million people in 2012 were attributable to outdoor air polluted with particulate matter - to which the transportation sector is accountable for roughly 30 and 50% in European cities and OECD countries, respectively [5]. Particulate matter is today (May, 2022) [6] responsible for 4.14 million deaths. Many of the unburnt hydrocarbons are by themselves carcinogenic [7]. Moreover, HC in combination with NO_2 may produce ground-level (tropospheric) ozone (O_3), which is a strong oxidizing irritant [8], killing roughly 370,000 people every year [6]. Lastly, NO_x, where on-road diesel vehicles is responsible for roughly 20% of all global anthropogenic NO_x emissions, cause acidification of ecosystems and inhalation may cause respiratory problems [9, 10].

1.2 Emission legislation

In 1960s' Los Angeles, the average tailpipe emissions were typically 9 g HC/km, 56 g CO/km and 4 g NO_x/km [8] - emitting upwards of 2800 times more than modern car! In combination with these high emissions, temperature inversions would trap the polluted air in the Los Angeles valley and during peak sunlight intensity a strong irritant was present in the city. The concentration of this oxidant correlated well with the sunlight intensity throughout the day - and so it was established that it was troposherpical O_3 that was formed from the polluted air. This problem became a major health concern in some American cities and to reduce this problem the 1970 Clean Air Act was signed

[11]. The same year in Europe, Directive 70/220/EEC, would become the foundation for the amendments that created the so-called *Euro Emission Standards*, which restricted the amount of emitted *gaseous pollutants* - at that time only carbon monoxide and hydrocarbons [12].

The Euro Emission Standards have since been revised to gradually reduce the permitted emission levels for different engine types and vehicle classes. These emission levels, between 1993 and 2027, are presented in figure 1.1. Since the legislation for HC and NO_x changed between Euro 2 and Euro 3 for respective fuel type, the sum for HC and NO_x is shown here. The year on the x-axis corresponds to the year for registration of new vehicles. Note that light duty is judged based on g/km while heavy duty is based on g/kWh. However, the heavy duty emissions levels can be recalculated (using e.g. the US HDD truck fleet fleet average of 1.68 kWh/km [13]), arriving at roughly the same emissions levels per km of travel. The boxes at the end of 2027 for light duty and 2026 for heavy duty corresponds to the, as of writing this thesis, expected Euro 7 limits.

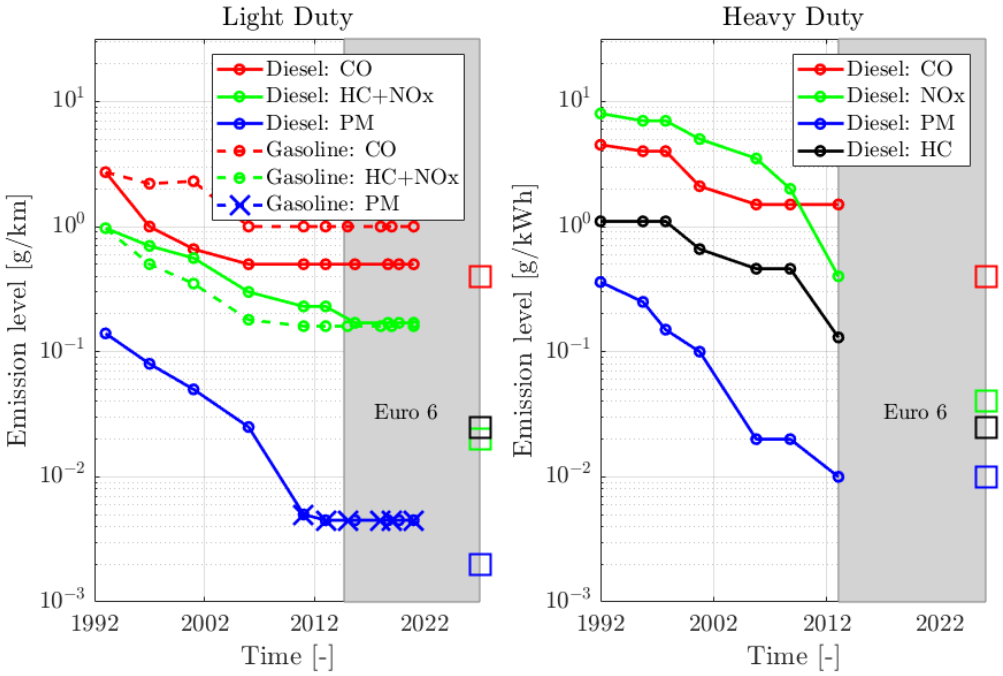

Figure 1.1: *Euro Emission Standard levels between 1992 and 2027.*

While many argue that the Euro 7 legislation might be the last legislation that comes in to place for major vehicle markets, studies still show that even though most European cities' pollutant levels are well below the allowed limits, the effects are still deleterious [14]. There is no safe limit.

1.3 Exhaust aftertreatment systems for diesel engines

Once the automotive industry realized that engine modifications alone could not meet the requirements of the 1970 Clean Air Act, various catalytic systems were investigated. However, aftertreatment for engines is very different from - and much more complex than for example that of a steady-state operated chemical plant process [15]. The exhaust aftertreatment system (EATS) must function at low temperatures, be able to handle thermal shocks and resist high temperatures, flow pulsations and tolerate various common catalysts poisons (e.g. SO_2). The EATS itself is also prone to vibrations [8]. Lastly, the catalyst itself consists of one or multiple different noble metals - which are some of the most expensive substances on earth and its use should therefore be minimized. This thesis is heavily focused on the diesel oxidation catalyst (DOC), therefore only a modern diesel engine EATS using a DOC is presented here.

A typical setup for a diesel engine EATS is shown in figure 1.2 (black substances are reactants that need to be removed, red, crossed out substances are removed for each catalyst). The DOC's main function is to oxidize (the excess O_2 being the oxidant) HC into CO_2 and H_2O, CO into CO_2 and lastly NO into NO_2, which in itself is actually more harmful than NO [1]. However, equimolar ratios of NO and NO_2 will lead to a different and faster reaction mechanism in the Ammonia Selective Catalytic Reduction (NH_3-SCR) catalyst [16]. The DOC also functions to generate an exotherm for active regeneration of the Diesel Particulate Filter (DPF) via e.g. in-cylinder post injection, or using an additional injector upstreams of the DOC, to increase HC concentration [17].

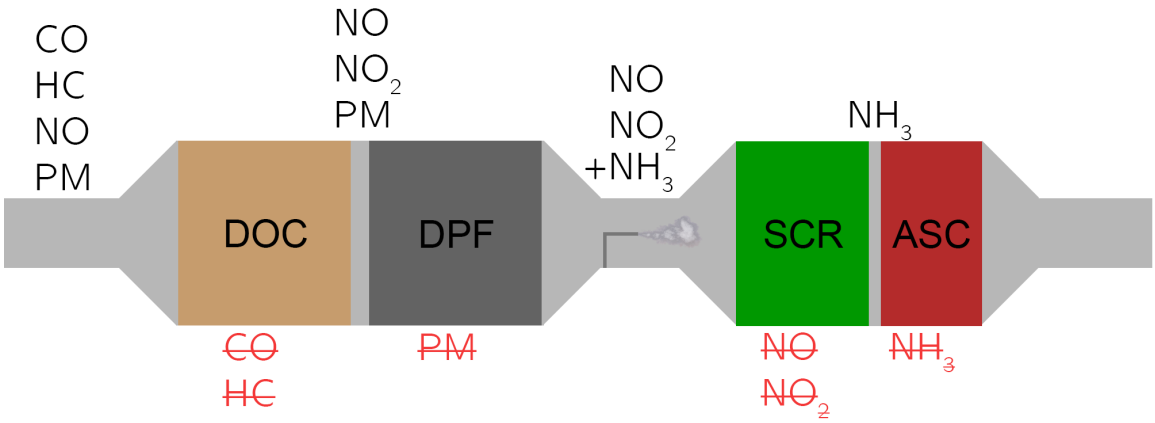

Figure 1.2: *Common components in a modern diesel engine exhaust aftertreatment system.*

The DPF's purpose is to trap and ultimately oxidize PM into CO_2. The Continuously Regenerating Trap (CRT) uses NO_2 created by the DOC and shows significant conversion already at around 300°C while the filter that relies on O_2 as oxidizing agent need temperatures above 550°C - thus active regeneration is sometimes necessary [18]. Modern

variations of the DPF incorporate DOC functionality into the filter walls to reduce thermal mass - i.e. less energy is required to heat the catalyst in order to get it functioning. This also lowers potential HC or CO slip from the DPF during active regeneration [1]. The third component deals with NO_x abatement. Common catalysts include the NH_3-SCR, the Lean NO_x Trap (LNT) and the NO_x Storage and Reduction (NSR) - either one of them or in a combination of two (e.g. NSR-SCR). For NH_3-SCR, Urea ($CO(NH_2)_2$) is injected upstreams the catalyst to later thermally decompose into NH_3 and CO_2 [19]. NH_3 then reduces NO_x into N_2 and H_2O [1]. Finally, to account for potential over-dosage of urea, an ammonia-slip catalyst (ASC) is placed after (or in combination with) the SCR to remove unreacted NH_3 [20].

1.4 Objectives

This thesis focuses on mathematical modelling along with relevant experiments. Experimental procedures include laboratory-scale synthetic catalyst activity tests (SCAT), scanning electron microscopy (SEM) analysis and intelligent gravimetric analysis (IGA). The DOC was chosen since its kinetics are a lot simpler than for example that of the $NH_3 - SCR$, but the findings could easily be extrapolated to different catalyst types, e.g. the three way catalyst (TWC) commonly found in gasoline vehicles [8].

The objective of this thesis is to combine relevant experiments and modelling to distinguish mass transfer from kinetics. By improving the separation of these phenomenon, the models will be more accurate and therefore more predictive when extrapolating the findings to new catalyst formulations. This thesis also intends to highlight the importance of validating various assumptions for modelling of monolith reactors: the assumption of a uniform washcoat and the single channel assumption. The purpose is also to highlight the role of the parameter estimation algorithm, the importance of a good initial parameter guess and accurate experimental observations.

The project caters to the United Nations Sustainable Development Goals (SDG); 3 - "*Good Health and Well-being*", 7 - "*Affordable and Clean Energy*" and 11 - "*Sustainable Cities and Communities*".

2 Background

This chapter will introduce some fundamental concepts of catalysis along with mathematical modelling of monolith reactors in general, thus distinguishing from next chapter which is solely focused on the reactor model used in this thesis along with analysis and description of the performed experiments.

2.1 History of Catalysis

In Jöns Jacob Berzelius' yearly review of the entire physics and chemistry society from 1835, he stated [21] (translated from Swedish):

> "It is, then, proved that several simple or compound bodies, soluble and insoluble, have the property of exercising on other bodies an action very different from chemical affinity. By means of this action they produce, in these bodies, decompositions of their elements and different recombinations of these same elements to which they remain indifferent".

This is indeed the very first definition of a catalyst - something (bodies) that will enable a reaction to take place (produce decompositions of their elements and different recombinations) while not being consumed itself (remain indifferent). Berzelius called this action "catalysis", from Greek "$\kappa\alpha\tau\alpha\lambda\acute{\upsilon}\omega$" meaning to loosen or to destroy. At the time it was far from understood what part of the chemical reaction that catalysts contribute to or alter. Some suggested that the metallic catalysts was only a mere heat source [22]. However, one early paper from Humphry Davy [23] suggested that a chemical reaction between two gaseous reactants (coal gas and oxygen) would only occur on specific metallic surfaces (e.g platinum), thus proving that the surface itself had additional important properties aside from its temperature.

Two hundred years later and roughly 90% of the products in the chemical industry are produced by means of some catalytic process. Still, the use of practical catalysis outgrows its fundamental understanding - however, many practical concepts helps us understand its basics [24].

2.2 Basics of Catalysis

By now, catalysts are defined by their ability to accelerate a chemical reaction through providing an energetically far superior reaction path compared to its non-catalytic counterpart [24]. Figure 2.1 shows the catalytic oxidation of CO by O_2; as a potential energy diagram and as a typical reaction mechanism. The uncatalyzed (red curve) requires high amounts of energy to produce a gas phase reaction whereas the catalyzed version (green curves) is a lot more favourable. However, the overall change in free energy is identical regardless if a catalyst is being used - the catalyst only changes the kinetics while thermodynamics and equilibrium are unaffected. The reaction mechanism includes

adsorption of CO and adsorption and dissociation of O_2 in the first step. The adsorbed CO and O then forms adsorbed CO_2 which either desorbs or decomposes back.

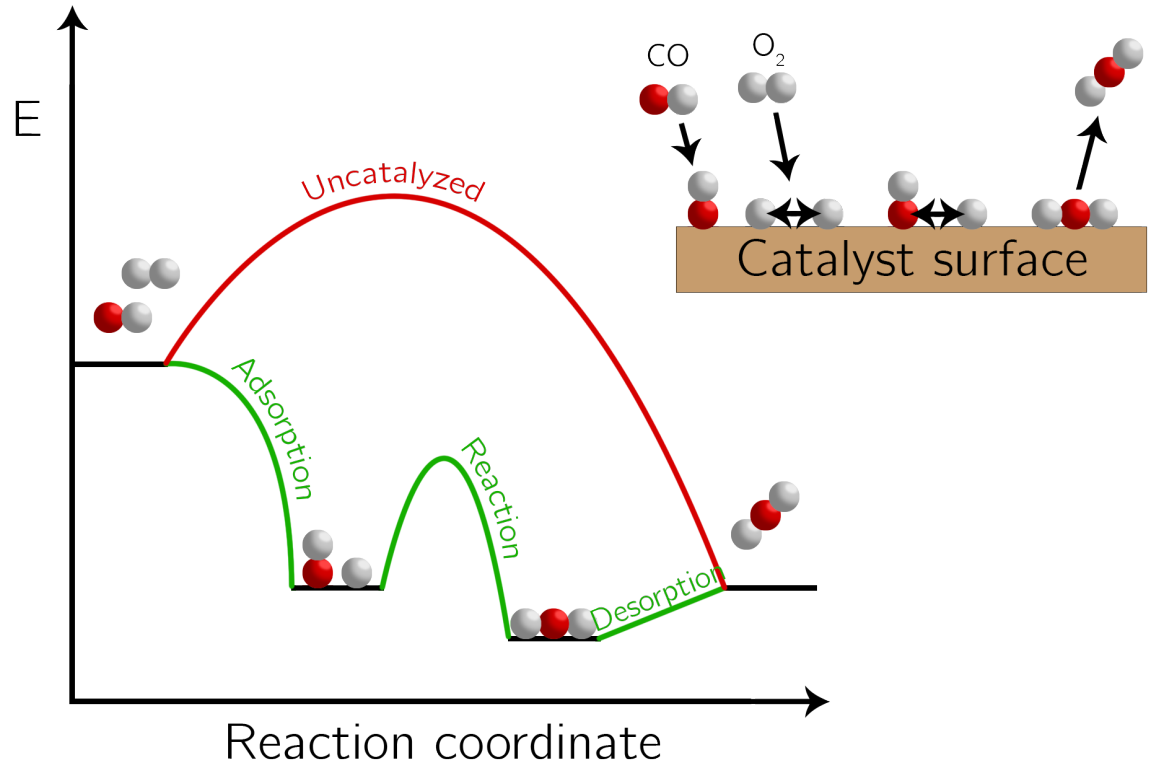

Figure 2.1: *Left: Potential energy diagram of a typical heterogeneous catalytic reaction. Right: Reaction mechanism of CO oxidation by O_2.*

As a consequence of the energetically favourable reaction path, industrial processes can operate at greatly reduced temperature and pressure. Furthermore, the catalyst design can be catered to increase selectivity (the ratio of desired to undesired products) towards a certain product - thus maximizing yield and potentially reducing the need for costly separations in industrial processes [24].

2.2.1 Heterogeneous catalysis

Catalysts comprise anything from atoms and molecules to complex enzymes and surfaces. However, this thesis only deals with heterogeneous catalysis - where the catalyst is a noble metal which catalyzes molecules in the gas phase. Different noble metals are suitable for different oxidation reactions, where according to the Sabatier principle, optimal catalytic performance is achieved where the interaction between the reacting species and the noble metal itself is "just right" [24]. If the bonds between the catalyst and the reactants are too weak, none of the reactants will stay long enough on the surface to dissociate or further react. On the other hand, if either of the required reactants, any potential intermediates or the final products bond to strongly to the surface, the catalyst will end up getting

poisoned and the reaction will die out. The interaction depends on the electron orbitals of the reactants and the metal, hence different transition metals are suitable for different reactions. Of course, catalyst price and susceptibility towards other poisons that might be prevalent in the inlet feed have to be considered as well [24].

As Humphry Davy established early on, in heterogeneous catalysis noble metal surface area is key. Since the surface area to volume ratio goes up as the particle diameter approaches zero, the smallest possible particles are desired (until a point where a too small particle will lose its catalytic properties). Additionally, to further improve the accessibility of the catalyst, the particles are typically dispersed in a highly porous material - commonly referred to as a washcoat, where γ-Al_2O_3 is the most common washcoat material used in automotive converters [24]. The washcoat typically has an extremely high specific surface area of around $150 - 175\, m^2/g$ because of its complex pore structure [24]. As a consequence of its high porosity the washcoat is very fragile and is therefore further applied onto a supporting body. In steady-state operated chemical plants this could be a packed-bed reactor while for automotive converters this is most likely a monolith.

2.3 Monolith reactors

Monolith reactors, also known as honeycomb monoliths, comprise a large number of axially parallel channels of an arbitrary shape (yet square channels are most common) [25]. They are used in a wide range of processes due to their compact nature and as a consequence of the highly structured design and small hydraulic diameter the flow is laminar. This leads to a low pressure drop which, in the automotive industry, is important for reducing fuel consumption and maintaining high power output. The monolith reactor has excellent heat transfer properties since it is usually ceramic, as can be seen in figure 2.2, or metallic [25] and typically has 400 cells per square inch (CPSI).

Figure 2.2: *Photograph of a 400 CPSI ceramic monolith placed inside a metal canning.*

One problem with monolith reactors is that once the reactants enter the structured channels it is not possible to change any potential concentration maldistributions across channels that e.g. arise from liquid injection of urea upstream the NH_3-SCR [26]. This can lead to lowered NO_x conversion and increased NH_3 slip. An emerging technology to solve such a problem is the periodic open cellular substrates (POCS) [27] which, at the cost of increased pressure drop, has improved radial heat and mass transfer. However, as of now, the monolith reactor is the state-of-the-art technology for supporting catalysts in the automotive industry [25]. Its operation occurs in a wide range of flow rates, temperature and concentrations. To characterize the operation for understanding of limiting factors, one may resort to using classical timescales [28]. To facilitate understanding, figure 2.3 shows the various important dimensions and geometries used in timescale calculations and later on transport equations.

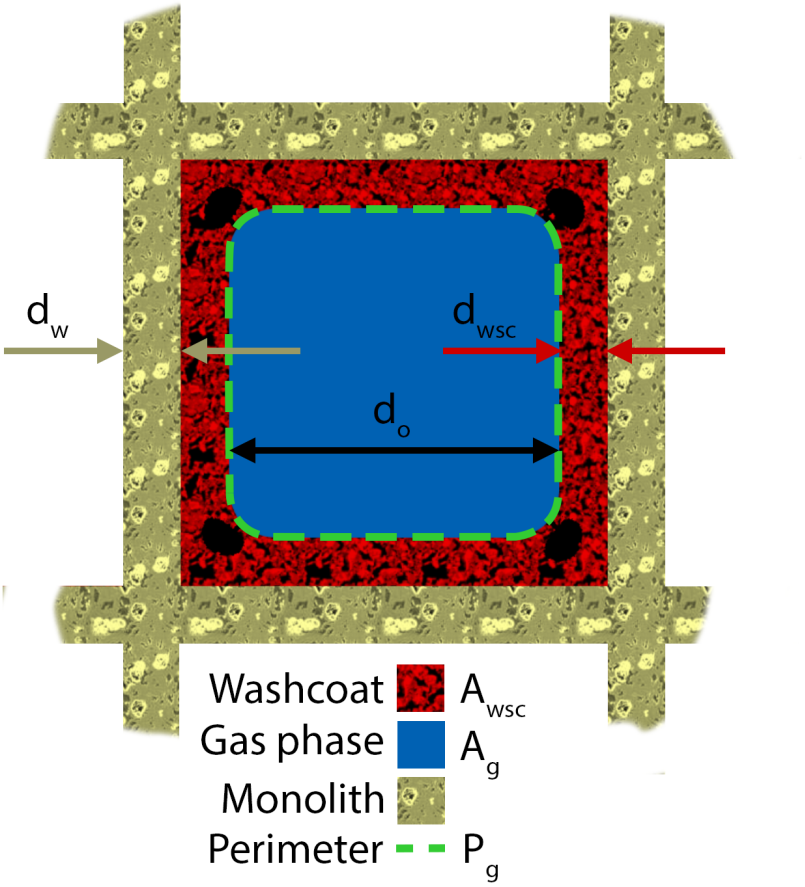

Figure 2.3: *Illustration of monolith channel cross-section along with various dimensions.*

Firstly, the timescale for convection (residence time) (t_c [s]) is:

$$t_c = \frac{l}{v} \tag{2.1}$$

where l [m] is the channel length and v [m s^{-1}] is the average channel velocity. The timescale for transverse (external) diffusion (t_{td} [s]) is:

$$t_{\mathrm{td}} = \frac{\Omega_{\mathrm{g}}^2}{D_{\mathrm{AB}}} = \frac{(A_{\mathrm{g}}/P_{\mathrm{g}})^2}{D_{\mathrm{AB}}} \tag{2.2}$$

where Ω_{g} [m] is the effective diffusion length scale for the gas phase, D_{AB} [$\mathrm{m}^2\,\mathrm{s}^{-1}$] is the free molecular diffusivity, A_{g} [m] is the cross-sectional area for the gas phase and P_{g} [m] is the perimeter of the gas phase. The timescale for washcoat (internal) diffusion (t_{wsc} [s]) is:

$$t_{\mathrm{wsc}} = \frac{\Omega_{\mathrm{wsc}}^2}{D_{\mathrm{e}}} = \frac{(A_{\mathrm{wsc}}/P_{\mathrm{g}})^2}{D_{\mathrm{e}}} \tag{2.3}$$

where Ω_{wsc} [m] is the effective diffusion length scale for the washcoat (solid phase), D_{e} [$\mathrm{m}^2\,\mathrm{s}^{-1}$] is the effective diffusivity of the washcoat and A_{wsc} [m] is the cross-sectional area of the washcoat. Finally, the observed timescale for reaction (t_r [s]) is:

$$t_{\mathrm{r}} = \frac{c_{i,\mathrm{surf}}\varepsilon_{\mathrm{wsc}}}{R_{\mathrm{wsc}}} \tag{2.4}$$

where $c_{i,\mathrm{surf}}$ [$\mathrm{mol\,m}^{-3}$] is the concentration of species i at the gas/solid interface, $\varepsilon_{\mathrm{wsc}}$ [$-$] is the porosity of the washcoat and R_{wsc} [$\mathrm{mol\,s}^{-1}\,\mathrm{m}^{-3}$] is the reaction rate per volume of washcoat. By relative comparison of these timescales, one can conclude whether the conversion is limited by slow kinetics or by internal or external mass transfer. The ratios between the timescales for internal diffusion and reaction form the classical Weisz modulus (Ψ) analogous to the Thiele modulus (Φ) or the second Damköhler number (Da_{II}):

$$\Psi^2 = \frac{t_{\mathrm{wsc}}}{t_{\mathrm{r}}} = \Phi^2\eta = Da_{\mathrm{II}} \tag{2.5}$$

where $\eta[-]$ is the effectiveness factor. Larger values for the Weisz modulus indicates increasing internal mass transfer limitations and vice versa. What sets the Weisz and Thiele modulus apart is that the Weisz modulus is based on the observed reaction timescale - making it useful since the intrinsic kinetics timescale is hard to measure. The effectiveness factor for a flat washcoat is given by:

$$\eta = \frac{\tanh(\Phi)}{\Phi} \tag{2.6}$$

and can be seen as how far into the the coating the reactants diffuse before reacting e.g. in the case of a very low effectiveness factor, only the outermost part of the the catalyst coating is being utilized for reaction and vice versa.

Since both external and internal mass transport phenomenon can limit the conversion in a monolith reactor, it is important to simultaneously compare all of these timescales. The timescales for internal and external mass transfer also forms the mass Biot number (Bi_{m} [$-$]):

$$Bi_{\mathrm{m}} = \frac{t_{\mathrm{wsc}}}{t_{\mathrm{td}}} = \frac{A_{\mathrm{wsc}}D_{\mathrm{AB}}}{A_{\mathrm{g}}D_{\mathrm{e}}} \tag{2.7}$$

Increasing values for the mass Biot number means that internal mass transfer dominates the mass transfer - i.e. the reactants reach the washcoat easily but cannot penetrate the washcoat as easily. Combining equation 2.7 with the model for effective diffusivity as shown in the coming sections, the mass Biot number boils down to geometric and material properties along with the ratio of the free molecular diffusivity (D_{AB}) to the Knudsen diffusivity (D_{Kn}):

$$Bi_{\mathrm{m}} = \frac{A_{\mathrm{wsc}}\tau}{A_{\mathrm{g}}\varepsilon_{\mathrm{wsc}}}\left(1 + \frac{D_{\mathrm{AB}}}{D_{\mathrm{Kn}}}\right) \tag{2.8}$$

where τ [$-$] is the tortuosity of the washcoat pores.

2.4 Mathematical modelling of monolith reactors

In gaining better fundamental understanding of catalyst performance, modelling can be a valuable tool. There have been huge efforts towards development of mathematical models of monolithic catalytic reactors [25, 29, 30], with a lot of attention on the DOC with varying degrees of complexity [1, 25, 31, 32]. Due to the vast range of scales (0.1 m to 1 nm) of processes occurring in a monolith reactor, several common simplifications are made to reduce computational cost. The extent of the simplifications depend on the purpose of the application - e.g. is it to model micro-flow in a single washcoat pore or to look at temperature profiles across the entire reactor? The assumptions affect dimensionality of the problem as well as the governing equations - regardless, some simplifying assumption regarding the fluid properties is typically made beforehand. Firstly, the fluid is typically handled as incompressible - overlooking fluid density changes along the channel length. Some models also neglects changes in total molar flow rates - which should be fine for low reactant concentrations [29]. However, the most commonly used assumption, that comes with a plethora of implications and experimental requirements, is the single-channel assumption. It should be mentioned that there exist highly detailed **washcoat models** for flow inside porous networks [33]. Even though their results are interesting for development of e.g. pore diffusion models, their detailed descriptions are simply not viable on a monolith modelling level [29], and so they are outside the scope of this thesis.

2.4.1 The single channel assumption

The **single-channel models** assume that the reaction-diffusion process that occurs within the large number of channels in a monolith reactor can be represented by a single channel [25]. This implies that each channel inlet has identical temperature, volumetric flow rate as well as same gas composition - regardless of its radial position. This also assumes that the manufactured reactor has no substantial changes in monolith or washcoat properties in the radial direction (i.e. from channel to channel). These implications should be controlled and verified on a lab scale catalyst. However, there still exists a distribution of volumetric flow rates in the channels, resulting from the upstream parabolic velocity profile of the typically laminar flow. Nevertheless, this is simply how these models are developed [29]. The single-channel assumption, along with the design of an experimental rig, is investigated in publication I.

For full-scale applications, where these gradients are significant, **multi-channel models** account for flow maldistributions, radial heat losses etc. They commonly use results from single-channel models to performing weighting between a number of representative channels [25]. However, also these models are outside the scope of this project. The three different modelling levels, multi-channel (a), single-channel (b) and washcoat models (c), can be seen in figure 2.4.

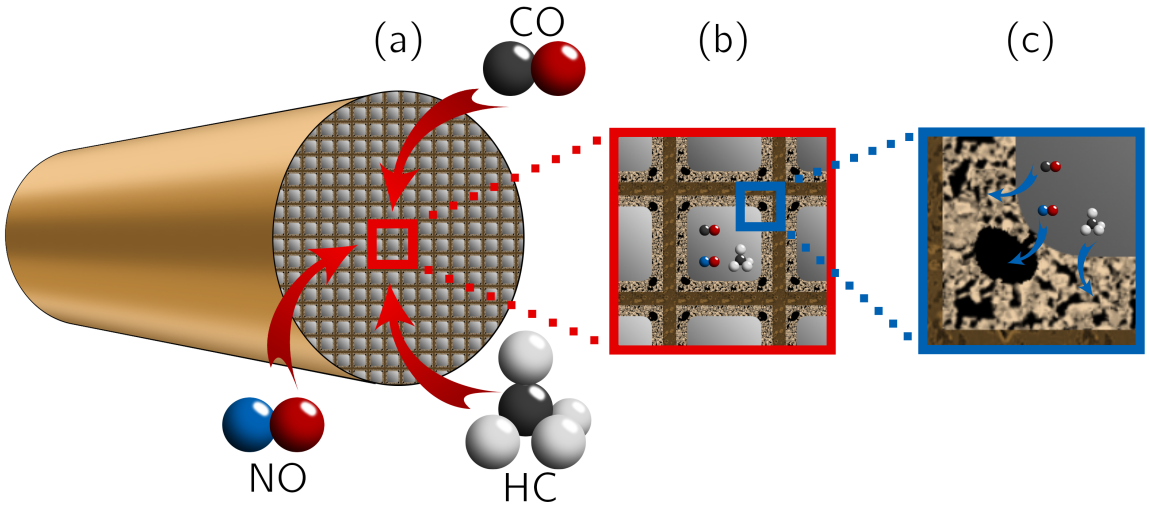

Figure 2.4: *Three common modelling levels of monolith reactors.*

2.5 Kinetics

This section covers some general aspects around kinetics found in heterogeneous catalysis. There are different kinetic expressions with varying complexity and different physical meaning. Generally, the most popular kinetic models used in heterogeneous catalysis are global and microkinetic models. However, there are also hybrid kinetic models, e.g. Stewart et al [34], who developed a detailed scheme for carbon monoxide oxidation in the presence of nitrogen monoxide - while modelling all other reactions occurring in the exhaust gas using a global scheme. Regardless of model type, the rate coefficients (k), are calculated using an Arrhenius type expression:

$$k = A_j e^{-\frac{Ea_j}{RT}} \tag{2.9}$$

where A_j $[-]$ is the pre-exponential factor (also known as frequency factor) accounting for the number of molecule collisions and Ea $[\mathrm{J\ mol^{-1}}]$ is the corresponding activation energy.

2.5.1 Global kinetics

Global models [35–38] describe the entire reaction with a single rate expression. The global kinetics describe the rate-determining step (usually the surface reaction step) and assume that the other steps are in equilibrium (e.g. adsorption and desorption). This

reduces the necessary state variables for the rate expression, reducing computational demand and the stiffness of the computation. The global models predict reaction rates based on the gas phase concentrations and the rate expression includes a denominator term, called an inhibition term, to account for species adsorption and poisoning of the catalyst surface or the reversible nature of a reaction. A typical reaction is [39]:

$$\mathrm{CO\,(g)} + \tfrac{1}{2}\,\mathrm{O_2(g)} \longrightarrow \mathrm{CO_2(g)}$$

It's corresponding rate expression would be:

$$r = mky_{\mathrm{CO}}y_{\mathrm{O_2}}/G \tag{2.10}$$

where $m\,[\mathrm{mol\,m^{-3}}]$ is the active site density, $y_{\mathrm{CO}}\,[-]$ and $y_{\mathrm{CO}}\,[-]$ are the gas phase species molar fractions and $k\,[\mathrm{m^3\,s^{-1}}]$. The inhibition term, G is based on the classical works by Voltz et al [35] and Oh and Cavendish [40], which is a function of the temperature and current gas phase concentrations [40]:

$$G = f(K_{\mathrm{inh}}, y_i, T) \tag{2.11}$$

where K_{inh} is the inhibition coefficient, also following an Arrhenius type expression for its temperature dependence. Global kinetics generally lack predictive ability and require extensive tuning as it contains non-physical or non-measurable constants. However, because of the less number of state variables (no surface coverages) it is far cheaper to compute - or can handle more reactions at the same computational cost.

2.5.2 Microkinetics

The microkinetic models [41–44] include all elementary steps in a certain reaction; adsorption, dissociation, surface diffusion, surface reaction and desorption (see figure 2.1) - therefore the stoichoimetric coefficients for each step i equal to unity. The steps corresponds to parts of a reaction that can be estimated through theory (e.g. collision to obtain the frequency factor) or experiments (e.g. temperature-programmed desorption (TPR)) [45]. There are different mechanisms for different reactions. Firstly, in an Eley-Rideal mechanism only one of the reactants (in this case oxygen) will adsorb onto the catalyst surface and dissociate ($*$ denotes a catalyst site):

$$\mathrm{O_2(g)} + 2* \longrightarrow 2\,\mathrm{O^*}$$

The other reactant will in gas phase react with the dissociated oxygen to form the adsorbed product:

$$\mathrm{O^*} + \mathrm{NO\,(g)} \longrightarrow \mathrm{NO_2(g)}$$

Its corresponding rate expression would be:

$$r = k\theta_{\mathrm{O}}c_{\mathrm{NO}} \tag{2.12}$$

where $\theta_{\mathrm{O}}\,[-]$ is the surface coverage of dissociated oxygen and $c_{\mathrm{NO}}\,[\mathrm{mol\,m^{-3}}]$ is the gas phase concentration for NO. In the Langmuir-Hinshelwood mechanism, both reactants adsorb onto neighbouring sites and then further react and desorb in the same step:

$$O^* + CO^* \longrightarrow NO_2(g)$$

Lastly, for some reactions it has been shown that the activation energy linearly decreases with some species surface coverage [45]:

$$Ea_j(\theta) = Ea_{0,j}(1 - \alpha_j \theta_i) \tag{2.13}$$

where $Ea_j(\theta)$ [J mol^{-1}] is the coverage dependent activation for oxygen desorption, $Ea_{0,j}$ [J mol^{-1}] is the activation energy for a clean surface and α_j [$-$] the coverage dependency. In this work all coverage dependencies (α_j) are set to zero.

2.6 Transport phenomenon

In order to predict the reaction rates along the channel, the mass transfer from the bulk gas to the solid surface (external) and throughout the washcoat (internal) must be taken into consideration. The same applies for heat transfer.

2.6.1 Tanks-in-series principle

The monolith channel can be treated as a plug flow reactor (PFR) which is modelled using the tanks-in-series model [46]. This non-ideal reactor model uses n continuously stirred tank reactors (CSTR) connected in series. As n assumes a larger number, the CSTRs behave increasingly like a PFR reactor as can be seen in figure 2.5.

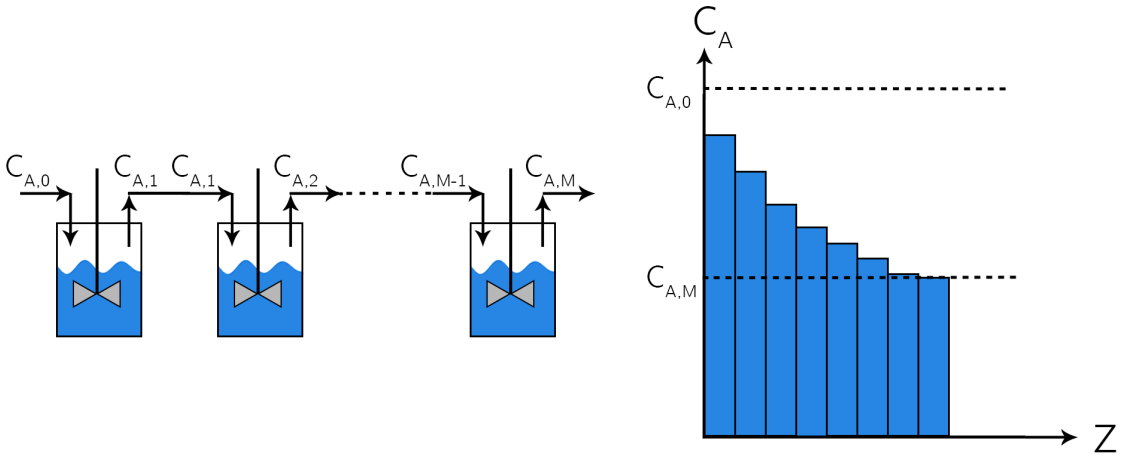

Figure 2.5: *Left: Tanks-in-series principle. Right: A typical graph for concentration vs axial reactor coordinate.*

2.6.2 External mass transfer

The flow inside the monolith channel is laminar and for the greater part of the reactor treated as fully developed (with the exception of potential turbulence decaying at the

very entrance of each channel [47]). The external mass transfer from the bulk gas to the solid surface is governed by molecular diffusion due to the concentration gradient that arises from the reaction within the washcoat. As such, the flux from the bulk gas to the solid interface is usually treated using film theory where the mass transfer coefficient is expressed in terms of the dimensionless Sherwood number [29]:

$$Sh = \frac{k_c \, d_o}{D_{AB}} \tag{2.14}$$

where Sh [−] is the Sherwood number (typically between 2 and 7 depending on channel geometry [48, 49]), k_c [m s^{-1}] is the external mass transfer coefficient, d_o [m] is the hydraulic diameter (typically the open channel diameter) and D_{AB} [m^2 s^{-1}] is the free molecular diffusivity. To account for the increased external mass transfer in the entrance region where the laminar velocity profile develops, there are correlations based on the dimensionless axial distance [48].

2.6.3 Internal mass transfer

There are a number of ways to treat the internal mass transfer through the washcoat. Some authors simply neglect internal mass transfer due to sufficiently thin washcoats or by operating at sufficiently low temperatures where the reaction is kinetically controlled [50, 51]. When it comes to operation of the automotive converters, internal diffusion limitations are apparent in normal operating conditions even with very thin washcoats [52, 53] – hence it is very common to include a separate model for the internal mass transfer [31, 54–62]. The option would be to lump the mass transfer effects into the kinetic expression [48], however it is not likely that such a model will accurately predict performance for an equally wide range of operating conditions as the models that separately model mass transfer.

2.6.3.1 Pore diffusion models

To model internal mass transfer on a low-dimensional level, an estimate of the effective diffusivity is needed [25]. It is typically modelled with one of the many available pore diffusion models; Wheeler's pore model [63], the model of Evans et al [64] and the model of Wakao and Smith [65] to name a few. Each author has their own idea of how the pore network is arranged - e.g. as a tree where the smaller pores are branched from larger ones or arranged in series, whether the coating has a pore size distribution that is unimodal (one distinct average pore size) or bimodal (two distinct pore sizes) [66]. To the best of my knowledge, all pore models describe the diffusion in macro- and micro-pores, as a combination of free molecular diffusivity and Knudsen diffusivity, to form the pore diffusivity [67]. The difference between the models being the description of where the transition between these two mechanisms occur. Since the mechanisms have different temperature dependencies ($T^{3/2}$ for free molecular diffusion and $T^{1/2}$ for Knudsen diffusion), the overall temperature dependency of each pore model would be different depending on various material characteristics (unimodal, bimodal, mean pore diameter).

Since this information was not available in the project (the assumed mean pore diameter was obtained from a previous project), and since the pore model was tuned to a single temperature point using intelligent gravimetric analysis (IGA), there is little to no reason for choosing any pore model over the others and so the chosen model in this work is the model by Wheeler [63]. To avoid repetition of all equations, the pore diffusion model is further presented in chapter 3.

The Knudsen diffusivity (D_{Kn}) is the diffusion mechanism when the mean free path of the molecule ($\lambda \approx 140\,\mathrm{nm}$ for O_2 at 1 atm and 300°C) is larger than the average micro pore diameter ($d_{\mu} \approx 5 - 10\,\mathrm{nm}$). When the opposite is true the diffusion mechanism is free molecular diffusivity (D_{AB}), which can be measured experimentally or calculated through the Chapman-Enskog method [68]. Together they form the pore diffusivity (D_{p}) according to the Bosanquet interpolation:

$$D_p = \left(\frac{1}{D_{AB}} + \frac{1}{D_{Kn}} \right)^{-1} \tag{2.15}$$

To further describe the complex nature of the pore network, two common constants are used - tortuosity ($\tau \approx 1 - 10$) and porosity ($\varepsilon_{wsc} \approx 0.8$). Figure 2.6 illustrates physical interpretations of these pore model constants.

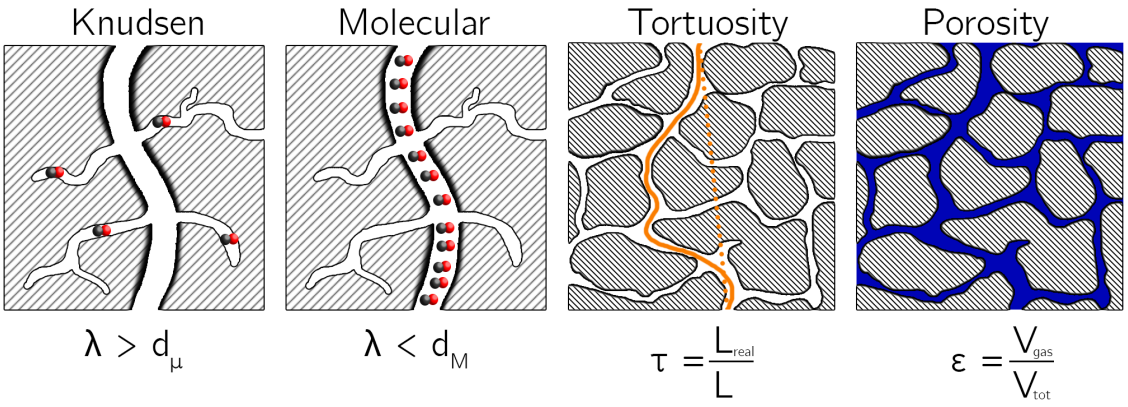

Figure 2.6: *Physical interpretations of pore model constants.*

The tortuosity is generally found to be inversely proportional to the washcoat porosity [69]. The porosity scales the pore diffusivity with the void fraction of the material while the tortuosity takes the curvature of the pores into account. This forms Wheeler's pore model for effective diffusivity (D_{e}):

$$D_{\boldsymbol{e}} = \frac{\varepsilon_{wsc}}{\tau} D_{\mathrm{p}} \tag{2.16}$$

2.6.3.2 Measurements of Effective Diffusivity

There are several methods for measuring effective diffusivity for washcoats applied onto monolith substrates [67, 70, 71]. Hayes et al [67] constructed a modified Wicke-Kallenbach cell to measure the diffusivity between channels for a washcoated monolith reactor. By also measuring the diffusive resistance of the uncoated monolith - the diffusivity of the coating alone could be distinguished. One problem with this method is that it assumes that the interface between the monolith and the washcoat doesn't result in any additional dead-end pores (compared to monolith or washcoat separately) that hinder diffusivity. Since this is highly likely, the experimentally measured diffusivities are likely underestimated. There are also classical chromatographic methods which rely on long columns ($>> 1\,m$) containing crushed monoliths with applied washcoat [70]. The chromatographic methods rely on small differences in residence time, across these columns, as a result from the effective diffusivity of some tracer substance. Lastly, there are gravimetric methods [71]. These are tedious experiments and only result in single data points per several of hours of experiments - however, they are accurate since they directly measure the uptake of some reactant with time.

2.6.4 Discretization schemes of single-channel models

The two most common ways to include internal mass transfer limitations in automotive converters are 1D models with the use of an effectiveness factor [54–58] as well as the 1+1D models [31, 59–62]. On a general level, these methods are distinguished by the fact that the 1+1D model also resolve the washcoat in the radial direction. Thus each tank, in the tanks-in-series model, includes a set of sub-tanks which correspond to washcoat layers [59].

2.6.4.1 1D models with effectiveness factor

The 1D reactor model, using an effectiveness factor, is far less complex than the 1+1D models. As a consequence it is less stiff and faster to compute [29]. The effectiveness factor is a simple but powerful tool that can account for different washcoat formulations, washcoat geometries, states of aging etc - but needs to be tuned or calculated for every state of the material and inlet conditions. Because it is so inexpensive, it is commonly used for commercial operation or control purposes [72]. Apart from simple tuning the constant to fit kinetic data there exist analytical solutions [73] as well as numerical solutions [55, 72, 74] to the problem.

2.6.4.2 1+1D models

For improved accuracy and understanding - which is key for reactor design and optimization, the 1+1D model is a better choice [54]. The name implies that the gas phase is resolved axially while the washcoat is resolved in radial direction as well ("+1D") as seen in figure 2.7. The tanks-in-series principle now approaches the finite volumes method. However, because of some geometric reasons and material properties further elaborated on in chapter 3 the model is not two dimensional by definition, since the axial mass transfer

within the washcoat is usually neglected. All of these models rely on the washcoat being axisymmetric, thus the tangential dimension is removed. However, this assumption has been reported to be quite erroneous and its penalties could unfortunately result in inaccurate light-off temperature predictions [75]. This assumption is elaborated on in publication III, where an alternative to the classical 1+1D model is presented - through which the axis-symmetric requirement can be circumvented.

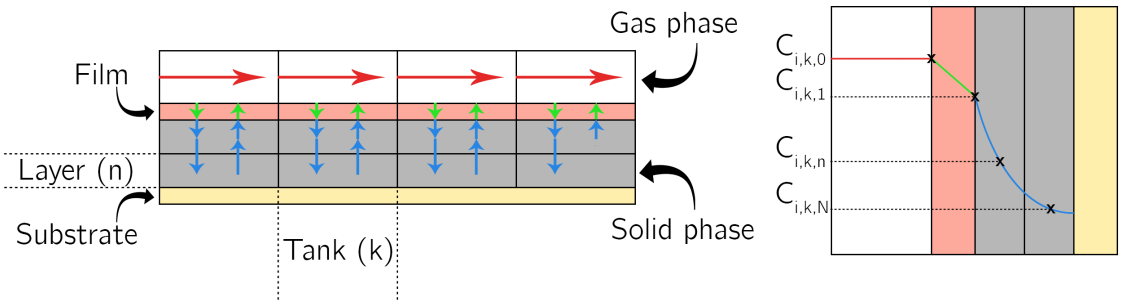

Figure 2.7: *Left: Tanks-in-series principle applied for a 1+1D discretization scheme. Right: Concentration profile.*

Lastly, there exist some attempts at performing full 3D CFD simulations of a single-channel [75]. As mentioned, they demonstrate some valuable insights for the validity of the underlying assumptions for the 1+1D models. However, these models are significantly more computationally demanding than the more common 1D and 1+1D models.

2.6.5 Heat transfer

Heat transfer in the monolith is to some extent analogous to the external mass transfer, i.e. a Nusselt correlation is used to describe the heat transfer from the gas phase to the solid [48]:

$$Nu_\infty = \frac{h\, d_\mathrm{o}}{\lambda_\mathrm{g}} \tag{2.17}$$

where Nu_∞ [−] is the asymptotic Nusselt number (typically between 3.0 and 4.5 [76]), h [W m^{-2} K^{-1}] is the heat transfer coefficient, d_o [m] is the hydraulic diameter (typically the open channel diameter) and λ_g [W m^{-1} K^{-1}] is the gas phase conductivity. Other important heat transport mechanisms include conduction within the washcoat and monolith substrates (especially important for metallic substrates) and reaction heat since the majority of the catalytic reactions in the EATS are exothermic. In the lab-scale kinetic experiments presented in chapter 3, the conditions are isothermal due to the low reactant concentration and high volumetric flow rates.

2.7 Parameter estimation in heterogeneous catalysis

In modelling of heterogeneous catalysis, there is a huge set of parameters that affect the overall conversion of the modelled reactor - kinetic parameters, heat and mass transfer properties and material properties to name a few. Material properties and mass transfer properties can be measured experimentally using e.g. gravimetric analysis (further explained in chapter 3). Furthermore, the kinetic parameters in a microkinetic model can be estimated a priori through various methodologies. For example, Florén et al [77] developed a kinetic model for methane oxidation on Palladium oxide, including over 200 kinetic parameters estimated from density-functional theory (DFT).

While most of these constants can in some way be determined, there are always experimental errors, there are assumptions in the derivation of a kinetic model (for example what is the most pronounced surface type), experiments are tedious and equipment is expensive. The alternative, and the complement, is to employ parameter estimation to tune the parameters so that difference between the reactive experiments and the simulations (known as the objective or cost function) is minimzed. Since the parameter values are relatively known by now through literature or using these above mentioned methods, the most common way of tuning the parameters is through using the method of gradients [78] (also known as steepest descent/ascent, gradient descent/ascent). The method, whose application is further described in chapter 3, utilizes the an approximation of the gradient of the objective function in an iterative manner to minimize it. The gradient could be an analytical expression, however, due to the complex solution of the set of partial differential equations that reactor models generally constitutes, a numerical approximation is necessary. It is this numerical approximation that, for a large set of parameters, can become very costly.

In the model presented in chapter 3, there is a total of 30 tunable parameters that affect the simulations. Tuning of such a large number of comes with a lot of challenges. One way to reduce this problem is to employ Partial Least Squares (PLS) [79], which helps to narrow down the number of parameters by selecting the parameters that affect the residual the most. Furthermore, it is a bad idea to tune both adsorption and desorption parameters for a certain reactant, since it will lead to high parameter correlation - i.e. it is very hard to differentiate what step increases or decreases the surface coverage for that reactant. In this thesis, a small, fixed set of parameters were chosen for tuning - generally the desorption parameters along with the forward reaction step as well as some mass transfer properties. Rather than focusing on which parameters should be tuned, the focus is instead to investigate various aspects regarding the tuning algorithm itself, such as the iterative stepping procedure.

The biggest drawback to the method of gradients is that its found minima is dependent on the starting point (initial guess), i.e. it cannot guarantee that the found minima is the global minima. An alternative to the gradient-based methods is to use global search methods. Pandya et al [80] used Matlab's *generalized pattern search* to achieve a good fit for

a complete DOC reactor model. However, even with a global search method, the algorithm could not guarantee a global minima because of the lack of experimental observations - i.e. multiple parameter sets would achieve the same low residual. There are also hybrid models, e.g. Park and Froment [81] developed a hybrid algorithm which employed a genetic algorithm to find a good starting point and then accurately located the global minima using the Levenberg-Marquardt optimization procedure. While global methods handle non-smooth objective functions containing noise (from the ordinary differential equation (ODE) solver for example), they become exponentially more expensive with increased number of parameters. Hence, the use of any global search method is outside the scope of this thesis.

3 Modelling and Experiments

This chapter describes the original 1+1D model, the suggested parallel model, the parameter estimation algorithm along with the performed experiments and their analysis.

3.1 Original 1+1D model

The 1+1D reactor model is based on the ones developed by Lundberg et al [59, 60] and in turn the one by Ericsson et al [82]. This model is a good trade-off between computational speed and accuracy [54].

3.1.1 Mass balance

The model contains a quasi-steady state formulation of mass and heat balances (assuming that the variations in inlet conditions are slow in comparison with the timescales for the modelled chemical processes). From hereafter, the discretized nodes in the reactor model are distinguished between axial nodes, referred to as *tanks* (index $k[1, K]$), and radial nodes, referred to as *layers* (index $l[0, L]$). Substances are indexed by i and reactions by j. The mass balance for the gas phase ($l = 0$) is given by:

$$0 = \left(V_{k,0} \frac{dc_{i,k,0}}{dt} \right) = \underbrace{F_{\text{tot}} \left(y_{i,[k-1],0} - y_{i,k,0} \right)}_{\text{Advection}} - \underbrace{\Gamma_{i,k,0} \left(c_{i,k,0} - c_{i,k,1} \right)}_{\text{Convection}} \tag{3.1}$$

where $V_{k,l}$ [m^3] is the volume of each tank and layer, $c_{i,k,l}$ [mol m^{-3}] is the gas phase concentration, F_{tot} [mol s^{-1}] is the total molar flow rate in the (assumed to be constant through-out the reactor due to low reactant concentration), $y_{i,k,l}$ [$-$] are the gas phase molar fractions and $\Gamma_{i,k,l}$ [$\text{m}^3\,\text{s}^{-1}$] is the lumped mass transfer coefficient. The axial diffusion in gas phase is assumed to be negligible compared to the advective term. For all layers ($l > 0$) the washcoat mass balance is given by:

$$\begin{aligned} 0 = \left(V_{k,l} \varepsilon_{\text{wsc}} \frac{dc_{i,k,l}}{dt} \right) = & \underbrace{\Gamma_{i,k,[l-1]} \left(c_{i,k,[l-1]} - c_{i,k,l} \right)}_{\text{Internal diffusion}} - \\ & - \underbrace{\Gamma_{i,k,l} \left(c_{i,k,l} - c_{i,k,[l+1]} \right)}_{\text{Internal diffusion}} + \underbrace{\sum_{j=1}^{j=J} \nu_{i,j} r_{j,k,l} m_{k,l}}_{\text{Reaction}} \end{aligned} \tag{3.2}$$

where $\nu_{i,j}$ [$-$] is the stoichiometric coefficient for reaction step j, $r_{j,k,n}$ [$\text{mol s}^{-1}\,\text{kg}^{-1}$] is the reaction rate per mass of catalyst and $m_{k,l}$ [kg] is the mass of catalyst. It is assumed that there is no mass transfer between tanks within the washcoat. This is simply due to the washcoat being very thin, and so the area between tanks is far smaller than the area between layers ($A_{tanks} << A_{layers}$). Furthermore, the distance used in the gradient

approximation is far larger between tanks ($\Delta x << \Delta z$). Combining these two geometric reasons makes the mass transfer coefficient roughly 10^6 times larger in the radial direction compared to the axial direction.

3.1.1.1 External mass transfer

The external lumped mass transfer coefficient, $\Gamma_{i,k,0}$ is calculated as:

$$\Gamma_{i,k,0} = A_0 \left(\frac{1}{k_{\mathrm{c},i,k,0}} + \frac{0.5\Delta x_1}{D_{\mathrm{e},i,k,l}} \right)^{-1} \tag{3.3}$$

where $A_0\,[\mathrm{m}^2]$ is the gas/washcoat interface area, $D_{\mathrm{e},i,k,l}\,[\mathrm{m}^2\,\mathrm{s}^{-1}]$ is the effective diffusivity and $k_{\mathrm{c},i,k,0}\,[\mathrm{m\,s}^{-1}]$ is the external mass transfer coefficient given by the local Sherwood number ($Sh_k\,[-]$):

$$k_{\mathrm{c},i,k,0} = \frac{Sh_k D_{\mathrm{AB},i,k,l}}{d_{\mathrm{o}}} \tag{3.4}$$

where $D_{\mathrm{AB},i,k,l}\,[\mathrm{m}^2\,\mathrm{s}^{-1}]$ is the free molecular diffusivity, $d_{\mathrm{o}}\,[\mathrm{m}]$ is hydraulic diameter (in other words the open channel dimension). The local Sherwood number is based on the correlation by Tronconi et al [48]:

$$Sh_k = Nu_{\infty,\mathrm{T}} + 8.827(1000z^*)^{-0.545} e^{-48.2z^*} \tag{3.5}$$

where $Nu_{\infty,\mathrm{T}}\,[-]$ is the asymptotic Nusselt number, $z^*\,[-]$ is the dimensionless axial coordinate, in other words the inverse Graetz number ($Gz\,[-]$):

$$z^* = \frac{1}{Gz} = \frac{d_o}{zReSc} \tag{3.6}$$

where $z\,[\mathrm{m}]$ is the axial coordinate and $Re\,[-]$ is the Reynolds number:

$$Re = \frac{v d_{\mathrm{o}}}{\nu} \tag{3.7}$$

where $\nu\,[\mathrm{m}^2\,\mathrm{s}^{-1}]$ is the kinematic viscosity. The Schmidt number ($Sc\,[-]$) is given by:

$$Sc = \frac{\nu}{D_{\mathrm{AB}}} \tag{3.8}$$

3.1.1.2 Internal mass transfer

The lumped internal mass transfer coefficient ($\Gamma_{i,k,l}$) is given by:

$$\Gamma_{i,k,l} = D_{\mathrm{e},i,k,l} A_l \left(0.5\Delta x_l + 0.5\Delta x_{[l+1]} \right)^{-1} \tag{3.9}$$

where $A_l\,[\mathrm{m}^2]$ is the area between layers (increasing with increased layer index). For the last layer ($l = L$), it is assumed that there is no flux into the monolith substrate, i.e. $\Gamma_{i,k,L} = 0$ (the corresponding concentration within the monolith substrate $c_{i,k,L+1}$ is not solved for).

3.1.1.3 Diffusion models

The free molecular diffusion is calculated using the Chapman-Enskog equation in the form found in [68]:

$$D_{\mathrm{AB}} = \frac{3}{16} \frac{\left(4\pi k_{\mathrm{B}} T / M_{\mathrm{AB}}\right)^{1/2}}{n\pi\sigma_{\mathrm{AB}}^2 \Omega_{\mathrm{D}}} \tag{3.10}$$

where k_{B} [$\mathrm{J\,K^{-1}}$] is Boltzmann's constant, M_{AB} [$\mathrm{g\,mol^{-1}}$] is the reduced molecular mass, n [$\mathrm{mol\,m^{-3}}$] is the number density of molecules in the mixture (given by the ideal gas law), σ_{AB}^2 [m] is the average collision diameter and Ω_{D} [$-$] is the collision integral. These constants are obtained from *Properties of Gases and Liquids* [68]. The pore diffusivity is given by the Bosanquet interpolation [83](cited therein).

$$D_{\mathrm{p}} = \left(\frac{1}{D_{\mathrm{AB}}} + \frac{1}{D_{\mathrm{Kn}}} \right)^{-1} \tag{3.11}$$

where D_{Kn} [$\mathrm{m^2\,s^{-1}}$] is the Knudsen diffusivity:

$$D_{\mathrm{Kn}} = \frac{d_p}{3} \sqrt{\frac{8RT}{\pi M_i}} \tag{3.12}$$

where d_{p} [m] the mean pore diameter, T [K] is the temperature, R [$\mathrm{m^3\,Pa\,K^{-1}\,mol^{-1}}$] is the gas constant and M_i [$\mathrm{kg\,mol^{-1}}$] is the molecular mass of species i. To account for the porous and tortuous nature of the pores, the pore model by Wheeler et al [63] is employed:

$$D_{\mathrm{e}} = \frac{\varepsilon_{\mathrm{wsc}}}{\tau} D_{\mathrm{p}} \tag{3.13}$$

where $\varepsilon_{\mathrm{wsc}}$ [$-$] is the porosity of the washcoat and τ [$-$] is the tortuosity of the pores.

3.1.2 Heat transfer

The heat balance resembles the mass balance, with one big exception; due to the excellent conductivity of the washcoat and monolith substrate, the solid (subscript s) only requires a one dimensional discretization - i.e. the monolith and washcoat has the same temperature in radial direction. The gas phase (subscript g) heat balance is given by:

$$0 = \left(V_{k,0} c_{\mathrm{p,g}} \frac{dT_{\mathrm{g},k}}{dt} \right) = \underbrace{F_{\mathrm{tot}} c_{\mathrm{p,g}} \left(T_{\mathrm{g},[k-1]} - T_{\mathrm{g},k} \right)}_{\text{Advection}} - \underbrace{h_k A_0 \left(T_{\mathrm{g},k} - T_{\mathrm{s},k} \right)}_{\text{Convection}} \tag{3.14}$$

where $T_{\mathrm{g},k}$ [K] is the gas phase temperature, $c_{\mathrm{p,g}}$ [$\mathrm{W\,K^{-1}\,mol^{-1}}$] is the gas phase specific heat capacity and $T_{\mathrm{s},k}$ [K] is the solid phase temperature. The external heat transfer coefficient (h_k [$\mathrm{W\,m^{-2}\,K^{-1}}$]) is given by:

$$h_k = \frac{Nu_{\infty,\mathrm{T}} \lambda_g}{d_{\mathrm{o}}} \tag{3.15}$$

where $Nu_{\infty,\mathrm{T}}$ [−] is the asymptotic Nusselt number and λ_g [W m^{-1} K^{-1}] is the gas phase heat conductivity. The solid phase heat balance is given by:

$$0 = \frac{dT_{\mathrm{s},k}}{dt}\left(m_{\mathrm{s},k}c_{\mathrm{p,s}} + \frac{s_\mathrm{heat}}{K}\right) = \underbrace{h_k A_0\left(T_{\mathrm{g},k} - T_{\mathrm{s},k}\right)}_{\text{Convection}} - \underbrace{A_k\left(q_{k+1} - q_k\right)}_{\text{Conduction}} + \\ + \underbrace{\sum_{l=1}^{L}\sum_{j=1}^{J} r_{j,k,l} m_{k,l}\left(-\Delta H_j\right)}_{\text{Heat of reaction}} - \underbrace{\frac{\alpha_\mathrm{tot}}{K}\left(T_{\mathrm{s},k} - T_\infty\right)}_{\text{Heat loss}} \tag{3.16}$$

where $c_{\mathrm{p,s}}$ [J K^{-1} kg^{-1}] is the mass weighted specific heat capacity of the solid (washcoat and monolith substrate), K is the total number of layers, s_heat [W K^{-1}] is a heat sink due to the added mass from catalyst canning and insulation, A_k [m^2] is the area between axial tanks, ΔH_j [J mol^{-1}] is the reaction enthalpy, α_tot [W K^{-1}] is the lumped heat loss coefficient and T_∞ [K] is the effective surrounding temperature. The axial solid heat flux (for $1 < k < K + 1$) is given by:

$$q_k = -\lambda_\mathrm{s}\frac{T_{\mathrm{s},k} - T_{\mathrm{s},[k-1]}}{0.5\Delta z_k + 0.5\Delta z_{[k-1]}} \tag{3.17}$$

where $\Delta z_k[m]$ is the distance between axial nodes and λ_s [W m^{-1} K^{-1}] is the solid phase heat conductivity. For the first and last tank the axial solid heat flux is zero:

$$q_k = 0 \tag{3.18}$$

3.1.3 Kinetics

The detailed kinetic model used includes oxidation of CO, NO and hydrocarbons lumped together and modelled as C_3H_6 oxidation. The full reaction scheme, based on Lundberg et al [59] who based the NO oxidation scheme on Olsson et al [45], can be seen in table 3.1. The mechanisms for NO and CO oxidation follows a typical Langmuir-Hinshelwood mechanism - i.e. it models adsorption for both reactants required for the forward reaction step. The C_3H_6 mechanism includes oxidation by dissociated oxygen or adsorbed NO_2, a typical Eley-Rideal mechanism where only one molecule is responsible for the adsorption and the formed products desorbs instantaneously. In the the last column showing the rate expression, θ_i [−] is the noble metal surface coverage of species i (subscript v denotes vacant).

Table 3.1: Reaction scheme for NO, C_3H_6 and CO.

#	Mechanism	Reaction	Rate
		NO reactions	
1	O_2 ads	$O_2(g) + 2* \longrightarrow 2\,O^*$	$r_1 = k_1 c_{O_2} \theta_v^2$
2	O_2 des	$2\,O^* \longrightarrow O_2(g) + 2*$	$r_2 = k_2 \theta_O^2$
3	NO_2 ads	$NO_2(g) + 1* \longrightarrow NO_2{}^*$	$r_3 = k_3 c_{NO_2} \theta_v$
4	NO_2 des	$NO_2{}^* \longrightarrow NO_2(g) + 1*$	$r_4 = k_4 \theta_{NO_2}$
5	fwd reaction	$NO(g) + O^* \longrightarrow NO_2{}^*$	$r_5 = k_5 c_{NO} \theta_O$
6	bwd reaction	$NO_2{}^* \longrightarrow NO(g) + O^*$	$r_6 = k_6 \theta_{NO_2}$
		C_3H_6 reactions	
7	fwd reaction	$C_3H_6(g) + 9\,O^* \longrightarrow 3\,CO_2(g) + 3\,H_2O(g) + 9*$	$r_7 = k_7 c_{C_3H_6} \theta_O$
8	fwd reaction	$C_3H_6(g) + 9\,NO_2{}^* \longrightarrow 9\,NO(g) + 3\,CO_2(g) + 3\,H_2O(g) + 9*$	$r_8 = k_8 c_{C_3H_6} \theta_{NO_2}$
		CO reactions	
9	CO ads	$CO(g) + 1* \longrightarrow CO^*$	$r_9 = k_9 c_{CO} \theta_v$
10	CO des	$CO^* \longrightarrow CO(g) + 1*$	$r_{10} = k_{10} \theta_{CO}$
11	fwd reaction	$CO^* + O^* \longrightarrow CO_2(g)$	$r_{11} = k_{11} \theta_{CO} \theta_O$
12	fwd reaction	$CO^* + NO_2{}^* \longrightarrow CO_2(g) + NO(g) + 1*$	$r_{12} = k_{12} \theta_{CO} \theta_{NO_2}$

It should be stressed that there are several missing reaction steps that have been shown to have importance for various conditions [39, 45, 84]. These include adsorption of HC and NO which could contribute to surface inhibition. The exclusion of these phenomena leads to overestimation of reaction step 3 and 9 - i.e. the surface is rather occupied by CO and NO_2. Additional steps could include HC oxidation by NO and formation of of noble metal oxides. It has been shown that PtO_x, formed during long-term oxidizing condition, lowers the activity for e.g. NO oxidation. Metallic Pt can be reintroduced by reducing conditions. To circumvent an unwanted change in the noble metal oxidation state, the SCAT experiments where conducted in excess oxygen with only short pulses where the reactivity was measured. However, in realistic engine cold-starts the noble metal oxidation state could easily be varying. It should also be mentioned that the kinetic scheme is developed for a modelling purpose DOC, i.e. it is strictly a Pt/Al_2O_3 DOC with very little other additives that could affect the kinetics. The rate coefficients (k_j $[m^3\,s^{-1}\,kg^{-1}]$ for $j[1,3,5,7,8,9]$ *or* $[mol\,s^{-1}\,kg^{-1}]$ for $j[2,4,6,10,11,12]$) are calculated using a standard Arrhenius type expression:

$$k_j = A_j e^{-\frac{Ea_j}{RT_s}} \tag{3.19}$$

where A_j $[-]$ is the pre-exponential factor (also known as frequency factor accounting for the number of molecule collisions) for reaction step j and $Ea_j[J\,mol^{-1}]$ is the corresponding activation energy. These two constants are typically estimated using experimental data, where they typically show very high correlation (in some cases close to unity even with

a decent design of experiments [85]), making the exact identification of each parameter impossible. One common way to combat this problem is to re-parameterize the equation to its centered form using a reference temperature [86]:

$$\begin{aligned} k_j &= A_j exp\left[-\frac{Ea_j}{R}\left(\frac{1}{T_s}\right)\right] = A_j exp\left[-\frac{Ea_j}{R}\left(\frac{1}{T_s}+\frac{1}{T_0}-\frac{1}{T_0}\right)\right] = \\ &= \underbrace{A_j exp\left[-\frac{Ea_j}{RT_0}\right]}_{k0_j} exp\left[-\frac{Ea_j}{R}\left(\frac{1}{T_s}-\frac{1}{T_0}\right)\right] = k0_j exp\left[-\frac{Ea_j}{R}\left(\frac{1}{T_s}-\frac{1}{T_0}\right)\right] \end{aligned} \tag{3.20}$$

where T_0 [K] is the reference temperature (note that $exp[x]$ is Euler's number e^x). This way the reference rate coefficient $k0_j$ captures the magnitude of the reactivity while the activation energy captures its temperature dependence. There are methods for choosing reference temperature in order to minimize the parameter correlation between A_j and Ea_j [87] (in this case the reference temperature becomes a function of the conversion along the experimentally observed temperatures). In this work the reference temperature is simply set to the average of all experimental observations.

Lastly, the NO backward reaction kinetics parameters ($j = 6$) was, for any kinetic parameter set, recalculated to maintain overall thermodynamic equilibrium of the NO oxidation reactions ($j[1, 6]$). Gibb's free energy (ΔG_{net}) for a reaction is given by:

$$\Delta G_{\text{net}} = \Delta G^0_{\text{net}} + RTln(Q) \tag{3.21}$$

where ΔG_{net} [J mol^{-1}] is Gibbs free energy (superscript 0 denotes standard state) and Q [$-$] is the reaction quotient. At equilibrium ($Q = K_{\text{eq}}$), ΔG_{net} is zero:

$$\Delta G^0_{\text{net}} = -RTln(K_{\text{eq}}) = \Delta H^0_{\text{net}} - T\Delta S^0_{\text{net}} \tag{3.22}$$

where ΔH^0_{net} [J mol^{-1}] is the overall change in enthalpy, ΔS^0_{net} [J mol^{-1} K^{-1}] is the overall entropy change and K_{eq} [$-$] is the equilibrium constant. Rearranging equation 3.22 and solving for the equilibrium constant gives:

$$K_{\text{eq}} = exp\left[\frac{\Delta S^0_{\text{net}}}{R}\right] exp\left[\frac{-\Delta H^0_{\text{net}}}{RT}\right] \tag{3.23}$$

The equilibrium constant can also be written in terms of the backward and forward reaction constants, using equation 3.19 (subscript fwd and bwd indicates the overall forward and backward reaction, respectively):

$$K_{\text{eq}} = \frac{k_{\text{fwd}}}{k_{\text{bwd}}} = \frac{A_{\text{fwd}}}{A_{\text{bwd}}} exp\left[\frac{-(Ea_{\text{fwd}} - Ea_{\text{bwd}})}{RT}\right] \tag{3.24}$$

Comparing equations 3.23 with 3.24 gives that:

$$\frac{A_{\text{fwd}}}{A_{\text{bwd}}} = exp\left[\frac{\Delta S^0_{\text{net}}}{R}\right] \tag{3.25}$$

from which A_6 can be calculated and

$$\Delta H^0_{\text{net}} = (Ea_{\text{fwd}} - Ea_{\text{bwd}}) \tag{3.26}$$

from which Ea_6 can be calculated.

3.1.4 Discretization

Due to the diffusion and consumption of reactants, along with the boundary conditions for the washcoat (given gas/washcoat interface concentration and zero mass flux at the washcoat/monolith interface) the concentration gradients are the largest at the top of the washcoat. This calls for a linear discretization for the washcoat layers (radial nodes):

$$\Delta x_l = d_{\text{wsc}} \left(\frac{0.02}{\sum_{i=1}^{L-1} i}(L-l) + \frac{0.98}{\sum_{i=1}^{L-1} i}(l-1) \right) \tag{3.27}$$

where Δx_l [m] is the thickness for layer l and d_{wsc} $[m]$ is the total washcoat thickness. The number of axial tanks is set to $K = 10$ and the number of radial layers is set to $L = 8$ in the case of a normal washcoat or $L = 10$ in the case of an additional inert washcoat layer on top of the normal one. This leads to a distribution corresponding to 0.5% and 25% of the total washcoat thickness for the first and last layer, respectively. The axial discretization was chosen to be constant as the axial gradients are never that large due to the desired differential reactor operation. Results for grid independence studies are shown in Appendix B.

3.1.5 Implementation and solver

The equations presented so far in this chapter forms a differential-algebraic system of equations (DAE). The time constants for each modelled phenomenon range several orders of magnitude - i.e. the problem is considered to be stiff which calls for a stiff ODE solver. The chosen solver is ODE15s (ordinary differential equation solver in Matlab explained in detail in Shampine et al [88, 89]. The initial guesses for e.g. surface coverages were robustly solved by [59]: the code ramps inlet temperature and species concentrations until a stable starting point is established.

3.2 Parallel 1+1D model

To be able to handle arbitrary washcoat geometries with local features such as cracks, thus circumventing the assumption of an axissymmetric washcoat, a sectionalizing principle was applied to the 1+1D model. Similarly to Papadias et al [58, 72] and later Hayes et al [56], the washcoat is sectionalized into multiple slices as seen in figure 3.1. Whereas Papadias et al and Hayes et al used this principle to calculate an overall effectiveness factor, in publication III this method is used to account for the importance of local or global washcoat properties (porosity, tortuosity and thickness). It is assumed that potential tangential mass transfer is negligible compared to the radial one. The local washcoat

properties are determined using a combination of scanning electron microscopy (SEM) analysis and gravimetric analysis (GA). Once these properties are established the model treats the problem, of a non-uniform washcoat, as a number of parallel computations using the original 1+1D model. After analyzing the thinner washcoats of the catalysts C and D, it was clear that the washcoat had a substantially more even distribution, making the continuation of the the parallel model development unnecessary.

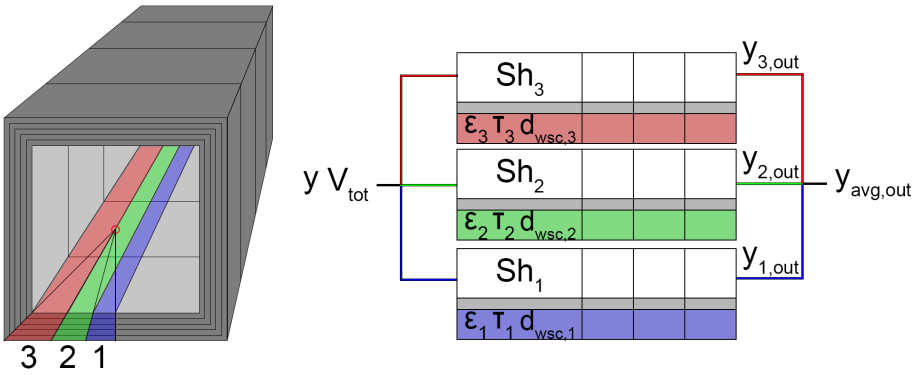

Figure 3.1: *Parallel 1+1D model discretization scheme and parallel computing scheme.*

3.3 Parameter estimation

This section will present the developed parameter estimation algorithm along with some key choices made along the way. The algorithm is described in more detail in paper IV, and so only the main features are presented here. The developed algorithm is based on response surface methodology (RSM), a methodology used in optimization. It should be stressed that by parameter estimation, the goal is in no way to find optimal parameter values or to optimize the performance of the catalyst, but to tune parameter values in order to minimize the weighted sum of squares error between experimental observations and simulations (also known as the objective or cost function):

$$g(p) = \sum_{o=1}^{O} w_o \left(\check{y_o}(p) - y_o\right)^2 \tag{3.28}$$

where $g(p)$ $[-]$ is the objective function, w_o $[-]$ is the weight function for observation o, $\check{y_o}(p)$ $[\%]$ is the simulated conversions using parameter set p and y_o $[\%]$ is the experimentally observed conversion. Outlet concentrations, instead of conversion, could technically also have been used. However, as different inlet concentrations was used (and NO oxidation is a much slower reaction and hence lower conversion) the species with highest outlet concentration would have a forced higher importance (due to the objective function being the error squared). Hence, the use of conversion more or less normalizes the importance

for each species. An illustration of the complete RSM algorithm can be seen in figure 3.2. The green box indicates the starting point, light green is the multi-stepping procedure, yellow is the Newton 2nd order method and red indicates stopping criteria.

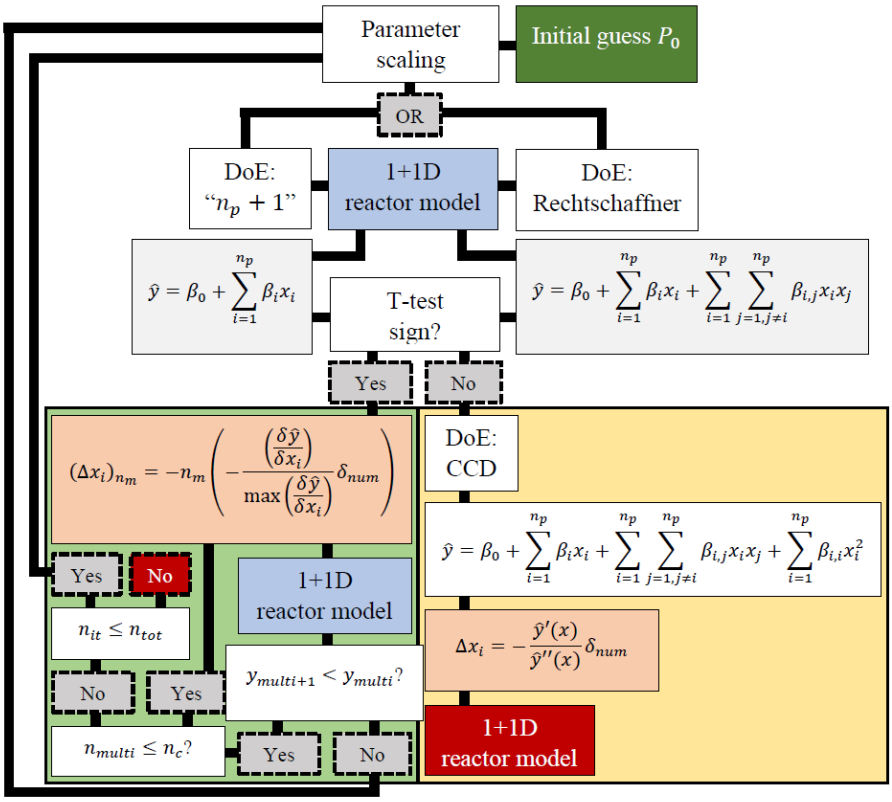

Figure 3.2: *Parameter estimation algorithm flow chart.*

Since the model contains parameter that span vastly different orders of magnitude ($A_j \approx 10^5 - 10^{15}$ vs $\tau \approx 1 - 10$), parameters are scaled so that they have roughly the same parameter sensitivity in a large part of the parameter space. For example, the reference reaction rate constants, activation energies and the constants for mass transfer are scaled according to:

$$k0_j = k0_j^{<i>} p_p^{<s>} \omega_p \tag{3.29}$$

$$Ea_j = Ea_j^{<i>} \left[(1 - \omega_p) + p_p^{<s>} \omega_p \right] \tag{3.30}$$

$$\tau = \tau^{<i>} p_p^{<s>} \omega_p \tag{3.31}$$

$$Sh_z = Sh_z^{<i>} p_p^{<s>} \omega_p \tag{3.32}$$

where $p_p^{<s>}$ $[-]$ is the scaled parameter value (that is actually tuned) and ω_p $[-]$ is the parameter weight to allow for parameters to have similar sensitivity. Superscripts i, f

and s denotes initial, final and scaled parameter values, respectively. The weights for the activation energies is typically around 0.2 while it is close to unity of the other shown parameter scalings. Next step is to use a design of experiments' design matrix to create a response surface model (polynomial) that resembles the objective function. The most simple kind of design matrix, shown in table 3.2, is one where each tuned parameter is varied independently. Levels 0 and 1 correspond to low and high levels, which in the case of paper IV is typically a ±1% scaled parameter variation (the influence of this numerical parameter variation is also examined in the paper).

Table 3.2: A simple design matrix.

$k0_1$	Ea_1	τ	Sh_z
0	0	0	0
1	0	0	0
0	1	0	0
0	0	1	0
0	0	0	1

A much more sophisticated DoE, namely the Rechtschaffner 8 parameter DoE with resolution V (i.e. 8 parameters are tuned and the main effects and 2-way interactions are only confounded with 4-way and 3-way interactions, respectively), was compared to the simple, cheap design matrix from 3.2 with respect to significance of interaction terms, potential benefits (e.g. a more elaborate response surface model) and cost for evaluation. Depending on the choice of DoE, a response surface model of varying complexity can be obtained:

$$\hat{y} = \underbrace{\hat{\beta}_0}_{\text{Intercept}} + \underbrace{\sum_{i=1}^{P} \hat{\beta}_i p_i}_{\text{Main}} + \underbrace{\sum_{i=1}^{P} \sum_{j=1, j\neq i}^{P} \hat{\beta}_{ij} p_i p_j}_{\text{Interaction}} + \underbrace{\sum_{i=1}^{P} \hat{\beta}_{ii} p_i^2}_{\text{Pure quadratic}} \tag{3.33}$$

where $\hat{y}$ [%] is the RSM predicted values, p_i [−] is the scaled parameter value and $\hat{\beta}$ [−] is the model coefficients according to:

$$\hat{\beta} = (X^T X)^{-1} X^T \vec{b} \tag{3.34}$$

where X [−] is the design matrix from the DoE (also including a column of ones for the intercept and any column combinations for the interaction or pure quadratic effects that should be approximated) and $\vec{b}$ [%] is a vector of the simulated responses ($\breve{y}_o(p)$). Once the response surface model is established a multi-stepping procedure along the steepest direction (negative gradient), to minimize the objective function, is established:

$$(\Delta p_p^{<s>})_{n_{multi}} = -n_{multi} \left(\frac{\frac{\partial \hat{y}}{\partial p_p^{<s>}}}{max\left(\frac{\partial \hat{y}}{\partial p_p^{<s>}}\right)} \right) \tag{3.35}$$

where n_{multi} [−] is the n-th multi-step along the gradient. The right-hand side ratio normalizes the gradients so that the most significant parameter always makes one δ_p step in the parameter space. A Student's T-test is performed to ensure that only significant parameters are tuned. Since modern CPUs typically support multi-core operation, all the steps can be computed at the same time, offering a more robust stepping procedure than the traditional Newton-Raphson method - at the same computational cost. The parameter combination that achieves the lowest objective function value is used as the center-point for next response surface model evaluation. The whole iteration is continued as long as there are significant parameters in the T-test.

3.4 Design of Experiments

In order to able to model monolith reactors properly experimental observations are required. To systematically examine these observations, and to get the most data out of the least number of experiments, design of experiment (DoE) is an invaluable tool. DoE aids in determining the relationship between state variables and some observed process variable [90]. To be able to model the processes that occur in the monolith, the data that is used to tune the model must also contain them. In order to create a broad experimental space, the effect of the the following parameters, presented in table 3.3 are investigated using.

Table 3.3: Investigated parameters for catalyst modelling.

Variable	Typical value
Temperature	100 to 550°C
Volumetric flow rate	23.6 and 38.6 $\mathrm{l_N/min}$
GHSV	110′000 and 180′000 $\mathrm{hr^{-1}}$
Reactants	CO, C_3H_6 and NO

The temperature span cover light-off for all species and also the thermodynamic equilibrium limitations of the NO oxidation. As HC and CO oxidation are the faster reactions that occur at lower temperatures compared to NO oxidation, the majority of the temperature points are placed to cover these light-off curves. The implications of the temperature points distribution, and its effects on the parameter tuning, is examined in paper IV. The volumetric flow rates correspond the upper and lower operating limits of the synthetic catalyst activity test (SCAT) bench, further described in the coming sections, but corresponds to reasonable Gas Hourly Space Velocities (GHSV [$\mathrm{hr^{-1}}$]) found in normal DOC operation. The 4 different catalysts used in the project is are shown in table 3.4 along with some design parameters and measured quantities.

Table 3.4: Catalysts used in the project.

Reference	Pt Loading	Washcoat Loading	Washcoat Thickness	Dispersion	Used in paper
A	15	2.6	110	23.9 ± 0.3	II, III
B	15	1.3	55	24.2 ± 0.9	II
C	5	$1 + 0$	35	–	IV
D	5	$1 + 1$	70	–	IV

The noble metal loadings are low to ensure a differential reactor - i.e. the catalysts have low conversion to allow for easy and accurate measurement of the outlet concentrations for tuning of the model at multiple reactor conditions. The washcoat loading of catalyst C and D mean that there is $1\,\mathrm{g\,in^{-3}}$ of washcoat that contains catalytic material, while there is additional $+1\,\mathrm{g\,in^{-3}}$ of *inert* washcoat on top of the normal layer for catalyst D. This barrier adds a pure internal diffusion limitation which allows for easy tuning of internal mass transport model parameters, e.g. τ. The thicknesses (assuming a flat slab) are calculated using a known overall washcoat porosity from a BET measurement and also verified using scanning electron microscopy (SEM), further explained in the coming sections. The dispersions where measured using CO chemisorption as explained in the coming sections. The last column shows in which paper each catalyst was used.

3.5 Synthetic Catalyst Activity Test

In engine tests the exhaust data, e.g. temperature, volumetric flow rate and concentrations, is often highly correlated [91]. To be able to cover a large experimental space and to freely adjust parameters in experiments, it is therefore common to use a synthetic catalyst activity test (SCAT) bench - also commonly known as flow reactor. An illustration of the SCAT bench supplied by Johnson Matthey AB is shown in figure 3.3.

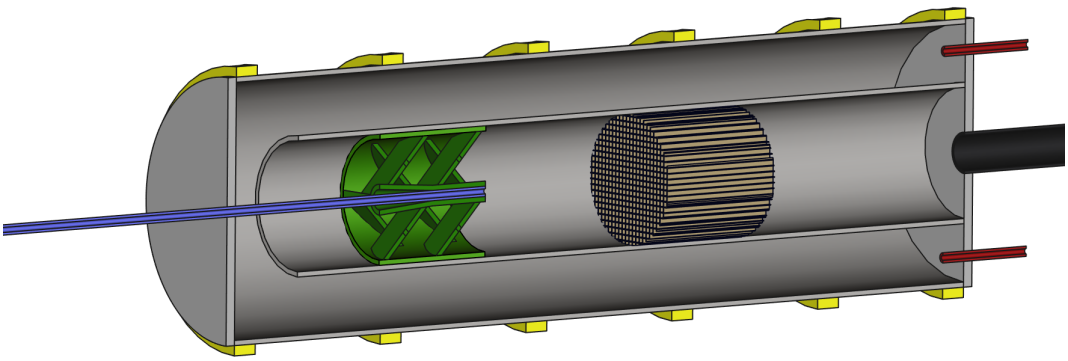

Figure 3.3: *Illustration of the SCAT bench.*

The SCAT bench consists of an inner and outer cylinder, where the outer cylinder is further encapsulated in an electrical heater (yellow) and a ceramic body along with insulation (not shown in the image). The carrier gas (typically nitrogen gas along with a desired oxygen level, injected through the red capillaries) flows in a two-pass configuration around the inner cylinder, where the test sample is placed, ensuring highly isothermal operation. The reactants themselves are kept in high concentrations, in separate capillaries (blue) minimizing unwanted reaction before the gases enter the tests sample itself. The short injection distance before the tests sample also reduces axial dispersion, compared to a premixed case, which is desirable for transient experiments. The SCAT bench also has far superior repeatability compared to an engine, which is a much more complex system. While not all combinations of species concentrations, volumetric flow rate and temperature are realistic engine operating conditions, the orthogonality of the experiments that SCAT bench can offer is highly desirable for parameter tuning in the reactor model. The mixer (green) developed in paper I is also shown in in figure 3.3.

3.5.1 Kinetic experiments

The kinetic experiments, summarized in publication II, comprise concentration step experiments for several reasons. Firstly, the transient experiments contain more useful information. Secondly, the short duration of the steps (where reaction occurs) limits the likelihood of a change in the noble metal oxidation state - which can alter the kinetics significantly [1]. As of now, this phenomenon is not included in the 1+1D model, hence, to observe this is experimentally undesired. The original idea was to simulate each individual step experiment, however, as the transient nature of the SCAT rig was never mapped, there is little to no additional information to be obtained through simulating a step. Instead, the steady state data from each pulse is used to form a light-off curve for each species - including one combination of all species for tuning of interaction reactions (step 8 and 12 in table 3.1).

3.5.2 CO Chemisorption

One of the most, if not the most, sensitive model parameters is the catalyst loading as it linearly scales the reaction rates. In tuning of the reactor model, having such a sensitive parameter can cause problems, hence it is smart to experimentally determine its value. The loading, or rather the noble metal dispersion - the ratio of the accessible mass of catalyst to the total mass of catalyst - can be determined using CO *chemisorption*.

At non-reactive temperatures ($T << 100°\mathrm{C}$), CO will adsorb (but not react further) onto the noble metal through two different mechanisms: chemisorption (strong, covalent bond, mono-layer) and physisorption (weak, van der vaals force, multi-layer). The chemisorbed amount, corresponding to the amount of active sites, need to be distinguished from the total amount adsorbed. This is done through exposing a catalyst sample to two, separate CO pulses with known concentration as can be seen in figure 3.4. During the first, the uptake of CO (i.e. the difference between inlet and outlet CO concentration) equals the chemisorbed and physisorbed CO. Once the first pulse is completed, the physisorbed CO

will desorb. During the second pulse the uptake equals only the physisorbed CO, as all the sites for chemisorption are already filled. The difference in uptake between the pulses then gives the chemisorbed amount of CO. By assuming a CO:Pt stoichiometry of 0.8 [92], the accessible mass of catalyst can be calculated.

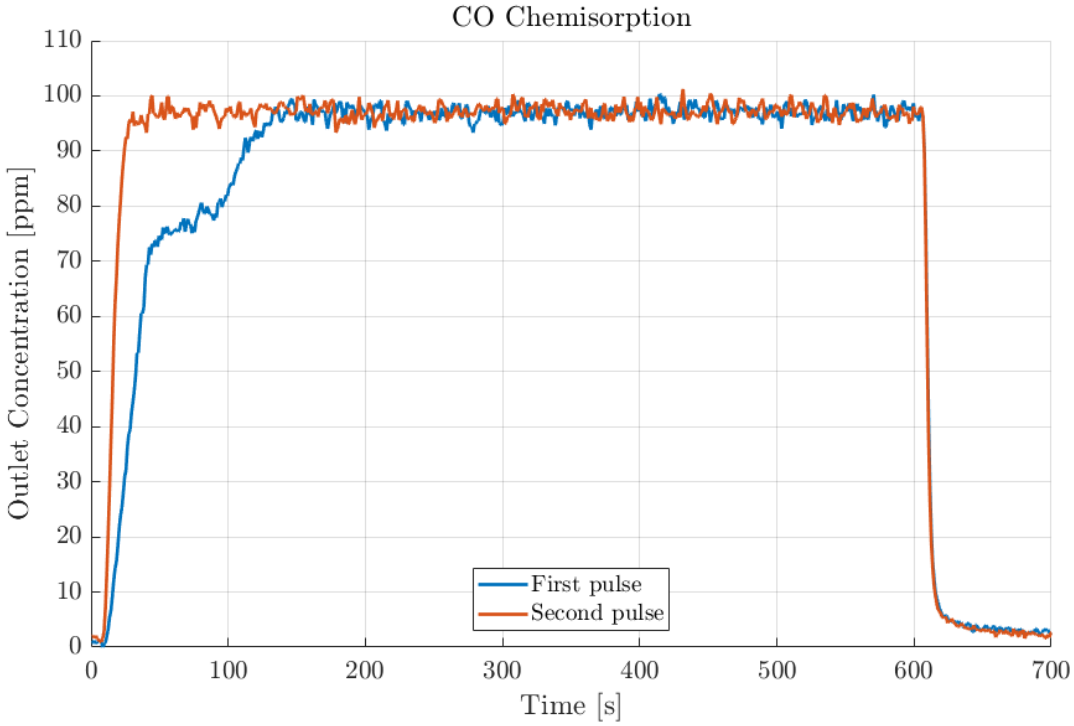

Figure 3.4: *CO Chemisorption pulses.*

There are off course commercially available, *dedicated* experimental instruments for dispersion measurements (e.g. CAT-LAB PCS from Hiden Isochema) designed for this very purpose. In this PhD project, it was investigated whether a normal SCAT bench could be used for this experimental technique. The obvious benefit would be that the exact same sample undergoes kinetic testing and chemisorption. To give an accurate measurement of the dispersion, the integral corresponding to the uptake of CO should be as large as possible. Since the accessible mass of catalyst is constant, this integral (a.k.a the breakthrough time) can be maximized through decreasing the volumetric flow rate, decreasing the CO concentration and increasing the total catalyst sample. This is where the use of a SCAT bench is problematic since it is optimized for reactive operating conditions.

The volumetric flow rates are generally to high, in order to achieve reasonable space velocities found in EATS operation and the analyzers used also require some minimum flow rate. Furthermore, the CO concentrations that make for a good DOC operating point would likely instantly saturate the active sites since they are not restored through reaction and desorption. Also, the use of a mass flow controller (MFC) could instantly saturate the active sites if it is not properly controlled (overshooting). Lastly, it is highly desirable

that the very same catalyst sample undergoes kinetic experiments and CO chemisorption so that there is no variation in dispersion due to having chosen a different catalyst sample from the original catalyst. The problem is that a too large sample would be to active (achieving integral reactor behaviour) in kinetic testing and a too small sample would have a too fast breakthrough time. Some of these limitations where solved by disconnecting the FTIR analyzer that required an additional 5 l/min and by using a switch to minimize the risk of an MFC overshoot. Because of these limitations, only some CO chemisorption tests were successful. An alternative solution for establishing potential differences in accessible amount of noble metal between catalysts would be to run a large set of different noble metal and washcoat loadings at a steady state temperature in the kinetically controlled region. The ratios in conversions would show the differences in amount of accessible noble metal. However, as this would only be a relative measurement, the kinetics would not be in absolute terms.

3.5.3 Verification of single channel assumption

One important assumption for the SCAT rig using this injection-based design is that it fulfills the single channel assumption experimentally - i.e. all channels have the same inlet conditions with regards to velocity, species concentrations and temperature. As the flow in the inner SCAT cylinder is laminar, the only mechanism to radially even out the concentrated reactants at the outlet of each capillary is molecular diffusion - which is slow compared to the advective axial transport. Hence, there is a risk of having a radial concentration gradient at the inlet of the test sample. The problem is that the SCAT rig only measures mixed-cup outlet concentration, which makes identification of local but large radial gradients impossible to identify - unless you design a smart experiment. The local inlet concentration is examined by placing a small 5x5 channels DOC coated with 30g Pt ft^{-3} at different radial positions (in the center or at the edge) in a larger, un-coated monolith as seen in figure 3.5.

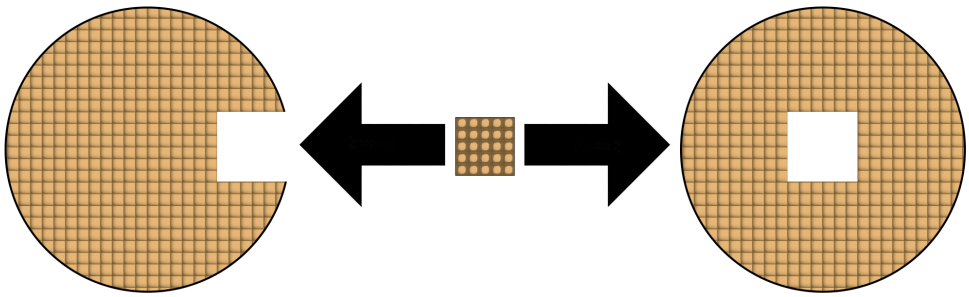

Figure 3.5: *Illustration of the positioning of the active 5x5 channels core at the edge (left) and in the center (right).*

The experiment has a simple yet effective analysis: if the mixed-cup conversion depends on the position of the inserted active core, then there is a concentration maldistribution. Or, if the conversion is higher than the relative cross-sectional area of the active core, there is a concentration maldistribution. The core testing results are presented in paper I,

however, additional results with a completely active DOC (normal size, no cutout) was tested with and without mixer to see if the found maldistribution affects the results even when the entire DOC is active. The results can be found in Appendix B.

3.6 Scanning Electron Microscope (SEM)

The scanning electron microscope (SEM) resembles the modern digital camera. However, instead of detecting the light reflected by an object, an accelerated electron beam (primary electrons) is bombarded onto a surface of interest. This surface allows for some electrons to pass through (transmitted). Some electrons originating in the beam itself are reflected back (backscattered) and through ionization the surface produces electrons (secondary). The intensity of these secondary and backscattered electrons can be recorded using special solid-state detectors. After the signal is amplified a pixel luminosity is formed. The electron beam is then moved (scanned) into a new position to record a new pixel - and slowly an image is captured [93]. A typical image of the monolith substrate (upper left), the open channel (lower right) and the applied washcoat can be seen in figure 3.6.

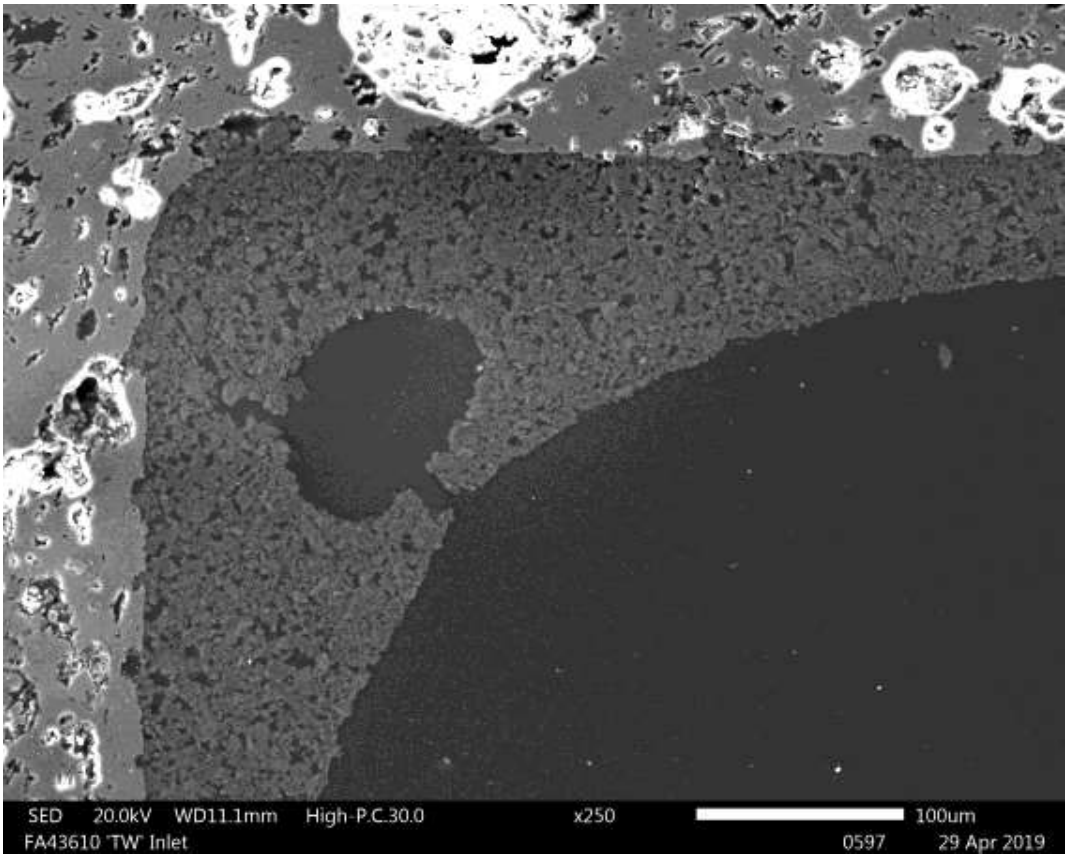

Figure 3.6: *SEM image of the washcoat used to approximate porosity.*

The SEM images are used for determining the washcoat porosity ($\varepsilon_{\mathrm{wsc}}$) and the local washcoat thickness (d_{wsc}). Its calculation and analysis are described in detail in appendix A for the interested reader.

3.7 Gravimetric analysis (GA)

Gravimetric analysis (GA) is a quantitative measurement technique that can aid in determining adsorption isotherms which are useful for determination of kinetics, but also for mass transport rates. In this work, the *Intelligent Gravimetric Analysis* (IGA) method using the IGA-001 from Hiden Isochema was employed. In this method, the transient weight data from the adsorption isotherms are used to determine the timescale for washcoat diffusion, which in turn can be used to calculate parameters in the model for effective diffusion. In IGA, similarly to CO chemisorption, a catalyst sample is exposed to an adsorbate. However, the adsorbate will diffuse into and adsorb onto the washcoat - not only onto the active sites of the noble metal. This diffusion process is very fast (tens of milliseconds for the SCAT rig at normal DOC operation). To accurately measure these phenomena, the experiment is performed at very low temperature and near vacuum. The lowered pressure decreases the adsorbate concentration and the lowered temperature decreases the diffusivity, thus prolonging the entire process. The low absolute pressure also removes need for modelling of drag and buoyancy forces of the catalyst sample during the experiment.

Initially, the catalyst sample is placed on a very sensitive scale inside a vacuum chamber. The sample is exposed to high temperature under vacuum in order to desorb any previously adsorbed molecules. The vacuum chamber is then placed inside a cryo chamber and the temperature is lowered to around 0°C. The scale is now tared, allowing for distinguishing between the sample and adsorbate weight. The adsorbate, a slowly diffusing hydrocarbon (Hexane), is contained in a liquid reservoir outside the chamber. A pressure regulator allows the adsorbate to fill the vacuum chamber in multiple ideal steps - going from near vacuum up to the adsorbate saturation pressure. As the diffusion and adsorption occurs, the weight of the adsorbate is monitored and the relative mass uptake is used to calculate the timescale for washcoat diffusion.

In IGA, as opposed to normal GA, the pressure regulator continuously maintains the pressure surrounding the catalyst sample as the adsorption starts. Furthermore, the cryo chamber maintains isothermal operation, removing the heat of adsorption through external cooling. IGA is suitable for slowly diffusing systems, e.g. zeolites where the mean pore size is small and Knudsen diffusion is the dominating diffusion mechanism. This means that there the chamber, along with monolith channels will fill up with adsorbate infinitely fast compared to the diffusion throughout the washcoat. When it comes to γ-Al_2O_3 used in this work, pore sizes are typically larger than that of zeolites and so the diffusion process is faster. To minimize the effects that the chamber and channel filling can have on the uptake curves, the chamber pressure is monitored and the start of uptake is defined to start once the surrounding pressure reaches 99% of the set value.
The time constant for washcoat diffusion is calculated through fitting a linear uptake equation to the IGA data:

$$\frac{m(t)}{m_\infty} = 1 - e^{-k_{\mathrm{wsc}}t} \tag{3.36}$$

where $m(t)/m_\infty$ $[-]$ is the ratio of mass adsorbed at time $t[s]$ to mass adsorbed at equilibrium. k_{wsc} $[\text{s}^{-1}]$ is the uptake rate coefficient:

$$k_{\text{wsc}} = \frac{D_{\text{e}}}{\Omega_{\text{wsc}}^2} = \frac{1}{t_{\text{wsc}}} \tag{3.37}$$

The uptake rate constant is also the inverse of the time constant for washcoat diffusion. The relative uptake for 0 to 12 mbar and 12 to 24 mbar along with the respective fit are shown in figure 3.7.

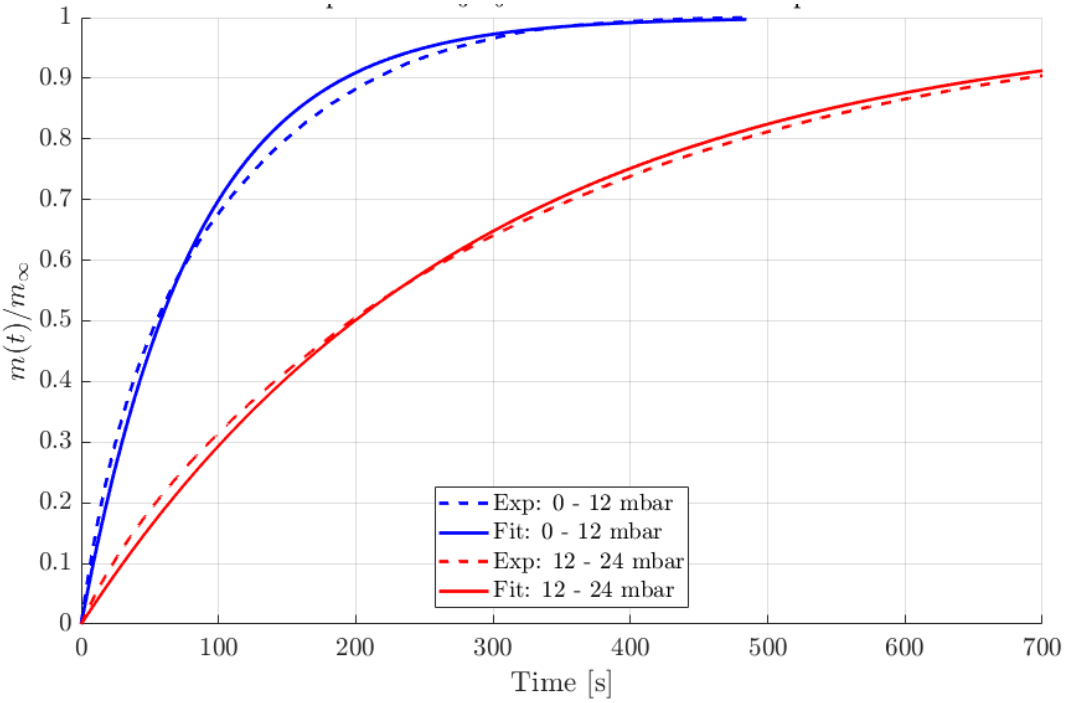

Figure 3.7: *Relative uptake of Hexane at* $-11°C$ *and* 12 mbar *steps.*

This simple uptake rate model works well for uniform diffusion processes - i.e. there is only one time constant for the entire sample. This holds true if there is a uniform effective diffusion length (monodisperse particles, uniform washcoat) and if the timescale for washcoat diffusion is far greater than any other occurring process. In the case of the 110 µm washcoat of catalyst A, the washcoat was obviously not uniform, and so there are multiple occurring time constants for the uptake. In this case the sectionalizing principle, further described in paper III, was also applied to the uptake rate equation. Equation 3.36 now becomes:

$$\frac{m(t)}{m_\infty} = \sum_{m=1}^{M} \frac{a_m}{a_{tot}} \left(1 - e^{-k_{\text{wsc}} t}\right) \tag{3.38}$$

where a_m $[\text{m}^2]$ is the washcoat cross-sectional area for segment m and a_{tot} $[\text{m}^2]$ is the total washcoat cross-sectional area.

4 Results and Discussion

This chapter summarizes the results from publications I, II, III and IV. Furthermore, there are also some important results on final model tuning. Finally, there are also results regarding grid independence and final mixer validation under reactive conditions in appendix B.

4.1 Summary of publication I

"Use of 3D-printed mixers in laboratory reactor design for modelling of heterogeneous catalytic converters"

Publication I presents a through investigation of the benefits and drawbacks of two typical SCAT bench designs - the premixed and injection-based design. The premixed design mixes the reactant flow before heating it to the desired operating temperature. As a result the premixed design unfortunately has high axial dispersion which is not desired in highly transient experiments. The injection-based design circumvents the problem with axial dispersion through injection of the reactants through a set of capillaries close to the reactor inlet. Because of this design principle, there is a risk of having a maldistribution of reactants across the monolith inlet - which is not accounted for in the single-channel models. The problem is that very few SCAT benches allow you to measure this local problem since you only have access to mixed-cup averages of the outlet conditions.

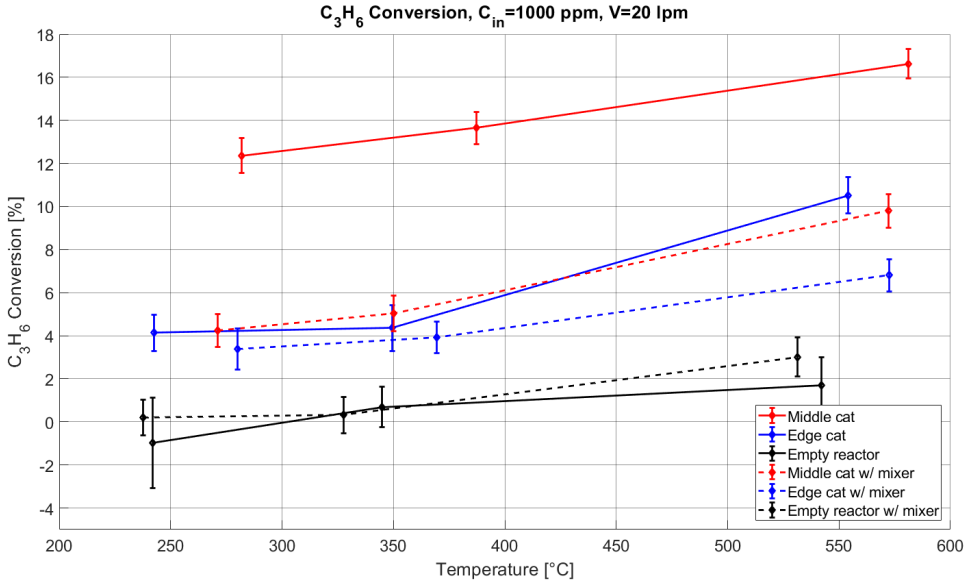

Figure 4.1: *Conversion vs temperature for various catalyst configurations, with or without mixer.*

To tackle this problem a set of smart catalysts were designed. The catalysts only induce local reactions and so the reactivity (and thus inlet concentrations) can be measured at various radial positions. The results can be seen in figure 4.1. By comparing the blue and red solid lines, it can be seen that the conversion depends on the radial position. To solve this maldistribution problem a modified SMX mixer was designed. Once the experiments were repeated using the mixer upstream the catalyst sample (dotted lines), conversions did not show a radial dependence. The SCAT bench, along with the modified SMX mixer, was also simulated using computational fluid dynamics (CFD). The effect on the flow field, caused by the mixer can be seen in figure 4.2.

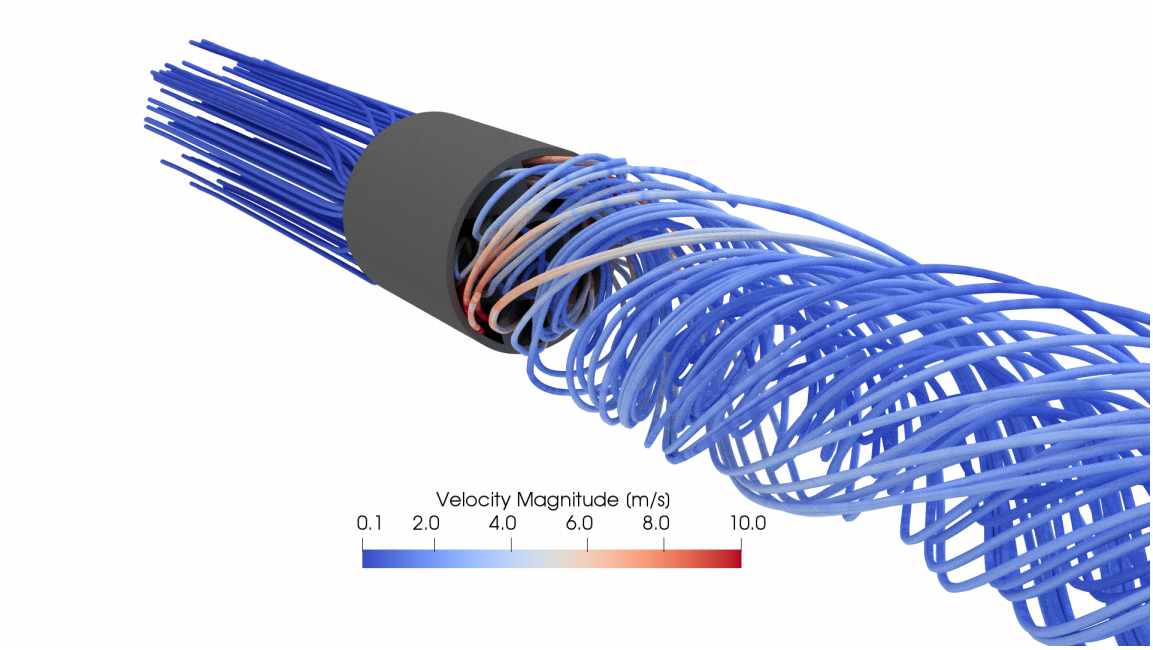

Figure 4.2: *Streamlines colored by velocity magnitude for CFD simulation of 20* l_N/min.

4.2 Summary of publication II

"Efficient Experimental Approach to Evaluate Mass Trans-fer Limitations for Monolithic DOCs"

In publication II, the diesel oxidation catalyst (DOC, Pt/γ-Al_2O_3) is used in a synthetic gas catalyst test bench to study internal and external mass transfer limitations during NO oxidation. By varying the washcoat thickness (55 and 110 µm) while keeping the total noble metal loading the same, two DOCs can be evaluated using classical timescales. Figure 4.3 shows the ratio between the time constant for reaction and washcoat diffusion. The conversion for the DOC with thinner washcoat shows to be kinetically controlled at lower temperatures. At intermediate temperatures it enters a region where internal mass transfer limitations start to play a role. The conversion for the DOC with thicker washcoat shows severe internal mass transfer limitations already at around 175°C.

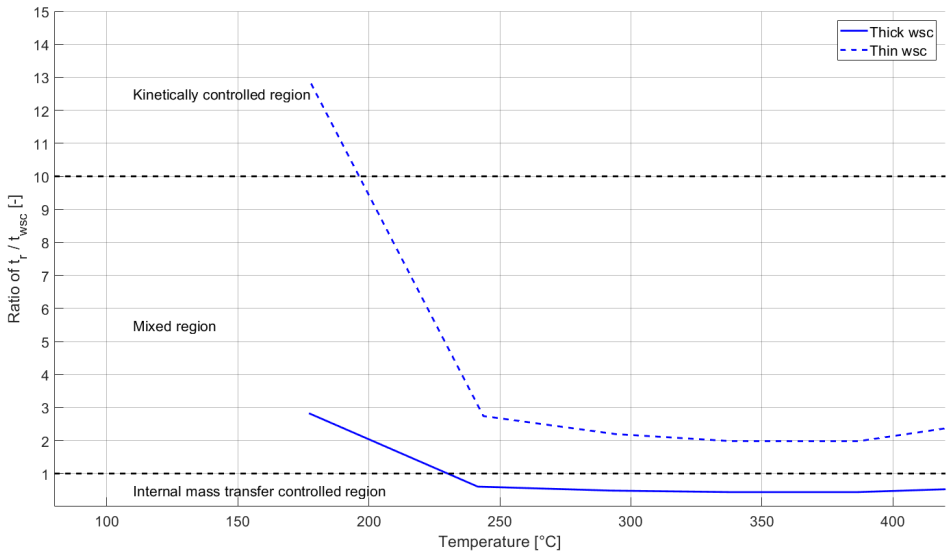

Figure 4.3: *Ratio of time scale for reaction and washcoat diffusion.*

4.3 Summary of publication III

"Modelling of mass-transfer resistances in non-uniformly washcoated monolith reactors"

The traditional 1D or 1+1D single-channel models fail to capture variations in mass transfer resulting from a non-uniform washcoat. Publication III presents a modelling framework where a sectionalizing principle is combined with a traditional 1+1D model to account for local variations in the washcoat. Intelligent gravimetric analysis (IGA) and scanning electron microscopy (SEM) are used in combination to calculate local effective diffusivity as an input for each simulation. The new model is compared to the original 1+1D model in figure 4.4, where NO light-off curves are shown. The new model predicted increased conversion at elevated temperatures, where mass transfer limitations are present, due to the higher porosity in the corners. Hence, these local features are important for predictive modelling of automotive converters where the axis-symmetric assumption for washcoat thickness is not fulfilled.

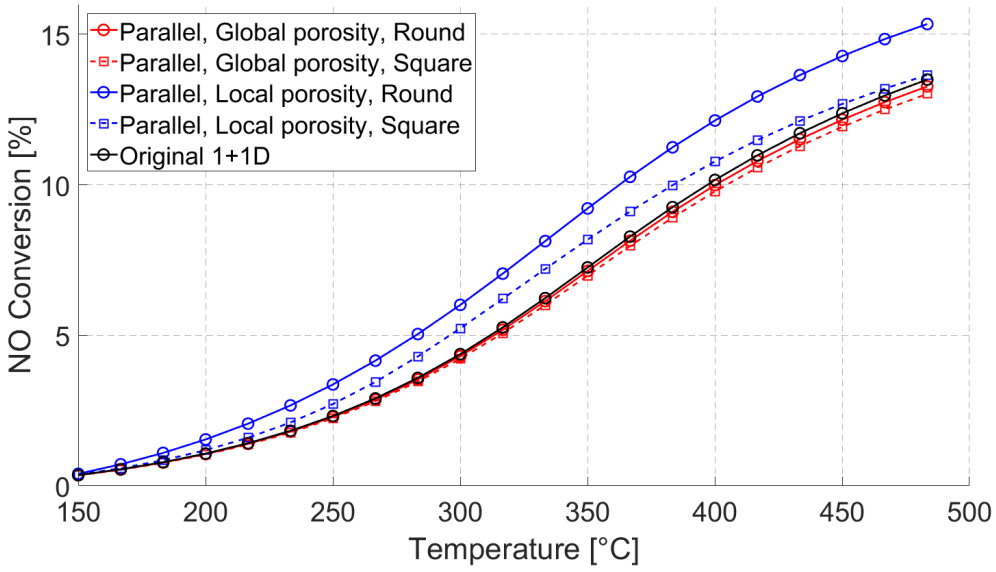

Figure 4.4: *Light-off curves for the original 1+1D model new (parallel) model using either global or local washcoat features*

4.4 Summary of publication IV

"Robust parameter estimation methodology for heterogeneous catalytic reactors"

Generally speaking, most EATS models found in literature are not predictive and thus they require tuning. Paper IV aims at implementing a robust steepest descent algorithm for tuning of the 1+1D reactor model used in this project. The algorithm employs a response surface methodology (RSM) for minimizing the error between simulations and experiments. It was shown that multiple parameters have interaction effects when the numerical parameter variation is large. Thus, combining a costly Rechtschaffner DoE (resolution V, 8 parameters), allowing for estimation of main and interaction effects, with a long step size allowed for a very fast tuning of the model. Similarly, it was shown that selecting a small step size and only estimating the main effects allowed for a robust, yet more costly, tuning procedure.

The paper further shows the importance of carefully designed experiments. Firstly, running kinetic experiments for catalysts having an additional, inert washcoat layer showed to be vital for tuning internal mass transport parameters. When performing parameter estimation for only the catalyst with a normal washcoat, the sensitivity for pore tortuosity completely disappeared. After extrapolating the final parameter values to the catalysts with inert washcoat, the internal mass transport limited region was shifted by 50°C. The overall fit also was a lot worse after extrapolation. The importance of having good initial guesses was also proven by comparing experimentally measured values for tortuosity with typical literature values. The experimentally measured value was far closer to the final value compared to the typical assumption of $\varepsilon/\tau \approx 0.1$ and the overall fit in the internally mass transport limited region was better in the case of using IGA as an initial guess.

Probably the most important wisdom from this paper is that the distribution of the steady-state temperatures strongly affects the parameter sensitivity. Figure 4.5 compares a case where the weight function is a vector of ones (case I) and a case where the weight function is temperature dependent (case III). It can be seen that weight dependent weight function achieves a better fit (left window). The parameters that differ the most are the parameters for internal and external mass transport (τ and Sh_z in the right window) which show higher sensitivity at those high temperatures that received a boost in importance from the temperature dependent weight function.

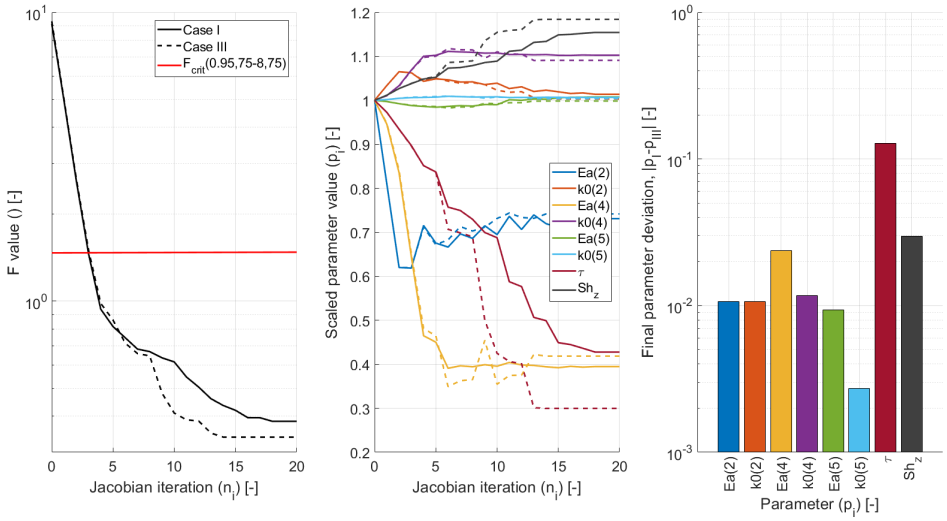

Figure 4.5: *Left: F-value for case I (normal weight function) and case III (temperature dependent weight function). Middle: Parameter values for case I (solid lines) and case III (dashed lines). Right: Final parameter value differences*

By comparing the final fit in figure 4.6 (case I to the left and case III to the right), it can be seen that the fit is still highly dependent on the densely populated temperature points between 100 and 300°C but that the fit is still slightly better in the span 300 to 450°C. An even more pronounced weight function at higher temperature would likely further improve the fit. Finally, the effect of final parameter values was compared by examining time constants for a 1x1 in DOC operating at 25000 to 300000 hr^{-1}, ranging between 100 and 550°C.

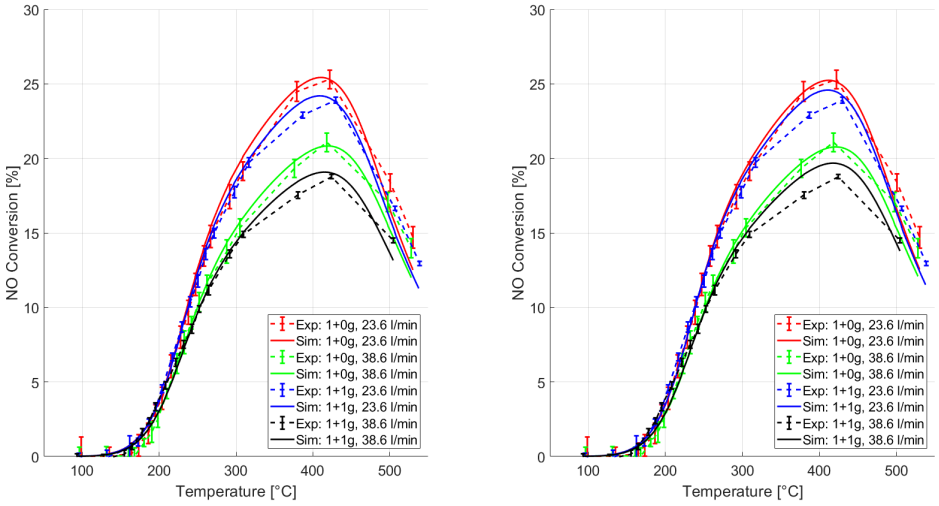

Figure 4.6: *Left: simulations vs experiments for case I. Right: simulations vs experiments for case III*

.

4.5 Further model tuning

To complement the findings in paper IV, the full DOC model was tuned to the SCAT data gathered for catalysts C and D (with and without inert washcoat) using a total of 5 different step experiments at various temperatures and different space velocities. The step experiment procedure from paper II were repeated for each individual reactant (hereafter referred to as single-component step) - CO, NO, C_3H_6 and $C_{10}H_{22}$ to individually tune the individual forward reaction of each specie as well as the corresponding desorption steps for each included reactant within those reactions and finally one step experiment with all reactant at the same time (hereafter labeled as multi-component step) to account for inhibitions and steps where NO_2 oxidizes CO or C_3H_6. However, several problems with the experimental data were encountered that ultimately led to a poor fit for all reactions if the multi-component reactions are included in the fit. The light-off curves for the multi-component step experiments can be seen in figure 4.7.

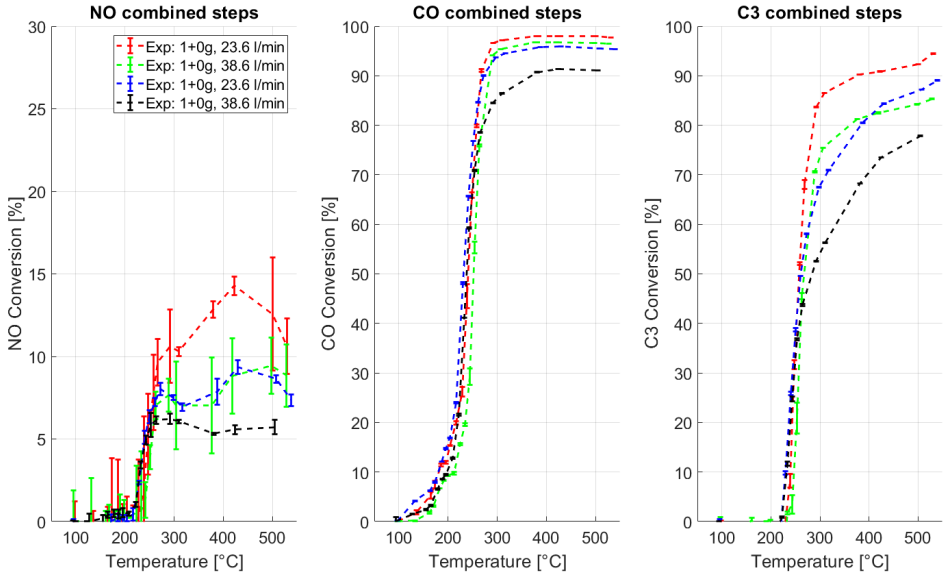

Figure 4.7: *Light-off curves for multi-component experiments. Left: NO. Middle: CO. Left: HC lumped as C_3H_6*

.

First of all, in the leftmost graph, it can bee seen that the error bars are unusually large compared to that of figure 4.6. Secondly, as hydrocarbon adsorption is not included in the model, but is likely apparent in the experimental data, CO adsorption had to act to inhibit the surface to explain the higher temperature required for CO oxidation. This led to CO oxidation separately would also occur at that same high temperature, which was not observed experimentally. The huge NO inlet concentration of roughly 1000 ppm also likely adsorbs to inhibit the reactions, again, something that is not included in the kinetic model - further forcing CO or NO_2 to inhibit the surface in the model. As CO has so strongly inhibited the surface - as soon as it desorbs even slightly the model predicted a too sharp light-off for all reactants in the multi-component step experiments.

There are also several issues with including $C_{10}H_{22}$ as a reactant. Firstly, Liu et al [94] reported that NO_x in the presence of $C_{10}H_{22}$, or even C_3H_6 (though stronger effect for higher carbon number), will produce a strong non-catalytic gas phase reaction - thus completely changing the catalyst inlet conditions. This effect showed a sharp consumption consumption of NO_x and $C_{10}H_{22}$ (roughly 67% of $C_{10}H_{22}$) at temperatures exceeding $350°C$. One could argue that this effect is visible in the right-most graph where the slope of the curve increases again at around $350 - 400°C$. As the SCAT bench only measures the outlet concentrations during the experiments (the desired gas mixtures are established before inserting the catalyst, at non-reacting, low temperature conditions) the inlet concentration for the catalyst is unknown. This effect would be even more pronounced in a premixed SCAT bench design where reactants are mixed together at an earlier stage compared to the injection-based SCAT bench design. While this gas phase reaction could easily be dealt with, the tedious experiments of running the SCAT rig without a catalyst sample to account for this effect were not performed, and so these multi-component experiments are unfortunately ruined. An alternative would be to perform the parameter estimation again and remove the data above these temperature threshold. Another issue would be the carbon number. Satsuma et al [95] showed the effect of carbon number on the light-off characteristics and found an almost two-step behaving light-off curve for longer hydrocarbons especially for alkenes. This might be caused by some reaction intermediate changes the activity for some specific part of the temperature span. Since all hydrocarbons are treated as C_3H_6 in the kinetic model, this effect would not be captured.

To exclude these effects that the multi-component step experiments would have on the parameter estimation, only the single-component experiments were included in the tuning. The final fit for NO, CO and C_3H_6 oxidation can be seen in figures 4.8, 4.9 and 4.10. For NO oxidation, the fit is just as good as in paper IV, where the trends and differences between each experiment were captured excellently. Similarly, the trends for the hydrocarbon oxidation is also captured well - with respect to light-off temperature and differences in conversion due to mass transfer limitations and residence time. There are some differences in the span $200 - 300°C$ where the experimental curves flatten out earlier than the simulations. Again, this might be due to some reaction intermediate the is not captured in the kinetic model or possible due to a change in noble metal oxidation state. This is where the application of the model is important. If the capturing the light-off temperature is the most important aspect of your EATS model this will do fine, but, if the EATS is operated frequently at elevated temperatures ($T > 200°C$) it might need further tuning or a different weight function for the experimental observations (as further explained in paper IV). Lastly, the CO light-off could be better. While the light-off temperature is captured decently, the model predicts a lowered conversion at higher temperatures. This is likely due to the first differential experimental data point for the black and blue curve. These specific data points gives high weight to the sum of squares error of the parameter estimation algorithm and the resulting model light-off curve is incredibly steep. This leads to CO desorbing very quickly and the surface is predicted to be almost free from CO at temperatures above $200°C$. Due to the lack of an Eley-Rideal type of CO oxidation mechanism the conversion goes down according to

the model. It would be interesting to perform the parameter estimation with a different weight to the above mentioned data point for the black and blue curves or to add a new mechanism for CO oxidation.

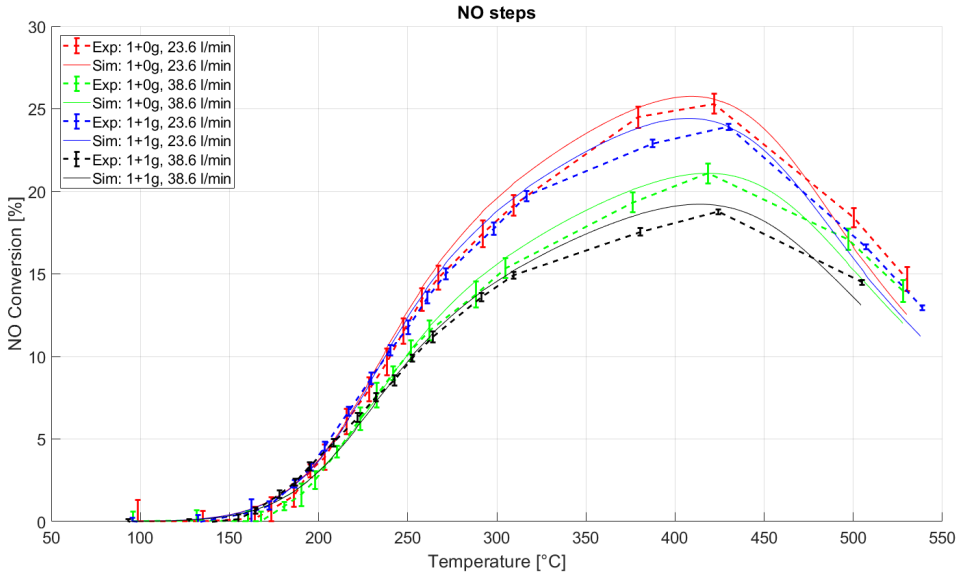

Figure 4.8: *Single-component light-off for NO*

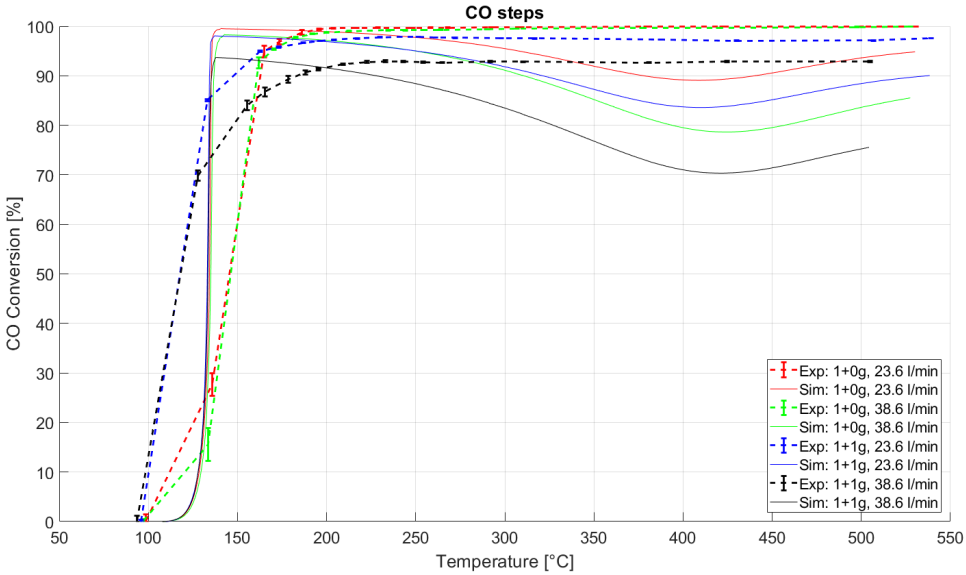

Figure 4.9: *Single-component light-off for CO*

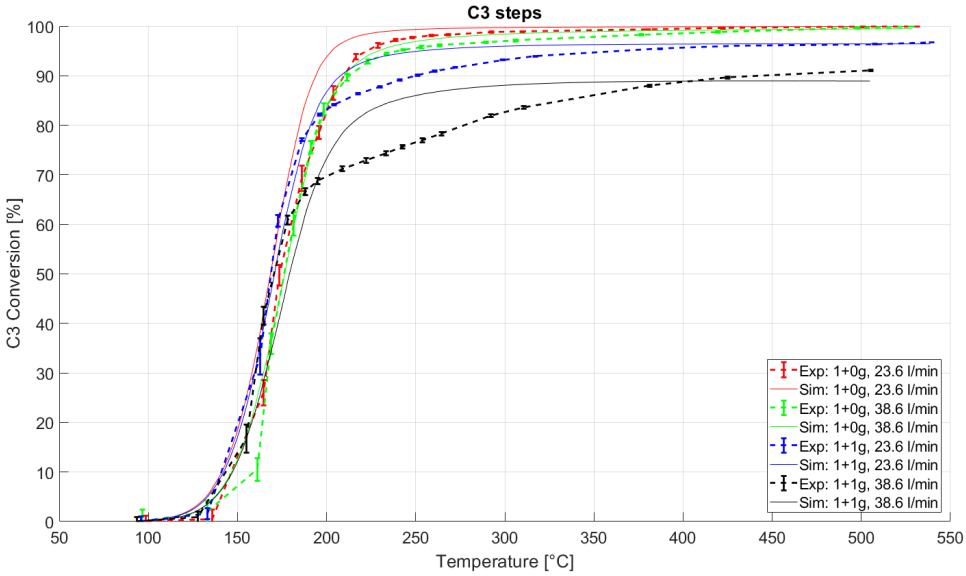

Figure 4.10: *Single-component light-off for C_3H_6*

5 Conclusion and Outlook

This thesis has been dedicated towards developing a predictive DOC reactor model using various experiments along with a robust tuning algorithm. The conclusions made regard both practical aspects around model tuning and design of experiments, but also general findings about NO oxidation using experiments and simulations.

From publications II and IV, it is evident that the NO oxidation on a $Pt/\gamma\text{-}Al_2O_3$ DOC experiences several operating limitations, relevant for actual driving conditions, that need to be modelled with great care. The limitations became the most evident in paper IV, in the cases where the tuned tortuosity ended up close to its lower limit ($\tau > 1$), the simulations did not capture the differences in conversion between 300 and 450°C. The DOCs tested in paper IV experienced kinetic, internal mass transfer and external mass transfer control - as well as many combinations of these regions. The tuning procedure in paper IV showed that many different cases, resulting in different parameter sets with very different time scales, achieved an acceptable residual. This means that there is not enough sensitivity in the experimental data to support one local minima, i.e. further experiments would be needed to tune the model and achieve better separation of mass transport phenomena and kinetics. As discussed in the final results within this thesis, it would be highly interesting to investigate a potential gas phase reaction between NO_x and HC and to further include multi-component reactions. This would be vital to get any realistic model that could be applied to real EATS applications with real exhaust gas.

It could also be that the used weight function forced a better fit at lower temperatures and that a more even distribution of temperatures would achieve a single local minima. The various experiments used proved to be invaluable. For example, the immense sensitivity of the noble metal dispersion was circumvented by employing chemisorption measurements. Hence, any differences in conversion could not be explained by a difference in total amount of active catalytic material. Furthermore, the IGA achieved a much more suitable starting point for tuning of the internal mass transfer rate than typical literature values. However, it would be interesting to see how the IGA results compare to alternative methods such as the classical Wicke-Kallenbach cell or chromatographic methods. Lastly, the use of an inert washcoat showed to be the most important experiment - as the variation of the effective diffusion length scale was vital to achieve good sensitivity for the tortuosity parameter. Simply by looking at the spread of the steady state data from the European stationary cycle, it can easily be concluded that using such a set of data for any tuning would have problems with tuning kinetics. For example, tuning a model with global kinetics that doesn't account for mass transfer phenomena would not capture intrinsic kinetics - leading to completely wrong cold start performances. Hence, having dedicated experiments covering a large operating span is important.

The developed mixer for the SCAT reactor showed a very inconsistent importance. On one hand, the core tests (presented in paper I) showed that there indeed was a large difference in inlet concentrations for different radial positions. On the other hand,

the fully active monolith showed very little differences for smaller reactants while only $C_{10}H_{22}$ showed differences with and without the mixer. This could be due to inconsistent positioning of the capillaries and the results are just mere coincidence. Regardless, since the core testing showed big problems with radial maldistributions the use of a mixer would always ensure proper validation of the single channel assumption for concentration.

The parallel model showed big promise early on in the project as several SEM images showed both increased washcoat thicknesses in the corners coupled with large cracks or pits. As the parallel model showed no significant sensitivity to local washcoat properties if the washcoat was uniformly distributed, and as the other catalysts used paper IV showed no problems with washcoat distributions, the parallel model remains more of a academic interest. Perhaps there are several uses for coated monolith reactors where the washcoat loading indeed results in a non-uniform distribution which calls for the use of a sectionalizing principle. One must not forget that square channels are not the only used channel geometry. Also, in any reactor that needs a thicker washcoat due to benefits in selectivity, the parallel model could still be useful. An alternative experimental procedure to isolate the corner effects in the case of high washcoat loading would be to use a round channel.

One major limitation of the current reactor model, when it comes to the kinetics, is the lack of a variable oxidation state for the noble metal. Since the SCAT experiments are conducted at a steady temperature, for roughly 30 minutes before moving on to the next one, it is possible that the oxidation state changes slowly between the first and last experimental point for that specific temperature. However, no time-dependent trends were ever found within each temperature point. That means that the oxidation state might be circumvented with the short step experiments that were conducted, or that the timescale for the oxidation state is even longer than 30 minutes. It would be highly interesting to investigate what the timescales are and what effects the oxidation state - e.g. temperature, inlet concentrations, pre-treatment and reaction time. Furthermore, it would be interesting to see whether different reactions exhibit stronger dependence on the oxidation state - and how large the differences really are compared to a case where the oxidation state is assumed to be constant.

Another obvious aspect to investigate would be catalyst aging state. As of now, all catalysts are prepared using the same method and all catalysts are pre-treated in the same way (for each experiment type). It would be interesting to compare synthetically aged, on-road aged as well as fresh catalyst sample to see what happens with dispersion (chemisorption), diffusion parameters (IGA and SEM) as well as reactivity (SCAT).

6 Contribution to the field

This main contribution of this work can be summarized as:

6.1 Publication I

"Use of 3D-printed mixers in laboratory reactor design for modelling of heterogeneous catalytic converters"

Validation of boundary conditions is of utmost importance - no matter the discipline. The novelty in this work comes from the smart way of identifying radial concentration maldistributions where local measurements are not possible. The modified SMX mixer assembled through additive manufacturing in α-Al_2O_3, having the reactant injection point in the turbulent wake of the mixer, is also new. I was responsible for designing the experiment, catalysts and the mixer - as well as writing the paper, analyzing the kinetic data and performing the dispersion calculations.

6.2 Publication II

"Efficient Experimental Approach to Evaluate Mass Trans-fer Limitations for Monolithic DOCs"

Experimental screening and its associated analysis, is of importance for time efficient experimental campaigns. These types of screenings have been done by others, however, the novelty here comes from using a sufficiently thin washcoat for one of the experiments - so that its reaction time scales can be carried over to the DOC with thick washcoat. Otherwise some modelling of reaction time scales would have been required. I was responsible for design of experiments, analysis as well as writing the paper.

6.3 Publication III

"Modelling of mass-transfer resistances in non-uniformly washcoated monolith reactors"

The often disregarded and erroneous assumption, regarding an axissymetric washcoat formulation, is typically found in all papers for 2D single-channel models. The novelty here comes from trying to circumvent this problem by resorting to the sectionalizing principle. Also, the combined use of IGA and SEM to tune a local effective diffusivity is also new. I was responsible for developing the idea, performing IGA experiments and analysis of SEM images, the modelling itself and lastly writing the paper.

6.4 Publication IV

"Robust parameter estimation methodology for heterogeneous catalytic reactors"

Generally in heterogeneous catalysis modelling, authors very rarely reveal findings on parameter tuning. The novelty is not the employed RSM method, which can be found in many different fields, but its application to EATS modelling. Showing several useful practical aspects on parameter estimation; whether there are significant interaction effects, what scaling and parameter variation is suitable, the importance of the dedicated experiments with inert washcoat and the importance of a temperature dependent weight function - should be highly interesting for the reader. I was responsible for developement and implementation of the RSM model into the main Matlab code, tuning exercises, analysis of results and finally writing and producing graphs.

Bibliography

[1] April Russell and William S. Epling. "Diesel Oxidation Catalysts". In: *Catalysis Reviews* 53.4 (2011), pp. 337–423. ISSN: 0161-4940. DOI: 10.1080/01614940.2011.596429. URL: https://doi.org/10.1080/01614940.2011.596429.

[2] European Environmental Agency (EEA). *Sulphur dioxide (SO2) emissions*. 2015. URL: https://www.eea.europa.eu/data-and-maps/indicators/eea-32-sulphur-dioxide-so2-emissions-1/assessment-3 (visited on 01/07/2020).

[3] Louise W. Kao and Kristine A. Nañagas. "Toxicity Associated with Carbon Monoxide". In: *Clinics in Laboratory Medicine* 26.1 (2006). Clinical Toxicology, pp. 99 –125. ISSN: 0272-2712. DOI: https://doi.org/10.1016/j.cll.2006.01.005. URL: http://www.sciencedirect.com/science/article/pii/S0272271206000060.

[4] Theo M.C.M. de Kok, Hermen A.L. Driece, Janneke G.F. Hogervorst, and Jacob J. Briedé. "Toxicological assessment of ambient and traffic-related particulate matter: A review of recent studies". In: *Mutation Research/Reviews in Mutation Research* 613.2 (2006), pp. 103 –122. ISSN: 1383-5742. DOI: https://doi.org/10.1016/j.mrrev.2006.07.001. URL: http://www.sciencedirect.com/science/article/pii/S1383574206000433.

[5] Organization World Health. *Ambient air pollution: a global assessment of exposure and burden of disease*. Geneva: World Health Organization, 2016. ISBN: 9789241511353. URL: https://apps.who.int/iris/handle/10665/250141.

[6] Richard Fuller, Philip J Landrigan, Kalpana Balakrishnan, Glynda Bathan, Stephan Bose-O'Reilly, Michael Brauer, Jack Caravanos, Tom Chiles, Aaron Cohen, Lilian Corra, Maureen Cropper, Greg Ferraro, Jill Hanna, David Hanrahan, Howard Hu, David Hunter, Gloria Janata, Rachael Kupka, Bruce Lanphear, Maureen Lichtveld, Keith Martin, Adetoun Mustapha, Ernesto Sanchez-Triana, Karti Sandilya, Laura Schaefli, Joseph Shaw, Jessica Seddon, William Suk, Martha María Téllez-Rojo, and Chonghuai Yan. "Pollution and health: a progress update". In: *The Lancet Planetary Health* (2022). ISSN: 2542-5196. DOI: https://doi.org/10.1016/S2542-5196(22)00090-0. URL: https://www.sciencedirect.com/science/article/pii/S2542519622000900.

[7] Roger O. McClellan, Thomas W. Hesterberg, and John C. Wall. "Evaluation of carcinogenic hazard of diesel engine exhaust needs to consider revolutionary changes in diesel technology". In: *Regulatory Toxicology and Pharmacology* 63.2 (2012), pp. 225 –258. ISSN: 0273-2300. DOI: https://doi.org/10.1016/j.yrtph.2012.04.005. URL: http://www.sciencedirect.com/science/article/pii/S0273230012000694.

[8] Martyn V. Twigg. "Rôles of catalytic oxidation in control of vehicle exhaust emissions". In: *Catalysis Today* 117.4 (2006). Selected papers presented at the 6th International Workshop on Catalytic Combustion, pp. 407 –418. ISSN: 0920-5861. DOI: https://doi.org/10.1016/j.cattod.2006.06.044. URL: http://www.sciencedirect.com/science/article/pii/S0920586106004196.

[9] V.I. Pârvulescu, P. Grange, and B. Delmon. "Catalytic removal of NO". In: *Catalysis Today* 46.4 (1998), pp. 233 –316. ISSN: 0920-5861. DOI: https://doi.org/10.1016/S0920-5861(98)00399-X. URL: http://www.sciencedirect.com/science/article/pii/S092058619800399X.

[10] Susan C. Anenberg, Joshua Miller, Ray Minjares, Li Du, Daven K. Henze, Forrest Lacey, Christopher S. Malley, Lisa Emberson, Vicente Franco, Zbigniew Klimont, and Chris Heyes. "Impacts and mitigation of excess diesel-related NOx emissions in 11 major vehicle markets". In: *Nature* 545.7655 (May 2017), pp. 467–471. DOI: 10.1038/nature22086. URL: https://doi.org/10.1038/nature22086.

[11] P. G. Rogers. "The Clean Air Act of 1970". In: *EPA Journal* 16.1 (1970), pp. 21 –23. URL: https://www.epa.gov/history/epa-history-clean-air-act-19701977.

[12] "COUNCIL DIRECTIVE of 20 March 1970 on the approximation of the laws of the Member States relating to measures to be taken against air pollution by gases from positive-ignition engines of motor vehicles". In: *Official Journal of the European Union* 1 (1970), pp. 171 –191. URL: https://eur-lex.europa.eu/legal-content/EN/ALL/?uri=CELEX:31970L0220.

[13] S. C. Davis and R. G. Boundy. *Transportation Energy Data Book*. English. Oak Ridge National Laboratory, Aug. 2019.

[14] Barbara Hoffmann, Nathalie Roebbel, Sophie Gumy, Francesco Forastiere, Bert Brunekreef, Dorota Jarosinska, Katherine D. Walker, Annemoon M. van Erp, Robert O'Keefe, Dan Greenbaum, Martin Williams, Michal Krzyzanowski, Frank J. Kelly, Michael Brauer, Hans Bruyninckx, and Hanna Boogaard. "Air pollution and health: recent advances in air pollution epidemiology to inform the European Green Deal: a joint workshop report of ERS, WHO, ISEE and HEI". In: *European Respiratory Journal* 56.5 (2020). ISSN: 0903-1936. DOI: 10.1183/13993003.02575-2020. eprint: https://erj.ersjournals.com/content/56/5/2002575.full.pdf. URL: https://erj.ersjournals.com/content/56/5/2002575.

[15] M. V Twigg and Imperial Chemical Industries PLC. Agricultural Division. Catalyst handbook. *Catalyst handbook*. 2nd ed. London : Manson Pub, 1996. ISBN: 1874545359. URL: http://www.loc.gov/catdir/enhancements/fy0638/97216179-t.html.

[16] Masaoki Iwasaki and Hirofumi Shinjoh. "A comparative study of "standard", "fast" and "NO2" SCR reactions over Fe/zeolite catalyst". In: *Applied Catalysis A: General* 390.1 (2010), pp. 71 –77. ISSN: 0926-860X. DOI: https://doi.org/10.1016/j.apcata.2010.09.034. URL: http://www.sciencedirect.com/science/article/pii/S0926860X10006885.

[17] Kanta Yamamoto, Keishi Takada, Jin Kusaka, Yasuharu Kanno, and Makoto Nagata. "Influence of Diesel Post Injection Timing on HC Emissions and Catalytic Oxidation Performance". In: *Powertrain Fluid Systems Conference and Exhibition*. SAE International, 2006. DOI: https://doi.org/10.4271/2006-01-3442. URL: https://doi.org/10.4271/2006-01-3442.

[18] P. Ehrburger, J.-F. Brilhac, Y. Drouillot, V. Logie, and P. Gilot. "Reactivity of Soot With Nitrogen Oxides in Exhaust Stream". In: *Spring Fuels Lubricants Meeting Exhibition*. SAE International, 2002. DOI: https://doi.org/10.4271/2002-01-1683. URL: https://doi.org/10.4271/2002-01-1683.

[19] Sung Dae Yim, Soo Jean Kim, Joon Hyun Baik, InSik Nam, Young Sun Mok, Jong-Hwan Lee, Byong K. Cho, and Se H. Oh. "Decomposition of Urea into NH3 for the SCR Process". In: *Industrial & Engineering Chemistry Research* 43.16 (2004), pp. 4856–4863. DOI: 10.1021/ie034052j. URL: https://doi.org/10.1021/ie034052j.

[20] Massimo Colombo, Isabella Nova, Enrico Tronconi, Volker Schmeißer, Brigitte Bandl-Konrad, and Lisa Zimmermann. "Experimental and modeling study of a dual-layer (SCR+PGM) NH3 slip monolith catalyst (ASC) for automotive SCR aftertreatment systems. Part 1. Kinetics for the PGM component and analysis of SCR/PGM interactions". In: *Applied Catalysis B: Environmental* 142-143 (2013), pp. 861 –876. ISSN: 0926-3373. DOI: https://doi.org/10.1016/j.apcatb.2012.10.031. URL: http://www.sciencedirect.com/science/article/pii/S0926337312005103.

[21] J. J. Berzelius. *Årsberättelse om framstegen i Fysik och Kemi*. P. A. Norstedt Söner, 1835. URL: https://books.google.se/books/about/\%C3\%85rsber\%C3\%A4ttelse_om_framstegen_i_fysik_oc.html?id=1DM1AAAAcAAJ&redir_esc=y.

[22] A. J. B. Robertson. "The Early History of Catalysis". In: *Platinum Metals Review* 19 (2 1975), pp. 64 –69. URL: https://www.technology.matthey.com/article/19/2/64-69/.

[23] "VIII. Some new experiments and observations on the combustion of gaseous mixtures, with an account of a method of preserving a continued light in mixtures of inflammable gases and air without flame". In: *Philosophical Transactions of the Royal Society of London* 107 (Jan. 1817), pp. 77–85. DOI: 10.1098/rstl.1817.0009. URL: https://doi.org/10.1098/rstl.1817.0009.

[24] I. Chorkendorff. *Concepts of Modern Catalysis and Kinetics*. Wiley-VCH, 2003. ISBN: 3527305742. URL: https://www.xarg.org/ref/a/3527305742/.

[25] Zeynep Ilsen Önsan and Ahmet Kerim Avci. "Monolith reactors". In: *Multiphase Catalytic Reactors - Theory, Design, Manufacturing, and Applications*. John Wiley Sons, 2016. ISBN: 978-1-118-11576-3. URL: https://app.knovel.com/hotlink/pdf/id:kt011BVFG1/multiphase-catalytic/performance-evaluation.

[26] Xiaobo Song, Jeffrey D Naber, and John H Johnson. “A study of the effects of NH3 maldistribution on a urea-selective catalytic reduction system”. In: *International Journal of Engine Research* 16.2 (2015), pp. 213–222. DOI: 10.1177/1468087414532462. URL: https://doi.org/10.1177/1468087414532462.

[27] Leonardo Giani, Gianpiero Groppi, and Enrico Tronconi. “Mass-Transfer Characterization of Metallic Foams as Supports for Structured Catalysts”. In: *Industrial & Engineering Chemistry Research* 44.14 (2005), pp. 4993–5002. DOI: 10.1021/ie0490886. URL: https://doi.org/10.1021/ie0490886.

[28] Pranit S. Metkar, Vemuri Balakotaiah, and Michael P. Harold. “Experimental study of mass transfer limitations in Fe- and Cu-zeolite-based NH3-SCR monolithic catalysts”. In: *Chemical Engineering Science* 66.21 (2011), pp. 5192–5203. ISSN: 00092509. DOI: 10.1016/j.ces.2011.07.014.

[29] Jinwen Chen, Hong Yang, Neil Wang, Zbigniew Ring, and Tadeusz Dabros. “Mathematical modeling of monolith catalysts and reactors for gas phase reactions”. In: *Applied Catalysis A: General* 345.1 (2008), pp. 1–11. ISSN: 0926-860X. DOI: https://doi.org/10.1016/j.apcata.2008.04.010. URL: http://www.sciencedirect.com/science/article/pii/S0926860X08002251.

[30] Shaibal Roy, Tobias Bauer, Muthanna Al-Dahhan, Peter Lehner, and Thomas Turek. “Monoliths as multiphase reactors: A review”. In: *AIChE Journal* 50 (2004), pp. 2918–2938. DOI: 10.1002/aic.10268.

[31] C. Depcik and A. Srinivasan. “One + One-Dimensional Modeling of Monolithic Catalytic Converters”. In: *Chemical Engineering Technology* 34.12 (2011), pp. 1949–1965. ISSN: 09307516. DOI: 10.1002/ceat.201100144.

[32] Anke Güthenke, Daniel Chatterjee, Michel Weibel, Bernd Krutzsch, Petr Kočí, Miloš Marek, Isabella Nova, and Enrico Tronconi. “Current status of modeling lean exhaust gas aftertreatment catalysts”. In: *Advances in Chemical Engineering*. Ed. by Guy B. Marin. Vol. 33. Academic Press, 2007, pp. 103–283. ISBN: 0065-2377. DOI: https://doi.org/10.1016/S0065-2377(07)33003-2. URL: http://www.sciencedirect.com/science/article/pii/S0065237707330032.

[33] Vladimír Novák, Petr Kočí, Tomáš Gregor, Jae-Soon Choi, František Štěpánek, and Miloš Marek. “Effect of cavities and cracks on diffusivity in coated catalyst layer”. In: *Catalysis Today* 216 (2013), pp. 142–149. ISSN: 0920-5861. DOI: https://doi.org/10.1016/j.cattod.2013.07.002. URL: http://www.sciencedirect.com/science/article/pii/S092058611300326X.

[34] Jonathan Stewart, Roy Douglas, and Alexandre Goguet. “Integrating intrinsic and global kinetics as a dual kinetic model for automotive catalysis”. In: *Proceedings of the Institution of Mechanical Engineers, Part D: Journal of Automobile Engineering* 228.3 (2014), pp. 285–294. DOI: 10.1177/0954407013508379. eprint: https://doi.org/10.1177/0954407013508379. URL: https://doi.org/10.1177/0954407013508379.

[35] Sterling E. Voltz, Charles R. Morgan, David Liederman, and Solomon M. Jacob. "Kinetic Study of Carbon Monoxide and Propylene Oxidation on Platinum Catalysts". In: *Product RD* 12.4 (1973), pp. 294–301. ISSN: 0091-1968. DOI: 10.1021/i360048a006. URL: https://doi.org/10.1021/i360048a006.

[36] Francois Lafossas, Yoshifumi Matsuda, Ali Mohammadi, Akinori Morishima, Mikio Inoue, Maria Kalogirou, Grigorios Koltsakis, and Zissis Samaras. *Calibration and Validation of a Diesel Oxidation Catalyst Model: from Synthetic Gas Testing to Driving Cycle Applications*. 2011. DOI: https://doi.org/10.4271/2011-01-1244. URL: https://doi.org/10.4271/2011-01-1244.

[37] G.P. Ansell, P.S. Bennett, J.P. Cox, J.C. Frost, P.G. Gray, A.-M. Jones, R.R. Rajaram, A.P. Walker, M. Litorell, and G. Smedler. "The development of a model capable of predicting diesel lean NOx catalyst performance under transient conditions". In: *Applied Catalysis B: Environmental* 10.1 (1996), pp. 183 –201. ISSN: 0926-3373. DOI: https://doi.org/10.1016/0926-3373(96)00030-6. URL: http://www.sciencedirect.com/science/article/pii/0926337396000306.

[38] Timothy C. Watling, Mehrdad Ahmadinejad, Monica Ţuţuianu, Åsa Johansson, and Michael A.J. Paterson. *Development and Validation of a Pt-Pd Diesel Oxidation Catalyst Model*. 2012. DOI: https://doi.org/10.4271/2012-01-1286. URL: https://doi.org/10.4271/2012-01-1286.

[39] Adéla Buzková Arvajová, Panagiotis Boutikos, Rudolf Pečinka, and Petr Kočí. "Global kinetic model of NO oxidation on Pd/-Al2O3 catalyst including PdOx formation and reduction by CO and C3H6". In: *Applied Catalysis B: Environmental* 260 (2020), p. 118141. ISSN: 0926-3373. DOI: https://doi.org/10.1016/j.apcatb.2019.118141. URL: https://www.sciencedirect.com/science/article/pii/S0926337319308884.

[40] Se H. Oh and James C. Cavendish. "Transients of monolithic catalytic converters. Response to step changes in feedstream temperature as related to controlling automobile emissions". In: *Industrial Engineering Chemistry Product Research and Development* 21.1 (1982), pp. 29–37. ISSN: 0196-4321. DOI: 10.1021/i300005a006. URL: https://doi.org/10.1021/i300005a006.

[41] James A. Dumesic. *The Microkinetics of Heterogeneous Catalysis (ACS Professional Reference Book)*. American Chemical Society, 1993. ISBN: 0841222142. URL: https://www.xarg.org/ref/a/0841222142/.

[42] I.A.W. Filot. *Introduction to microkinetic modeling*. English. Technische Universiteit Eindhoven, Dec. 2018. ISBN: 978-90-386-4520-9.

[43] Louise Olsson, Erik Fridell, Magnus Skoglundh, and Bengt Andersson. "Mean field modelling of NOx storage on Pt/BaO/Al2O3". In: *Catalysis Today* 73.3 (2002). Environmental Catalysis, pp. 263 –270. ISSN: 0920-5861. DOI: https://doi.org/10.1016/S0920-5861(02)00009-3. URL: http://www.sciencedirect.com/science/article/pii/S0920586102000093.

[44] S. Salomons, M. Votsmeier, R.E. Hayes, A. Drochner, H. Vogel, and J. Gieshof. "CO and H2 oxidation on a platinum monolith diesel oxidation catalyst". In: *Catalysis Today* 117.4 (2006). Selected papers presented at the 6th International Workshop on Catalytic Combustion, pp. 491 –497. ISSN: 0920-5861. DOI: https://doi.org/10.1016/j.cattod.2006.06.001. URL: http://www.sciencedirect.com/science/article/pii/S0920586106003683.

[45] L. Olsson, B. Westerberg, H. Persson, E. Fridell, M. Skoglundh, and B. Andersson. "A Kinetic Study of Oxygen Adsorption/Desorption and NO Oxidation over Pt/Al2O3 Catalysts". In: *Journal of Physical Chemistry B* 103.47 (1999). cited By 167, pp. 10433–10439. URL: https://www.scopus.com/inward/record.uri?eid=2-s2.0-0033604675&partnerID=40&md5=dcfb66ff8029ec281d5e34ce25c7bc2b.

[46] H. S. Fogler. "Chapter 18 - Models for Nonideal Reactors". In: *Elements of Chemical Reaction Engineering*. Prentice Hall PTR, 2006, pp. 848–849. ISBN: 0130473944.

[47] I. Cornejo, P. Nikrityuk, and R. E. Hayes. "Turbulence Decay Inside the Channels of an Automotive Catalytic Converter Monolith". In: *Emission Control Science and Technology* 3.4 (2017), pp. 302–309. ISSN: 2199-3629 2199-3637. DOI: 10.1007/s40825-017-0070-6.

[48] Enrico Tronconi and Pio Forzatti. "Adequacy of lumped parameter models for SCR reactors with monolith structure". In: 38.2 (1992), pp. 201–210. DOI: doi:10.1002/aic.690380205. URL: https://onlinelibrary.wiley.com/doi/abs/10.1002/aic.690380205.

[49] A. Holmgren and B. Andersson. "Mass transfer in monolith catalysts–CO oxidation experiments and simulations". In: *Chemical Engineering Science* 53.13 (1998), pp. 2285 –2298. ISSN: 0009-2509. DOI: https://doi.org/10.1016/S0009-2509(98)00080-3. URL: http://www.sciencedirect.com/science/article/pii/S0009250998000803.

[50] G. Groppi, W. Ibashi, M. Valentini, and P. Forzatti. "High-temperature combustion of CH4 over PdO/Al2O3: kinetic measurements in a structured annular reactor". In: *Chemical Engineering Science* 56.3 (2001), pp. 831–839. ISSN: 0009-2509. DOI: https://doi.org/10.1016/S0009-2509(00)00295-5. URL: http://www.sciencedirect.com/science/article/pii/S0009250900002955.

[51] St Walter, St Malmberg, B. Schmidt, and M. A. Liauw. "Mass transfer limitations in microchannel reactors". In: *Catalysis Today* 110.1 (2005), pp. 15–25. ISSN: 0920-5861. DOI: https://doi.org/10.1016/j.cattod.2005.09.019. URL: http://www.sciencedirect.com/science/article/pii/S0920586105006310.

[52] M. Walander, J. Sjöblom, D. Creaser, B. Lundberg, S. Tamm, and J. Edvardsson. "Efficient Experimental Approach to Evaluate Mass Transfer Limitations for Monolithic DOCs". In: *Topics in Catalysis* 62.1 (2019), pp. 391–396. ISSN: 1572-9028. DOI: 10.1007/s11244-018-1111-2. URL: https://doi.org/10.1007/s11244-018-1111-2.

[53] R. E. Hayes and S. T. Kolaczkowski. “Mass and heat transfer effects in catalytic monolith reactors”. In: *Chemical Engineering Science* 49.21 (1994), pp. 3587–3599. ISSN: 0009-2509. DOI: https://doi.org/10.1016/0009-2509(94)00164-2. URL: http://www.sciencedirect.com/science/article/pii/0009250994001642.

[54] N. Mladenov, J. Koop, S. Tischer, and O. Deutschmann. “Modeling of transport and chemistry in channel flows of automotive catalytic converters”. In: *Chemical Engineering Science* 65.2 (2010), pp. 812–826. ISSN: 0009-2509. DOI: https://doi.org/10.1016/j.ces.2009.09.034. URL: http://www.sciencedirect.com/science/article/pii/S000925090900637X.

[55] R. E. Hayes, B. Liu, and M. Votsmeier. “Calculating effectiveness factors in non-uniform washcoat shapes”. In: *Chemical Engineering Science* 60.7 (2005), pp. 2037–2050. ISSN: 0009-2509. DOI: https://doi.org/10.1016/j.ces.2004.11.041. URL: http://www.sciencedirect.com/science/article/pii/S0009250904008954.

[56] R. E. Hayes, B. Liu, R. Moxom, and M. Votsmeier. “The effect of washcoat geometry on mass transfer in monolith reactors”. In: *Chemical Engineering Science* 59.15 (2004), pp. 3169–3181. ISSN: 0009-2509. DOI: https://doi.org/10.1016/j.ces.2004.05.002. URL: http://www.sciencedirect.com/science/article/pii/S0009250904002830.

[57] Saurabh Y. Joshi, Michael P. Harold, and Vemuri Balakotaiah. “On the use of internal mass transfer coefficients in modeling of diffusion and reaction in catalytic monoliths”. In: *Chemical Engineering Science* 64.23 (2009), pp. 4976–4991. ISSN: 00092509. DOI: 10.1016/j.ces.2009.08.008.

[58] D. Papadias, L. Edsberg, and P. Björnbom. “Simplified method of effectiveness factor calculations for irregular geometries of washcoats: A general case in a 3D concentration field”. In: *Catalysis Today* 60.1 (2000), pp. 11–20. ISSN: 0920-5861. DOI: https://doi.org/10.1016/S0920-5861(00)00312-6. URL: http://www.sciencedirect.com/science/article/pii/S0920586100003126.

[59] Björn Lundberg, Jonas Sjöblom, Åsa Johansson, Björn Westerberg, and Derek Creaser. “DOC modeling combining kinetics and mass transfer using inert washcoat layers”. In: *Applied Catalysis B: Environmental* 191 (2016), pp. 116–129. ISSN: 09263373. DOI: 10.1016/j.apcatb.2016.03.024.

[60] Björn Lundberg, Jonas Sjoblom, Åsa Johansson, Björn Westerberg, and Derek Creaser. “Parameter Estimation of a DOC from Engine Rig Experiments with a Discretized Catalyst Washcoat Model”. In: *SAE International Journal of Engines* 7.2 (2014), pp. 1093–1112. ISSN: 1946-3944. DOI: 10.4271/2014-01-9049.

[61] David Kryl, Petr Kočí, Milan Kubíček, Miloš Marek, Teuvo Maunula, and Matti Härkönen. “Catalytic Converters for Automobile Diesel Engines with Adsorption of Hydrocarbons on Zeolites”. In: *Industrial Engineering Chemistry Research*

44.25 (2005), pp. 9524–9534. ISSN: 0888-5885. DOI: 10.1021/ie050249v. URL: https://doi.org/10.1021/ie050249v.

[62] Petr Kočí, Miloš Marek, Milan Kubíček, Teuvo Maunula, and Matti Härkönen. "Modelling of catalytic monolith converters with low- and high-temperature NOx storage compounds and differentiated washcoat". In: *Chemical Engineering Journal* 97.2 (2004), pp. 131–139. ISSN: 1385-8947. DOI: https://doi.org/10.1016/S1385-8947(03)00151-7. URL: http://www.sciencedirect.com/science/article/pii/S1385894703001517.

[63] A. Wheeler. "Catalysis". In: ed. by Paul H. Emmett. Vol. 2. New York: Reinhold Publishing Corporation, 1955. Chap. 2, p. 105. ISBN: 0095-9553. DOI: 10.1002/jps.3030440531. URL: https://onlinelibrary.wiley.com/doi/abs/10.1002/jps.3030440531.

[64] R. B. Evans, G. M. Watson, and E. A. Mason. "Gaseous Diffusion in Porous Media at Uniform Pressure". In: *The Journal of Chemical Physics* 35.6 (1961), pp. 2076–2083. DOI: 10.1063/1.1732211. eprint: https://doi.org/10.1063/1.1732211. URL: https://doi.org/10.1063/1.1732211.

[65] N. Wakao and J. M. Smith. "Diffusion in catalyst pellets". In: *Chemical Engineering Science* 17.11 (1962), pp. 825–834. ISSN: 0009-2509. DOI: https://doi.org/10.1016/0009-2509(62)87015-8. URL: http://www.sciencedirect.com/science/article/pii/0009250962870158.

[66] Marvin F.L. Johnson and Warren E. Stewart. "Pore structure and gaseous diffusion in solid catalysts". In: *Journal of Catalysis* 4.2 (1965), pp. 248 –252. ISSN: 0021-9517. DOI: https://doi.org/10.1016/0021-9517(65)90015-1. URL: http://www.sciencedirect.com/science/article/pii/0021951765900151.

[67] R. E. Hayes, S. T. Kolaczkowskib, P. K. C. Li, and S. Awdry. "Evaluating the effective diffusivity of methane in the washcoat of a honeycomb monolith". In: *Applied Catalysis B: Environmental* 25.2 (2000), pp. 93–104. ISSN: 0926-3373. DOI: https://doi.org/10.1016/S0926-3373(99)00122-8. URL: http://www.sciencedirect.com/science/article/pii/S0926337399001228.

[68] E. Poling Bruce, M. Prausnitz John, and P. O'Connell John. *Properties of Gases and Liquids, Fifth Edition*. 5th ed. New York: McGraw-Hill Education, 2001. ISBN: 9780070116825. URL: https://www.accessengineeringlibrary.com/content/book/9780070116825.

[69] Ramesh K. Sharma, David L. Cresswell, and Esmond J. Newson. "Effective diffusion coefficients and tortuosity factors for commercial catalysts". In: *Industrial Engineering Chemistry Research* 30.7 (1991), pp. 1428–1433. ISSN: 0888-5885. DOI: 10.1021/ie00055a004. URL: https://doi.org/10.1021/ie00055a004.

[70] Tomáš Starý, Olga Šolcová, Petr Schneider, and Miloš Marek. "Effective diffusivities and pore-transport characteristics of washcoated ceramic monolith for automotive

catalytic converter". In: *Chemical Engineering Science* 61.18 (2006), pp. 5934–5943. ISSN: 00092509. DOI: 10.1016/j.ces.2006.05.014.

[71] Douglas M. Ruthven. "Diffusion in type A zeolites: New insights from old data". In: *Microporous and Mesoporous Materials* 162 (2012), pp. 69–79. ISSN: 13871811. DOI: 10.1016/j.micromeso.2011.12.025.

[72] D. Papadias, L. Edsberg, and P. Björnbom. "Simplified method for effectiveness factor calculations in irregular geometries of washcoats". In: *Chemical Engineering Science* 55.8 (2000), pp. 1447–1459. ISSN: 0009-2509. DOI: https://doi.org/10.1016/S0009-2509(99)00375-9. URL: http://www.sciencedirect.com/science/article/pii/S0009250999003759.

[73] D. J. Gunn. "Diffusion and chemical reaction in catalysis and absorption". In: *Chemical Engineering Science* 22.11 (1967), pp. 1439–1455. ISSN: 0009-2509. DOI: https://doi.org/10.1016/0009-2509(67)80071-X. URL: http://www.sciencedirect.com/science/article/pii/000925096780071X.

[74] Vemuri Balakotaiah. "On the relationship between Aris and Sherwood numbers and friction and effectiveness factors". In: *Chemical Engineering Science* 63.24 (2008), pp. 5802–5812. ISSN: 00092509. DOI: 10.1016/j.ces.2008.08.025.

[75] P. Canu and S. Vecchi. "CFD simulation of reactive flows: Catalytic combustion in a monolith". In: *AIChE Journal* 48.12 (2004), pp. 2921–2935. DOI: 10.1002/aic.690481219. eprint: https://aiche.onlinelibrary.wiley.com/doi/pdf/10.1002/aic.690481219. URL: https://aiche.onlinelibrary.wiley.com/doi/abs/10.1002/aic.690481219.

[76] R. K. Shah and A. L. London. "Chapter VII - Rectangular Ducts". In: *Laminar Flow Forced Convection in Ducts*. Ed. by R. K. Shah and A. L. London. Academic Press, 1978, pp. 196–222. ISBN: 978-0-12-020051-1. DOI: https://doi.org/10.1016/B978-0-12-020051-1.50012-7. URL: http://www.sciencedirect.com/science/article/pii/B9780120200511500127.

[77] Carl-Robert Florén, Maxime Van den Bossche, Derek Creaser, Henrik Grönbeck, Per-Anders Carlsson, Heikki Korpi, and Magnus Skoglundh. "Modelling complete methane oxidation over palladium oxide in a porous catalyst using first-principles surface kinetics". In: *Catalysis Science Technology* 8.2 (2018), pp. 508–520. ISSN: 2044-4753 2044-4761. DOI: 10.1039/c7cy02135f.

[78] Henry J. Kelley. "Method of Gradients". In: *Optimization Techniques*. Ed. by George Leitmann. Vol. 5. Mathematics in Science and Engineering. Elsevier, 1962, pp. 205–254. DOI: https://doi.org/10.1016/S0076-5392(08)62094-9. URL: https://www.sciencedirect.com/science/article/pii/S0076539208620949.

[79] Jonas Sjöblom and Derek Creaser. "New approach for microkinetic mean-field modelling using latent variables". In: *Computers Chemical Engineering* 31.4 (2007), pp. 307–317. ISSN: 0098-1354. DOI: https://doi.org/10.1016/j.compchemeng.

2006.07.008. URL: https://www.sciencedirect.com/science/article/pii/S0098135406002006.

[80] A. Pandya, J. Mmbaga, R. E. Hayes, W. Hauptmann, and M. Votsmeier. "Global Kinetic Model and Parameter Optimization for a Diesel Oxidation Catalyst". In: *Topics in Catalysis* 52.13-20 (July 2009), pp. 1929–1933. DOI: 10.1007/s11244-009-9361-7. URL: https://doi.org/10.1007/s11244-009-9361-7.

[81] Tae-Yun Park and Gilbert F. Froment. "A hybrid genetic algorithm for the estimation of parameters in detailed kinetic models". In: *Computers Chemical Engineering* 22 (1998). European Symposium on Computer Aided Process Engineering-8, S103–S110. ISSN: 0098-1354. DOI: https://doi.org/10.1016/S0098-1354(98)00043-X. URL: https://www.sciencedirect.com/science/article/pii/S009813549800043X.

[82] Ericson Claes, Westerberg Björn, and Odenbrand Ingemar. *A State-Space Simplified SCR Catalyst Model for Real Time Applications*. technical-paper. 2008. DOI: 10.4271/2008-01-0616. URL: http://proxy.lib.chalmers.se/login?url=http://search.ebscohost.com/login.aspx?direct=true&db=edsstp&AN=edsstp.2008.01.0616&lang=sv&site=eds-live&scope=site.

[83] W. G. Pollard and R. D. Present. "On Gaseous Self-Diffusion in Long Capillary Tubes". In: *Phys. Rev.* 73 (7 1948), pp. 762–774. DOI: 10.1103/PhysRev.73.762. URL: https://link.aps.org/doi/10.1103/PhysRev.73.762.

[84] Martin Leskovjan, Petr Kočí, and Teuvo Maunula. "Simulation of diesel exhaust aftertreatment system DOC—pipe—SCR: The effects of Pt loading, PtOx formation and pipe configuration on the deNOx performance". In: *Chemical Engineering Science* 189 (2018), pp. 179–190. ISSN: 0009-2509. DOI: https://doi.org/10.1016/j.ces.2018.05.031. URL: https://www.sciencedirect.com/science/article/pii/S0009250918303282.

[85] Douglas J. Pritchard and David W. Bacon. "Prospects for reducing correlations among parameter estimates in kinetic models". In: *Chemical Engineering Science* 33.11 (1978), pp. 1539–1543. ISSN: 0009-2509. DOI: https://doi.org/10.1016/0009-2509(78)85205-1. URL: http://www.sciencedirect.com/science/article/pii/0009250978852051.

[86] D.J. Pritchard and D.W. Bacon. "Statistical assessment of chemical kinetic models". In: *Chemical Engineering Science* 30.5 (1975), pp. 567–574. ISSN: 0009-2509. DOI: https://doi.org/10.1016/0009-2509(75)80028-5. URL: https://www.sciencedirect.com/science/article/pii/0009250975800285.

[87] Marcio Schwaab and José Carlos Pinto. "Optimum reference temperature for reparameterization of the Arrhenius equation. Part 1: Problems involving one kinetic constant". In: *Chemical Engineering Science* 62.10 (2007), pp. 2750–2764. ISSN: 0009-2509. DOI: https://doi.org/10.1016/j.ces.2007.02.020. URL: https://www.sciencedirect.com/science/article/pii/S0009250907001777.

[88] Lawrence F. Shampine, Mark W. Reichelt, and Jacek A. Kierzenka. "Solving Index-1 DAEs in MATLAB and Simulink". In: *SIAM Review* 41.3 (1999), pp. 538–552. DOI: 10.1137/S003614459933425X. eprint: https://doi.org/10.1137/S003614459933425X. URL: https://doi.org/10.1137/S003614459933425X.

[89] Lawrence F. Shampine and Mark W. Reichelt. "The MATLAB ODE Suite". In: *SIAM Journal on Scientific Computing* 18.1 (1997), pp. 1–22. DOI: 10.1137/S1064827594276424. eprint: https://doi.org/10.1137/S1064827594276424. URL: https://doi.org/10.1137/S1064827594276424.

[90] Douglas C. Montgomery. *Design and Analysis of Experiments*. Wiley, 2012. ISBN: 9781118097939. URL: https://www.xarg.org/ref/a/1118097939/.

[91] Björn Lundberg, Jonas Sjoblom, Åsa Johansson, Björn Westerberg, and Derek Creaser. "New Methodology for Transient Engine Rig Experiments for Efficient Parameter Tuning". In: *SAE International Journal of Engines* 6.4 (2013), pp. 1995–2003. ISSN: 1946-3944. DOI: 10.4271/2013-01-9043.

[92] Ayman D. Allian, Kazuhiro Takanabe, Kyle L. Fujdala, Xianghong Hao, Timothy J. Truex, Juan Cai, Corneliu Buda, Matthew Neurock, and Enrique Iglesia. "Chemisorption of CO and Mechanism of CO Oxidation on Supported Platinum Nanoclusters". In: *Journal of the American Chemical Society* 133.12 (Mar. 2011), pp. 4498–4517. DOI: 10.1021/ja110073u. URL: https://doi.org/10.1021/ja110073u.

[93] Debbie Stokes. *Principles and Practice of Variable Pressure / Environmental Scanning Electron Microscopy (VP-ESEM)*. Wiley, 2008. ISBN: 0470065400. URL: https://www.xarg.org/ref/a/0470065400/.

[94] Chih-Han Liu, Kevin Giewont, Todd J. Toops, Eric A. Walker, Caitlin Horvatits, and Eleni A. Kyriakidou. "Non-catalytic gas phase NO oxidation in the presence of decane". In: *Fuel* 286 (2021), p. 119388. ISSN: 0016-2361. DOI: https://doi.org/10.1016/j.fuel.2020.119388. URL: https://www.sciencedirect.com/science/article/pii/S001623612032384X.

[95] Akihiro Tsuchiya, Sota Masaoka, Junya Ohyama, Kyoichi Sawabe, and Atsushi Satsuma. "Effects of carbon number and bond saturation on hydrocarbon combustion over a diesel oxidation catalyst". In: *Catal. Sci. Technol.* 10 (12 2020), pp. 3868–3874. DOI: 10.1039/D0CY00017E. URL: http://dx.doi.org/10.1039/D0CY00017E.

[96] Caroline A Schneider, Wayne S Rasband, and Kevin W Eliceiri. "NIH Image to ImageJ: 25 years of image analysis". In: *Nature Methods* 9.7 (2012), pp. 671–675. DOI: 10.1038/nmeth.2089. URL: https://doi.org/10.1038%2Fnmeth.2089.

Appendix A - Supplementary Material

Porosity from SEM

The SEM images are used to approximate two important parameters for mass transport; washcoat thickness (d_{wsc}) and porosity (ε_{wsc}). Firstly, the open source image analysis program *ImageJ* by National Institutes of Health [96] is used to identify differentiate between the solid washcoat and the void space. By measuring their respective areas the porosity can easily be approximated. The only parameter required from the user is a threshold, i.e. what pixel luminosity differentiates between solid and void. As the SEM images has very high contrast (its corresponding histogram of luminosity is highly bimodal), the effect of the user's chosen threshold on the porosity is negligible. However, the most important aspect of this method, and similar methods such as X-ray Tomography (XRT), is the coupled magnification and resolution. In the SEM images used, this was limited to 6.56 px/µm (pixels per micrometer). This at least a hundred times lower than what would be required to capture the mesopores in γ-Al_2O_3 ($d_{\mathrm{m}} \approx 10\,\mathrm{nm}$). Thus the captured porosity should be limited to the macroporosity (ε_{M}) - covering only macropores ($d_M \approx 1 - 10\,\mu\mathrm{m}$) and cracks ($\sim 10 - 100\,\mu\mathrm{m}$). Modern SEM imaging goes down to Ångström (0.1 nm) level in magnification so it is possible to capture the micro- (ε_i) or at least mesoporosity (ε_{m}) of the washcoat. Even at this level of magnification, it is better to use something like Brunauer–Emmett–Teller (BET) or Mercury Intrusion Porosimetry (MIP) which not only gives you more accurate porosity measurements down to nanometer scale, but also gives achieves a pore size distribution. The value for porosity used in this work has been established in an earlier project for a similar catalyst formulation using BET. The method established here can be used to evaluate local differences in macroporosity which can be used in combination with the sectionalization principle to find local effective diffusivities.

Washcoat thickness from SEM

An in-house MATLAB code is used to evaluate the thickness of the washcoat along with its local deposition along the monolith wall. The code is given two boxes; one somewhere in the gas phase (its exact location is so far irrelevant) and one somewhere on the monolith wall. Each box is used to calculate an average luminosity that corresponds to either void or monolith, the luminosity corresponding to the washcoat lies somewhere in between. The pixel luminosity for the void and monolith boxes are pushed to assume values 0 and 255 (minimuim and maximum values in a 8-bit image). This increases the contrast of the entire image which enables easy detection of each area. The code moves from pixel to pixel in increasing x-direction (through each row in the pixel matrix) starting at the upper left corner $(1, 1)$. If it detects a big drop in pixel luminosity, it has found the edge of the monolith, and the coordinates (matrix indices recalculated to distance using the magnification) are recorded. The same procedure is repeated in decreasing x-direction starting at the upper right corner $(n_x, 1)$. The entire procedure is then repeated going pixel to pixel in y-direction (through each column in the pixel matrix) starting from $(1, 1)$ and $(1, n_y)$. The saved coordinates for the monolith edge (c_{mon}) are saved in a polygon vector ζ_{mon} and subsequently arranged in order of increasing angle (α_{mon}) in relation to the gas phase box. This allows for computation of its centeroid, i.e. a very accurate determination of the center of the monolith and also the center of the channel:

$$c_{\text{center}} = \left\{ \sum_{i=1}^{k} (x_i/k), \sum_{i=1}^{k} (y_i/k) \right\} \tag{6.1}$$

where $c_{\text{center}}[-]$ is the centeroid and $x_i[-]$ and $y_i[-]$ are the indices for coordinate number i (ranging from 1 to k), respectively. With the new actual centeroid determined, the coordinates for the monolith, along with the corresponding angle in relation to the new centeroid, are recalculated. The procedure is now reversed; starting at a known angle (α_{wsc}) and moving in increased radius away from the centeroid the washcoat edge is found when there is a big jump in pixel luminosity. The found coordinates for the washcoat edge c_{wsc} is converted into cartesian coordinates and saved in a polygon vector ζ_{wsc}. The use of an angle, instead of the going pixel to pixel in the image matrix, minimizes problems that arise with uneven washcoats (e.g. cracks). Finally, by looping over the angle and comparing washcoat and monolith coordinates that fall within a small enough tolerance (sector), the local washcoat thickness for angle α is:

$$d_{wsc,\alpha} = \sqrt{(c_{\text{mon},\alpha} - c_{\text{center}})^2} - \sqrt{(c_{\text{wsc},\alpha} - c_{\text{center}})^2} \tag{6.2}$$

where $d_{\text{wsc},\alpha}[m]$ is the local washcoat thickness and $c_{\text{mon},\alpha}$ and $c_{\text{wsc},\alpha}$ and the coordinates for the monolith and washcoat that fall within within sector α $[-]$, respectively. The average washcoat thickness, assuming that the it forms a perfect uniform slab, can also be calculated using the areas for the polygons vectors:

$$d_{\text{wsc,avg}} = \frac{\left(d_{\text{w}} - \frac{1}{\sqrt{N}}\right) \pm \sqrt{\left(\frac{1}{\sqrt{N}} - d_w\right)^2 + \left(\int_1^k \zeta_{mon}\, dx - \int_1^k \zeta_{wsc}\, dx\right)}}{2} \tag{6.3}$$

where $d_{\text{wsc,avg}}$ [m] is the average washcoat thickness, d_{w} $[-]$ is the monolith wall thickness, N [cpsi] is the cell density and $\int_1^k \zeta_{\text{mon}}\, dx[m^2]$ and $\int_1^k \zeta_{\text{wsc}}\, dx[m^2]$ are the areas for the polygon vectors.

Appendix B - Supplementary Results

Verification of mixer performance

In paper I it was shown that for a small active core, the local differences in inlet concentration was huge and thus the conversions were very different. However, one could easily argue that for a small catalyst (1x1 in) and isothermal conditions, the effects of any radial concentration maldistribution might be negligible - i.e. some channels have higher inlet concentration while others a little less, but the area-weighted average conversion is the same. However, there is also a velocity gradient which gives higher residence time with increased radius. The light-off curves, with (solid) and without mixer (dashed),for CO, C_3H_6, $C_{10}H_{22}$ and NO are shown in figure 6.1. It can be seen that for the smaller curves there is little to no difference - which could indicate that there was no maldistribution to begin with - or that the area-weighted conversion is the same by sheer luck. I.e. some channels have different concentrations but that is counteracted by a difference in residence time. It can also be that the capillaries where in this case very straight (i.e. pointing towards the center of the test sample). When comparison the results for $C_{10}H_{22}$ it can be seen that the case without mixer achieves higher conversion, especially between 150 to 300°C. It could be that its capillary was pointed in a different way and that there is really no maldistribution. It can also be that there is a maldistribution and that the lower diffusivity of the larger hydrocarbon makes the maldistribution more apparent. This seems like the most plausible explanation as the differences diminish at higher temperatures where the diffusivity is higher.

One experiment that could verify the maldistribution is to perform a chemisorption with and without the mixer. Differences in breakthrough time, shape of the curve and total amount of dispersed Pt should be different.

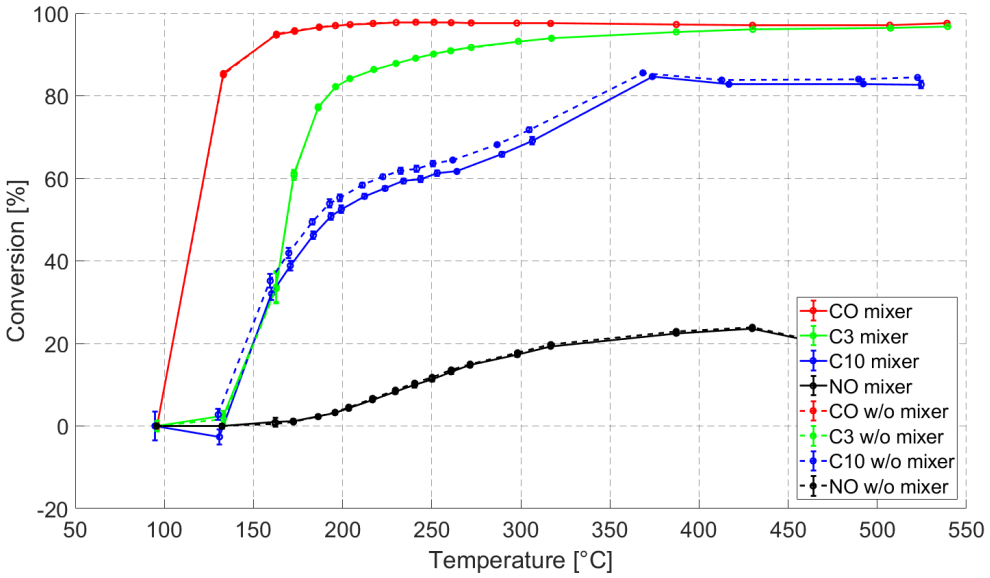

Figure 6.1: *SCAT experiments with and without mixer*

Grid independence study

For verification of the results being independent of the chosen discretization (original 1+1D model), the total number of axial tanks (K) and total number of layers (L) where varied between the standard used in this work ($K = 10$, $L = 8$ in the case of a normal washcoat formulation and $K = 10$, $L = 10$ in the case of an additional inert washcoat) and two other values shown in figures 6.2, 6.3 and 6.4. It can be seen that over the large span of 150 to 375°C there is only 0.51% difference in conversion for the light-off for catalyst A from paper II (therein labeled as "thick washcoat"). This is considered negligible compared to the experimental noise.

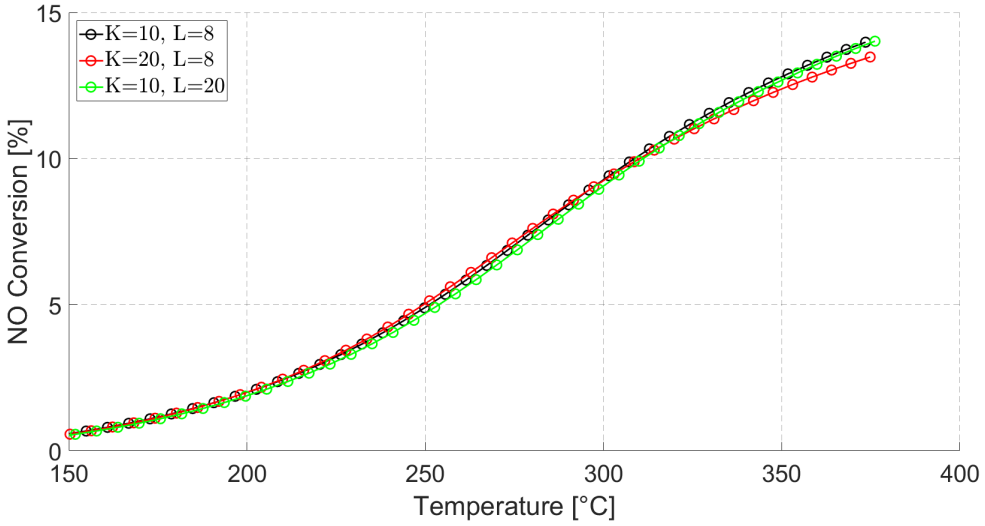

Figure 6.2: *Grid independence comparison - light-off*

The corresponding axial and radial concentration profiles are shown in 6.3 and 6.4, respectively. It can be seen that the concentrations differences are on the level of 1 $\sin ppm$, which is also very small. The largest differences was when moving from the standard grid to doubling the number of axial tanks, i.e. there might be a small difference in the very first tank where concentrations and driving forces are the highest.

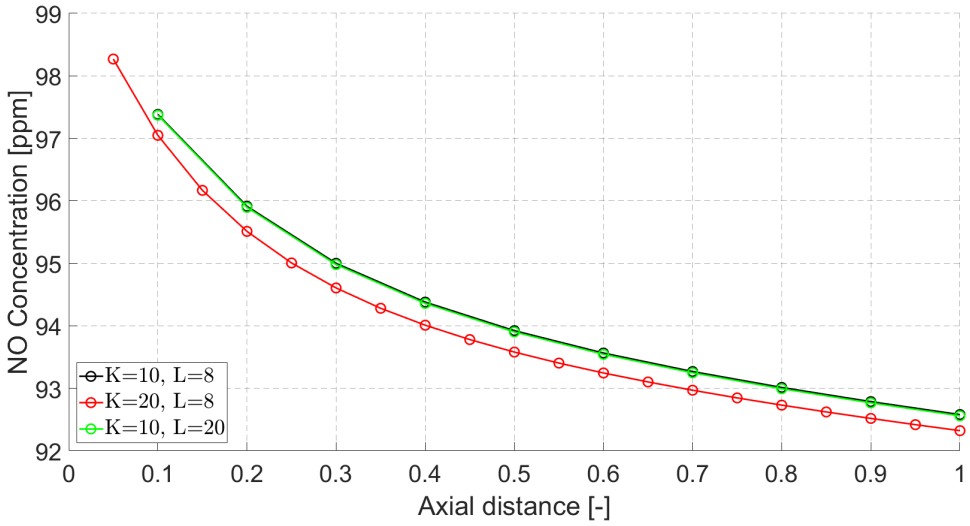

Figure 6.3: *Grid independence comparison - axial concentrations*

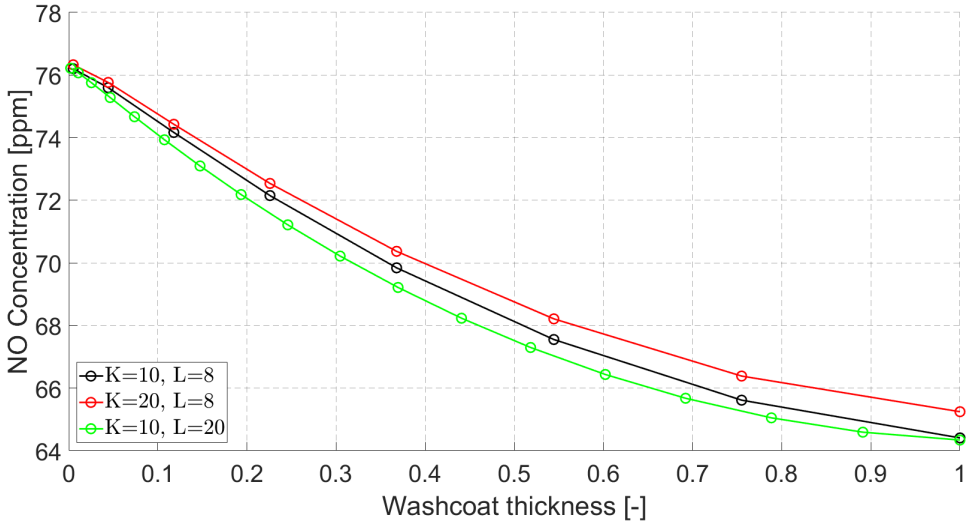

Figure 6.4: *Grid independence comparison - radial concentrations*